Fermions on a Quantum Ring

Joshua Cesca

A thesis submitted for the degree of
Bachelor of Philosophy - Science with Honours in Physics of
The Australian National University

October, 2022

Declaration

This thesis is an account of research undertaken between February 2022 and October 2022 at The Department of Physics, Faculty of Science, The Australian National University, Canberra, Australia.

Except where acknowledged in the customary manner, the material presented in this thesis is, to the best of my knowledge, original and has not been submitted in whole or part for a degree in any university.

Joshua N. Cesca

October, 2022

Acknowledgements

I acknowledge the Ngunnawal and Ngambri people, upon whose land this work was conducted. I acknowledge the traditional owners of land throughout Australia, and pay my respects to their elders past, present and emerging.

I would like to thank Cédric Simenel, my supervisor, for his significant amount of support, guidance, and feedback for this project. His demonstrations of particles on a ring using whiteboard markers in a coffee mug were particularly helpful.

I also thank Rose Ahlefeldt and James Sullivan for their help in the Honours research training course and Ilya Shadrivov for organising the physics Honours year.

I would like to thank my parents for providing me with education, support, and laying the foundations for me to reach this point.

Finally, I would like to thank my partner, Ellie Cooper, and her dog, Jasper, for their love and support which helped me get through this year as well as for the proofreading of this thesis (which was done by Ellie not Jasper since he can't read).

Abstract

Model systems are an effective tool for testing approximate methods for solving the quantum many-body problem. This thesis used an idealised 1-D quantum ring of fermions to test rotational symmetry breaking and rotational symmetry restoration in the Hartee-Fock method when applied to Coulomb and nuclear-like systems. This was achieved by comparing the exact ground state energy, which was found using the variational Monte Carlo method, to the predicted ground state energies of the Hartree-Fock method without rotational symmetry breaking, with rotational symmetry breaking, and with rotational symmetry restored. It was found that the effectiveness of symmetry breaking in systems with repulsive interactions between particles increased with the strength of the interaction. In systems with attractive interactions, symmetry breaking significantly improved the Hartree-Fock energy but still failed to account for all of the correlation energy of the ground state. Symmetry restoration was able to account for almost all of the correlation energy in repulsive systems but typically gave little improvement to the symmetry-broken energy in attractive systems.

Contents

List of Figures

List of Tables

Chapter 1

Introduction

1.1 The quantum many-body problem

One of the major successes of quantum mechanics lies in its ability to describe systems across a wide range of energy, length and time scales. For non-relativistic particles, the dynamics and structure of these quantum systems can be found by solving a single, second-order partial differential equation called the Schrödinger equation. Unfortunately, exact analytical solutions to the Schrödinger equation generally cannot be found for most real physical systems of many particles, an issue known as the quantum many-body problem (QMBP). There are two options for further study of the QMBP. The first is to study model systems which are simple enough to solve analytically, yet share important properties with real systems. In this way, conclusions can be made about the dynamics and structure of real systems by considering the properties of the model system solutions. The second option for further study is to solve the Schrödinger equation using approximate methods. A wide variety of approximate methods exist; the choice of which one to use for a given system depends on the type of system studied, the desired accuracy of the solution, and the amount of computational power available. The two options each have their own advantages and disadvantages. When studying model systems, confidence can be had in the accuracy of the solutions but these solutions have limited relevance to real systems. When using approximate methods, real systems are able to be studied but the accuracy of your solutions is difficult to determine.

In this thesis, I apply approximate methods to a model system which can be solved exactly in order to test their accuracy. I focus only on systems of identical interacting fermions (particles with half integer spin whose wave functions must be antisymmetric on the exchange of each pair of particles). These systems can be found in a range of different fields of physics including: quantum chemistry in which the fermions are electrons around a molecule, atomic physics in which the fermions are electrons around an atom or the atoms themselves are fermions in the case of ultracold atomic physics, solid states physics where the fermions are valence or conducting electrons, and nuclear physics in which the fermions are protons and neutrons in a nucleus.

1.2 The mean-field approach and the nuclear QMBP

The mean-field approach is a class of approximate methods for solving the QMBP. Generally, the approach treats the system as a collection of independent, one-body systems in which each particle only interacts with the others indirectly via a mean-field potential which aims to average the effect of the interactions with other particles. By reducing the N-body problem to a one-body problem, this approach greatly reduces the computational effort required to find a solution. One of the first applications of the mean-field approach to a QMBP was conducted by Douglas Hartree in 1929, who used it to model the energy level structure of electrons around an atom [1]. His method did not account for the anti-symmetry requirement for fermions and so the method was improved by Vladimir Fock in 1930 [2] by adding an exchange term to the mean-field calculation. With this addition, the method is now known as the Hartree-Fock method. The mean-field approach was reasonably successful in describing the energy level structure of electrons around an atom, primarily thanks to a weak interaction between the particles leading to less correlations and a large mean free path for each electron, resulting in a low chance of collisions.

A mean-field approach called the shell model, which was first proposed by Ivanenko and Gapon in 1932 [3], has also had a large degree of success in describing the energy levels of nucleons in a nucleus. In the early versions of the shell model, the mean-field was a three-dimensional harmonic oscillator potential and the nucleons filled the lowest energy single particle states of this potential as a result of the Pauli exclusion principle. With the inclusion of the spin-orbit interaction to the shell model by Maria G. Mayer in 1949 [4], it was able to correctly predict the so-called magic numbers of nuclear stability [5] (the specific number of neutrons or protons in a nucleus which result in a higher average binding energy per nucleon than other similar nuclei and thus a more stable nucleus). It is not immediately clear why the mean-field, independent-particle approach was so successful in describing nuclear structure. From nucleon scattering experiments, it is known that the nucleon-nucleon interaction consists of a strong, short-ranged attraction along with an even stronger hard-core repulsion [6] and it would be natural to expect that these strong interactions would lead to large correlations between nucleons which would invalidate an independent-particle picture. In reality, collisions between particles which would lead to these strong correlations are blocked by the Pauli exclusion principle which prevents fermions from existing in the same quantum state. In order for two nucleons to scatter, their final energy and momentum states after the collision must be unoccupied by other nucleons which is frequently not the case inside the nucleus. As a result, the mean free path for a nucleon is of the order of the size of the entire nucleus which justifies the assumption of particle independence in the nucleus used by the mean-field approximation [7].

The shell model has been extended in several ways since its introduction. The Nilsson model [8] extends the shell model by using a deformed mean-field potential to predict the single particle energy levels in a non-spherical nucleus as a function of the degree of deformation. Modern usage of the shell model is typically in a configuration interaction method [9] which is considered a 'beyond mean-field' model. In this method, the basis

states of the system (which are called configurations) are formed from particle excitations of the independent-particle states of the shell model. Including all possible configurations quickly becomes numerically intractable, so it is necessary to exclude excitations from lower energy single particles (called an inert core) as well excitations to high energy single particle states. With these exclusions, the method just deals with the occupation of single particle states in a 'valence space'. An effective Hamiltonian which accounts for the excluded configurations is then diagonalised in this basis to find the energy eigenstates of the system which are given as superpositions of the allowed configurations.

The Hartree-Fock method is also used to predict nuclear structure (where it is often called the self-consistent mean-field method). As in the shell model, it assumes that the many-body state is comprised of independent, single-particle states. However, instead of starting with some fixed mean-field potential, as in the shell model, the Hartree-Fock method calculates the potential iteratively by averaging the wave functions of its single-particle states which in turn are the lowest energy states of a system with the mean-field potential. In this way, the Hartree-Fock method requires self consistency between the single-particle states and the mean-field Hamiltonian. The non-linearity of the resulting equations means that Hartree-Fock method is typically solved through an iterative process until self-consistency is achieved. Modern implementations of the Hartree-Fock method also account for nuclear pairing phenomena and are called the Hartree-Fock-Bogoliubov method [10].

1.3 Correlations through symmetry breaking and restoration

The interactions between particles in the QMBP are often invariant under a number of symmetries. One example is translational symmetry; the strength of an interaction is unaffected if the particles are translated in space by some distance. Other common symmetries include rotational, parity and a range of gauge symmetries. As a result, the solutions to the QMBP are also expected to have these symmetries. However, mean-field approaches often work in bases which do not respect the symmetries of the system and thus allow for symmetry-broken solutions. In many cases, these symmetry-broken solutions give more accurate results than solutions which are constrained to have that symmetry. This feature of mean-field methods is referred to as spontaneous symmetry breaking and provides a way for the method to account for correlations between particles while still working in the simple independent-particle picture.

The spontaneous symmetry breaking of the mean-field solutions does come at a price. Noether's theorem tells us that each continuous symmetry of a system is associated with a conservation law for that system, for example translational symmetry leads to conservation of linear momentum and rotational symmetry leads to conservation of angular momentum. As a result, the mean-field symmetry-broken solutions are no longer states with well defined values of the relevant conserved quantity. If translational symmetry is broken, then the mean-field solution will not be an eigenstate of total linear momentum;

if rotational symmetry is broken, it will no longer be an eigenstate of total angular momentum and so on. These previously conserved values are often used in the calculation of physically relevant quantities, for instance, the electromagnetic transition probabilities between electronic states in an atom are subject to selection rules which depend on the parity and total angular momentum of the initial and final states. The loss of this information in the symmetry-broken states makes these calculations difficult.

The symmetry restoration method [11] offers a solution to the problems of spontaneous-symmetry breaking in the mean-field approach. The method projects the symmetry-broken state back onto a state with a well-defined symmetry-relevant quantity. It does this by taking an appropriately weighted superposition of each of the states in the broken symmetry group. This superposition results in a state with the correct symmetry while still keeping the symmetry-broken solution's account of correlations. Since the resultant superposition is no longer an independent-particle state, symmetry restoration is considered to be another beyond mean-field method.

1.4 Simplified models for benchmarking approximate methods

Although powerful, approximate methods for solving the QMBP have a significant drawback. Any approximation we include is expected to cause the approximate solution to deviate from the true solution, however, the degree of deviation is largely unknown. To calculate the deviation, we would need to know the true solution which, as mentioned above, is not possible for most real many-body systems. The fact that we cannot assess approximate methods in this way is a problem since a large degree of deviation may make a given approximate method unsuitable for a particular system.

This motivates the use of model systems to benchmark approximate methods, which is what will be done in this thesis. A model system is a system which is simple enough for its QMBP to be solved exactly yet still shares important features with the real physical system which we wish to apply the approximate method to. By using the approximate method in the model system, we can compare the approximate solution with the true solution to assess the suitability of the approximate method for this system. This in turn, allows us to make some conclusions about the suitability of the method in other real systems. Additionally, the properties of a model system's solution can also be used to make conclusions about its real counterpart's solution.

So far, I have discussed solutions to the QMBP and deviations to the solutions in an abstract way, which begs the question: what actually are these solutions and how would one go about benchmarking them? The answer depends on whether one is interested in the dynamics or the energy level structure of the system (which can often be a useful tool in calculating its dynamics). The dynamics of the system can be found by solving the time-dependent Schrödinger equation, in which case the solution is a time-dependent many-body wave function of the evolving system (or equivalently the time-dependent operators of the system in the Heisenberg picture). Benchmarking approximate methods

in this case typically involves comparing the expectation values of observables of the real system over time (which have been experimentally measured) with those predicted by the approximate method. The energy level structure of the system is found by solving the time-independent Schrödinger equation, in which case the solution is a set of energy eigenstates and their eigenenergies. In particular, the ground state wave function (the many-body state with the lowest energy) makes for a good target for benchmarking as it allows us to compare just a single number, the ground state energy, between methods. As a result of the variational principle, which will be discussed in more detail in a later section, a lower ground state energy typically implies a better approximation of the true ground state.

I shall now briefly discuss some of the model systems commonly used to test approximate methods in nuclear systems in order to justify the choice of system used in this thesis.

The first model system is infinite nuclear matter (also referred to as homogeneous matter) which consists of an infinite number of protons and neutrons with a finite density and ratio, interacting with each other via nuclear forces. Infinite nuclear matter has been used to study the binding energy of nuclei [12], the structure of neutron stars and other compact stars [13], and is used in the fitting of parameters for energy density functionals [14]. The major limitation of this model comes from its translational invariance which prevents the study of nuclear effects which depend on gradients of nucleon densities such spin-orbit splitting. Given that its translational symmetry is key to its simplicity, infinite nuclear matter is a poor choice to investigate the effects of symmetry breaking and restoration.

Another model system, called neutron drops, consist of a small number of neutrons (typically on the order of 10) trapped in an external potential and interacting with each other via an interaction potential which models the nuclear force. Neutron drops have been used to estimate neutron pairing energies in real nuclei [15] and to fit the parameters of energy density functionals [16]. Typically, neutron drops offer insight into systems where the isospin degree of freedom plays a significant role such as neutron stars or exotic neutron-rich nuclei. Isospin physics is beyond the scope of this project, so neutron drops were not used in this thesis.

The final model system to introduce is the quantum ring (also referred to as a ringium) which was the model used in this thesis. A quantum ring is a one-dimensional system consisting of particles constrained to exist and move around the edge of circle [17]. Quantum rings contain a number of parameters which can be varied in order to model a range of real systems. Among these are: the ring radius to model systems of different scales, the number of particles on the ring, and the strength and type of the interactions between the particles. In particular, I can choose a model nuclear interaction and a femtometre scale radius to model nuclear systems, or a Coulomb interaction and an angstrom scale radius to model electronic systems. A major advantage of the quantum ring over nuclear matter is that it is not required to be translationally invariant (which for the quantum ring is equivalent to rotational invariance). This allows for the investigation of symmetry breaking and restoration in mean-field methods when applied to quantum rings. Another

advantage of the quantum ring lies in its ability to be extended to higher dimensions in order to explore the dependence of the effectiveness of approximate methods on the dimensionality of the system. As an example, a two-dimensional quantum ring, called a spherium, consists of particles constrained to be on the surface of a sphere. This thesis will focus only on one-dimensional quantum rings, however, extending the investigation to higher dimensions is a clear direction for future work.

I will now briefly outline some of the previous work with quantum rings. Quantum rings have been studied in a range of fields as they approximate several real systems. These include semiconductor structures where their electronic and optical properties have been studied [18, 19], molecular rings formed from circular polymers [20], and heavy ion storage rings [21]. These physical systems all possess some finite width to the ring and are considered quasi-one-dimensional. In terms of the idealised, purely one-dimension quantum ring, the exact ground state wave function of two electrons on the ring has been found analytically as an infinite series for all ring radii [22] and as a series with a finite number of terms for particular radii [23]. In addition, the variational Monte Carlo method was shown to be effective at accounting for correlations in the ground state of a N-electron quantum ring (for N up to 6) [24]. Finally, Bray and Simenel have benchmarked the Hartree-Fock method with enforced rotational symmetry by finding the ground state of an N-fermion quantum ring (for N up to 10) with a range of different ring radii and interaction types intended to model nuclear and electronic systems [25]. They found that the symmetry-unbroken Hartree-Fock method gave a good approximation to the ground state in some cases but failed in the case of dense systems with strong short-ranged repulsion as well as attractive systems. A more in-depth description of their results can be found in the next chapter.

1.5 Aim and outline of the thesis

Bray and Simenel's results [25] lead naturally to the question of the effectiveness of symmetry breaking and restoration in the Hartree-Fock method when applied to the quantum ring, which is the subject of this thesis. The aim of thesis was to systematically search the parameter space of the quantum ring to find under which conditions the Broken-Symmetry Hartree-Fock (BSHF) and Restored-Symmetry Hartree-Fock (RSHF) methods are able to significantly improve on the Unbroken-Symmetry Hartree-Fock (USHF) results found by Bray and Simenel. To compare the accuracy of these methods, I also use the Variational Monte Carlo (VMC) method to find an effectively exact ground state.

I will now outline the remainder of this thesis. In Chapter 2, I explore some additional background of the quantum ring. I first introduce the interactions and Hamiltonian for the system and define some notation, then cover some properties that the ground state must possess. Then, I reproduce the analytical solution for two electrons on a quantum ring, explore the results of Bray and Simenel [25] in more depth, and also cover some results for electrons on higher dimensional quantum rings. In Chapter 3, I describe each method (USHF, BSHF, VMC then RSHF) used in this work as well as give some details on their numerical implementations. Finally, in Chapter 4, I compare the results of each

method and discuss the implications of the results on their relative effectiveness.

Chapter 2

Background on the Quantum Ring

2.1 Interactions and system Hamiltonians

In this work, the quantum ring consists of N fermions constrained to be on the edge of a circle of radius R. This work does not focus on any effects involving the spin of the particles, so for simplicity, every particle is in the same spin eigenstate in the direction of the axis of the ring, which I call spin up.

The state of the system can be described by N coordinates, one for the angular position of each particle which I label $\theta_1, \theta_2, ...\theta_\alpha, ..., \theta_n$. Throughout this thesis, I will use Greek letters subscripts or labels when referring to particle numbers. The particles interact via two-body potential operators, $\hat{V}_{int}(\alpha, \beta)$. In the position basis, these operators are functions only of the distance between the particles, $V_{int}(r_{\alpha\beta})$, where

$$r_{\alpha\beta} = 2R\left|\sin\left(\frac{\theta_\alpha - \theta_\beta}{2}\right)\right| \tag{2.1}$$

is the distance through the ring[1] between particles α and β. Following the work of Bray and Simenel [25], several interaction potentials are considered in this thesis, each aimed at approximating real systems. The first is the Coulomb potential, the electrostatic interaction between charged particles,

$$V_C(r_{\alpha\beta}) = \frac{V_0}{r_{\alpha\beta}}. \tag{2.2}$$

V_0 is an additional parameter controlling the magnitude and direction of the force between the particles depending on the product of their charges. V_0 is positive for a repulsive interaction which I label as V_{C+} and negative for an attractive one which I label V_{C-}. Throughout this thesis, I treat positive and negative V_0 as two different interaction types as they result in very different behaviour. I also consider two interactions intended to model the nuclear force between nucleons, both taken from Bray and Simenel. Both interactions consist of a 'hard-core' repulsion at short distances followed by an attractive component at at moderate distances which then decays to zero at larger distances. The

[1] As opposed to around the ring which would be $R|\theta_\alpha - \theta_\beta|$.

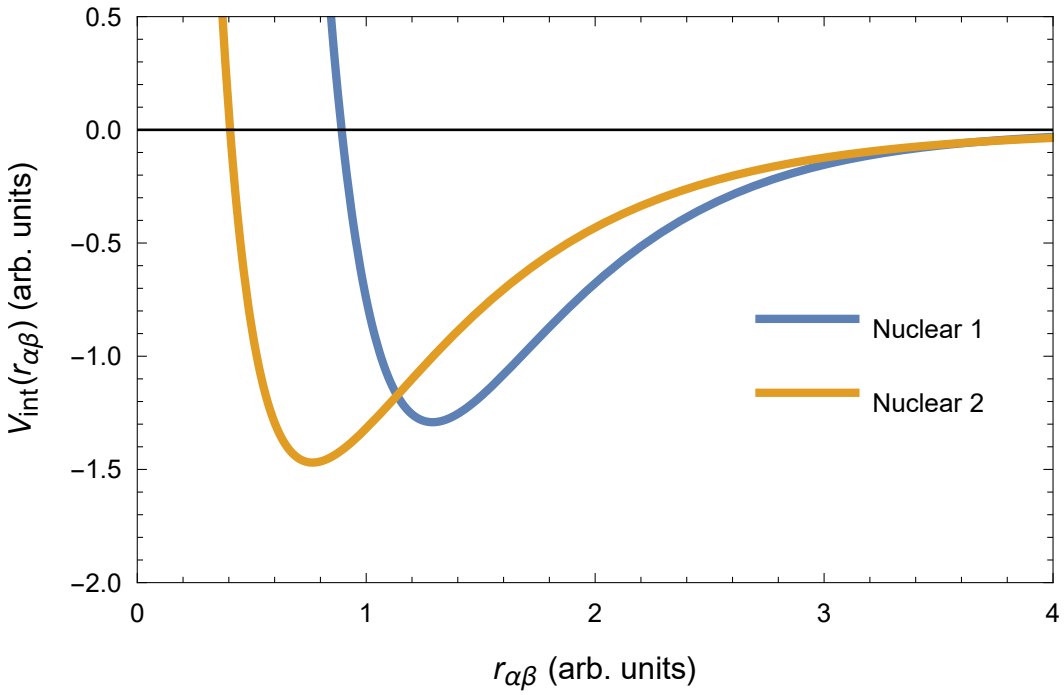

Figure 2.1: A comparison between the two nuclear potentials used in this thesis with $V_0 = 1$.

interaction potentials, which I refer to as Nuclear 1 and Nuclear 2 respectively, are each the sum of attractive and repulsive Yukawa potentials,

$$V_{N1}(r_{\alpha\beta}) = \frac{V_0}{r_{\alpha\beta}}\left(100e^{-2r_{\alpha\beta}} - 64e^{-1.5r_{\alpha\beta}}\right), \tag{2.3}$$

$$V_{N2}(r_{\alpha\beta}) = \frac{V_0}{r_{\alpha\beta}}\left(12e^{-2r_{\alpha\beta}} - 8e^{-r_{\alpha\beta}}\right), \tag{2.4}$$

where again V_0 determines the strength of the potential and is positive for these interactions. A comparison of the two interaction potentials can be seen in figure (2.1) with $V_0 = 1$. The main difference between the two is the strength and range of the hard-core repulsion and the classical equilibrium distances (that is, the minimum of the potential). Nuclear 1 has the larger hard-core repulsion and has an equilibrium distance of $r_{\alpha\beta} = 1.29$ arbitrary units, while Nuclear 2 has a weaker hard-core repulsion and an equilibrium distance of $r_{\alpha\beta} = 0.77$ arbitrary units. The two interactions have similar well depths at their respective equilibrium distances of around -1.4 arbitrary units, provided that their potential strengths, V_0, are the same.

In this thesis, I use dimensionless distances and energies and set the mass of the fermions on the ring, m, and the reduced Planck constant, $\hbar$, to be 1. In this format, the system Hamiltonian in the angular coordinate basis is

$$H = -\frac{1}{2R^2}\sum_{\alpha=1}^{N}\frac{\partial^2}{\partial\theta_\alpha^2} + \sum_{\alpha<\beta}^{N} V_{\text{int}}(r_{\alpha\beta}), \tag{2.5}$$

where the sum over the potential terms runs over each pair of particles α and β and V_{int} can be V_{C+}, V_{C-}, V_{N1} or V_{N2}.

To recover the standard kinetic energy term we can multiply equation (2.5) throughout by $\frac{\hbar^2}{mR_{\text{unit}}^2}$, where R_{unit} is an appropriately chosen distance scale for the system. In that case, the true energy of the ground state becomes $E_{0\,\text{actual}} = \frac{\hbar^2}{mR_{\text{unit}}^2} E_{0\,\text{dimensionless}}$ and the strength of the potential is $V_{0\,\text{actual}} = \frac{\hbar^2}{mR_{\text{unit}}} V_{0\,\text{dimensionless}}$. Some extra care must be taken when interpreting the range of the nuclear interactions. If the distance $r_{\alpha\beta}$ has units of R_{unit}, then the range parameter a in the Yukawa terms of the form $e^{-ar_{\alpha\beta}}/r_{\alpha\beta}$ has units of R_{unit}^{-1}.

2.2 Properties of the ground state

There are a number of conditions we know the ground state wave function must satisfy. Firstly, since the particles are identical fermions, the wave function must be antisymmetric under the exchange of two particles, that is

$$\Psi(..., \theta_\alpha, ..., \theta_\beta, ...) = -\Psi(..., \theta_\beta, ..., \theta_\alpha, ...). \tag{2.6}$$

Next, we have that the wave function must be continuous everywhere and have bounded first order partial derivatives everywhere except at singular points in the potential [26] (in this case, singular points are when two particles are at the same position so $r_{\alpha\beta} = 0$). Finally, the local energy of the wave function $\Psi^{-1}\hat{H}\Psi$ must be constant everywhere (a short proof can be found in appendix A) and so cannot diverge at singular points in the potential. This leads to a condition on the second partial derivative of the wave function analogous to the Kato cusp condition [26] in 3D systems,

$$\left.\frac{\partial^2 \Psi}{\partial r_{\alpha\beta}^2}\right|_{r_{\alpha\beta}\to 0} = \left.\frac{V_1}{r_{\alpha\beta}}\Psi\right|_{r_{\alpha\beta}\to 0}, \tag{2.7}$$

where V_1 is the strength of the diverging part of the Coulomb-like component of the potential as $r_{\alpha\beta} \to 0$. For the Coulomb potential, $V_1 = V_0$, for the Nuclear 1 potential, $V_1 = 36V_0$ and for Nuclear 2, $V_1 = 4V_0$. See Appendix B for the derivation of this condition.

2.3 Analytical solution for two electrons on a ring

As mentioned previously, a major advantage of the quantum ring is that there exists analytical solutions for the ground state of two electrons on a ring interacting via the Coulomb potential, found by Loos and Gill [23]. For completeness I will reproduce their derivation of the solutions here. The time-independent Schrödinger equation (TISE) for this system in the standard angular position basis (that is the basis of particle positions

on the ring θ_1 and θ_2) is

$$H\Psi(\theta_1,\theta_2) = \left(-\frac{1}{2R^2}\left(\frac{\partial^2}{\partial\theta_1^2}+\frac{\partial^2}{\partial\theta_2^2}\right)+\frac{1}{r_{12}(\theta_1,\theta_2)}\right)\Psi(\theta_1,\theta_2) = E\Psi(\theta_1,\theta_2). \tag{2.8}$$

A change of variables is made to the angular separation between the particles, $\omega = \theta_1 - \theta_2$, and the average position of the particles, $\Omega = \frac{\theta_1+\theta_2}{2}$. The second derivatives terms become

$$\frac{\partial^2}{\partial\theta_\alpha^2} = \left(\frac{\partial\Omega}{\partial\theta_\alpha}\right)^2\frac{\partial^2}{\partial\Omega^2}+\left(\frac{\partial\omega}{\partial\theta_\alpha}\right)^2\frac{\partial^2}{\partial\omega^2}+2\frac{\partial\omega}{\partial\theta_\alpha}\frac{\partial\Omega}{\partial\theta_\alpha}\frac{\partial^2}{\partial\Omega\partial\omega}+\frac{\partial^2\Omega}{\partial\theta_\alpha^2}\frac{\partial}{\partial\Omega}+\frac{\partial^2\omega}{\partial\theta_\alpha^2}\frac{\partial}{\partial\omega}, \tag{2.9}$$

for $\alpha = 1$ or 2. Using $\frac{\partial\Omega}{\partial\theta_1} = \frac{\partial\Omega}{\partial\theta_2} = \frac{1}{2}$, $\frac{\partial\omega}{\partial\theta_1} = 1$, $\frac{\partial\omega}{\partial\theta_2} = -1$, and $\frac{\partial^2\Omega}{\partial\theta_1^2} = \frac{\partial^2\Omega}{\partial\theta_2^2} = \frac{\partial^2\omega}{\partial\theta_1^2} = \frac{\partial^2\omega}{\partial\theta_2^2} = 0$, equation (2.8) becomes

$$\left(-\frac{1}{2R^2}\left(\frac{1}{2}\frac{\partial^2}{\partial\Omega^2}+2\frac{\partial^2}{\partial\omega^2}\right)+\frac{1}{r_{12}(\omega)}\right)\Psi(\theta_1,\theta_2) = E\Psi(\theta_1,\theta_2). \tag{2.10}$$

The Hamiltonian can be split into two parts, one which depends only on the average position coordinate, $H_\Omega = -\frac{1}{4R^2}\frac{\partial^2}{\partial\Omega^2}$ and the other which depends only on the difference in angular position, $H_\omega = -\frac{1}{R^2}\frac{\partial^2}{\partial\omega^2}+\frac{1}{r_{12}(\omega)}$. This separation of the Hamiltonian means that the wave function can be written as the product of two functions which depend on independent coordinates $\Psi(\Omega,\omega) = \Lambda(\Omega)\Phi(\omega)$. Thus, the TISE becomes

$$(H_\Omega + H_\omega)\Lambda(\Omega)\Phi(\omega) = E\Lambda(\Omega)\Phi(\omega) \tag{2.11}$$

$$\frac{H_\Omega\Lambda(\Omega)}{\Lambda(\Omega)}+\frac{H_\omega\Phi(\omega)}{\Phi(\omega)} = E. \tag{2.12}$$

Being independent functions, the two terms of the left hand side of the equation above must be equal to constants which I will call $\mathcal{E}$ and ε such that $\mathcal{E}+\varepsilon = E$. This leads to two one-coordinate TISEs,

$$H_\Omega\Lambda(\Omega) = -\frac{1}{4R^2}\frac{\partial^2}{\partial\Omega^2}\Lambda(\Omega) = \mathcal{E}\Lambda(\Omega) \tag{2.13}$$

$$H_\omega\Phi(\omega) = \Big(-\frac{1}{R^2}\frac{\partial^2}{\partial\omega^2}+\frac{1}{r_{12}(\omega)}\Big)\Phi(\omega) = \varepsilon\Phi(\omega). \tag{2.14}$$

The first equation has a simple solution, $\Lambda_J(\Omega) = \exp(iJ\Omega)$, with energy levels $\mathcal{E}_J = \frac{J^2}{4R^2}$. Using the boundary condition, $\Lambda(0) = \Lambda(2\pi)$, J must be an integer and the lowest energy state has $J = 0$ which corresponds to no motion of the average position of the two electrons. The second equation is more difficult to solve and requires changing the coordinate from ω to $r_{12} = 2R\left|\sin\frac{\omega}{2}\right| = R\sqrt{2-2\cos(\omega)}$ (since there is a one to one relation between r_{12} and ω). Then the second derivative term becomes

$$\frac{\partial^2}{\partial\omega^2} = \left(\frac{\partial r_{12}}{\partial\omega}\right)^2\frac{\partial^2}{\partial r_{12}^2}+\frac{\partial^2 r_{12}}{\partial\omega^2}\frac{\partial}{\partial r_{12}}. \tag{2.15}$$

Using $\left(\frac{\partial r_{12}}{\partial \omega}\right)^2 = R^2 - \frac{1}{4}r_{12}^2$ and $\left(\frac{\partial^2 r_{12}}{\partial \omega^2}\right)^2 = -\frac{1}{4}r_{12}$, the second TISE becomes

$$\left(\frac{r_{12}^2}{4R^2} - 1\right)\frac{\partial^2\Phi(r_{12})}{\partial r_{12}^2} + \frac{r}{4R^2}\frac{\partial\Phi(r_{12})}{\partial r_{12}} + \frac{1}{r_{12}}\Phi(r_{12}) = \epsilon\Phi(r_{12}), \tag{2.16}$$

which is classified as a Heun-like equation. This has the general power series solution of

$$\Phi(r_{12}) = r_{12}\left(1 + \frac{r_{12}}{2R}\right)^{a/2}\left(1 - \frac{r_{12}}{2R}\right)^{b/2}\sum_{k=0}^{\infty} c_k^{(a,b)} r_{12}^k, \tag{2.17}$$

with a and b equal to 0 or 1 [27]. The coefficients of the power series follow the recurrence relation

$$c_{k+2}^{(a,b)} = \frac{1}{(k+2)(k+3)}\left[\left(\frac{(k+2)(b-a)}{2R}+1\right)c_{k+1}^{(a,b)} + \left(\frac{k(k+2+a+b)+\sigma^{(a,b)}}{4R^2} - \sigma^{(a,b)}\epsilon\right)c_k^{(a,b)}\right], \tag{2.18}$$

with starting values $c_0^{(a,b)} = 1$ and $c_1^{(a,b)} = \frac{1}{2}\left(1 + \frac{b-a}{2R}\right)$ and the additional terms $\sigma^{(0,0)} = 1$, $\sigma^{(1,0)} = \sigma^{(0,1)} = 1 + \frac{5}{4-16R^2\epsilon}$, and $\sigma^{(0,1)} = 1 + \frac{3}{1-4R^2\epsilon}$. Only the $(a,b) = (0,0)$ and $(a,b) = (1,0)$ solutions contain the ground state of the ring for any radius. Loos and Gill found closed form solutions for particular values of R by solving the equations $c_{k+1}^{(a,b)} = 0$ and $c_{k+2}^{(a,b)} = 0$ for ϵ and R. These ground state solutions are given in table (2.1). In this thesis, I will use these exact solutions as a starting point to test the accuracy of the other many-body methods.

Ring radius R	Ground state wave function $\Phi(r_{12})$	Ground state energy ϵ
$1/2$	$r_{12}\left(1 + \frac{r_{12}}{2R}\right)^{1/2}$	$9/4$
$\sqrt{3/2}$	$r_{12}\left(1 + \frac{1}{2}r_{12}\right)$	$2/3$
$\sqrt{\frac{3}{4}(7+\sqrt{33})}$	$r_{12}\left(1 + \frac{r_{12}}{2R}\right)^{1/2}\left(1 + \frac{15-\sqrt{33}}{24}r_{12}\right)$	$\frac{25}{96}(7-\sqrt{33})$
$\sqrt{23/2}$	$r_{12}\left(1 + \frac{1}{2}r_{12} + \frac{5}{92}r_{12}^2\right)$	$9/46$

Table 2.1: Exact closed-form solutions for two electrons on a quantum ring. Energy and radii are in arbitrary units.

2.4 Previous investigations

Now that we have an exact solution for a two-electron quantum ring, I will discuss the previous numerical results conducted by Bray and Simenel [25], that inspired the work in this thesis.

In their paper, Bray and Simenel compare the effectiveness of the Hartree-Fock method without broken rotational symmetry to quantum Monte Carlo methods in predicting the

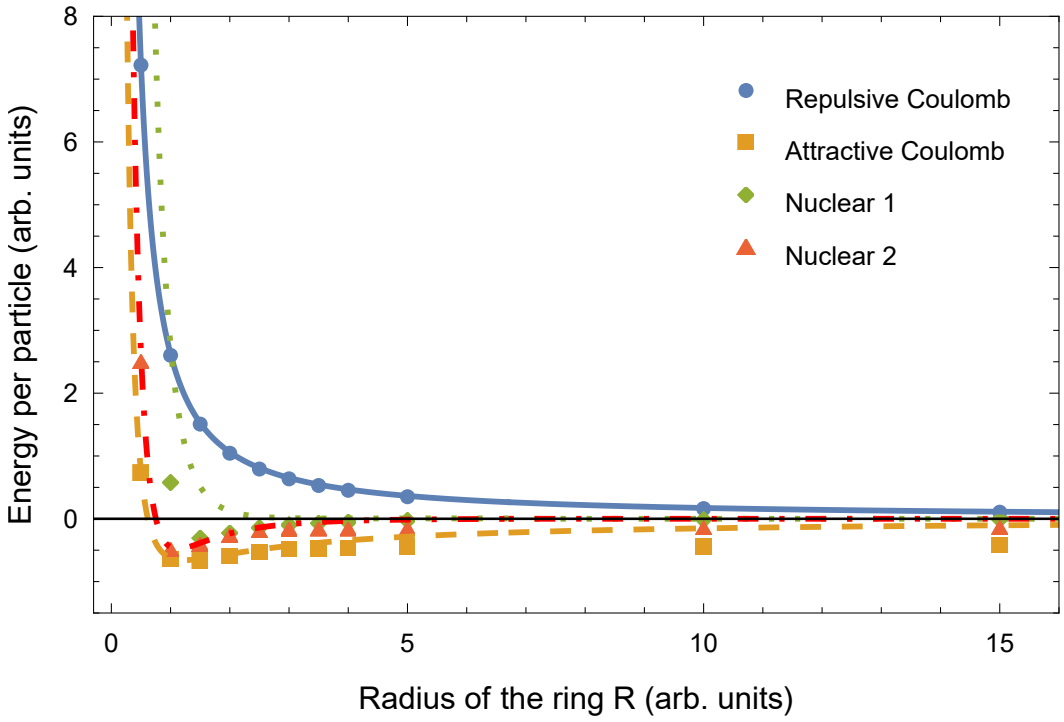

Figure 2.2: Energy per particle for a quantum ring with $N = 5$ particles, potential strength $V_0 = 1$, and varying ring radii R. Points indicate the exact energy for each interaction while the corresponding lines indicate the unbroken-symmetry Hartree-Fock energy. Figure adapted from [25].

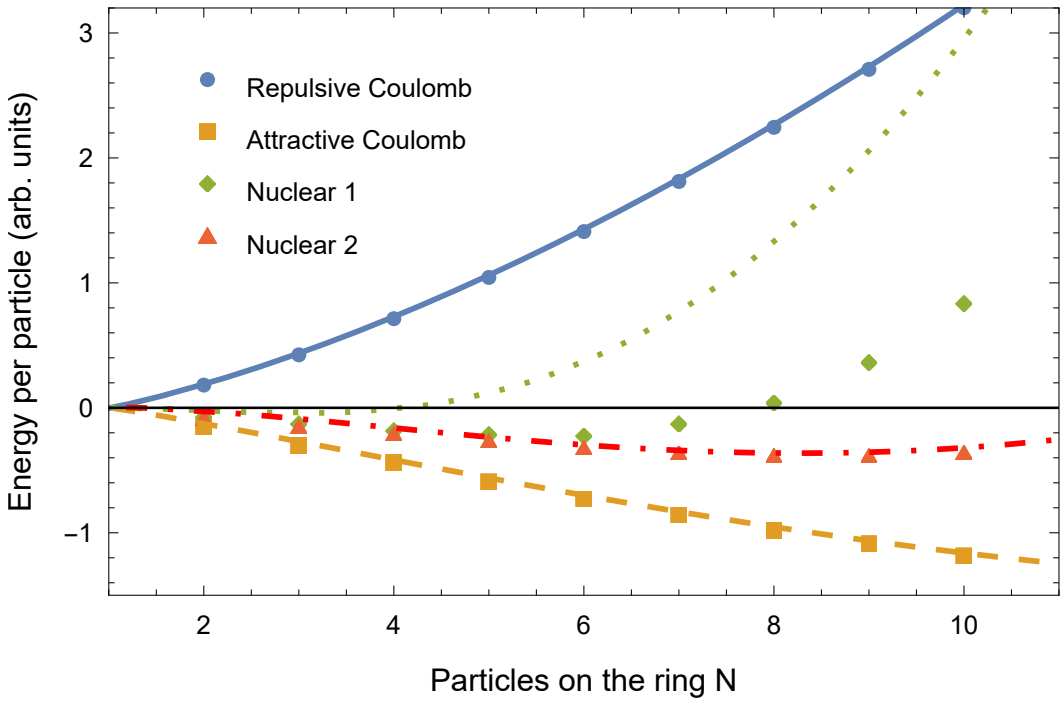

Figure 2.3: Energy per particle for a quantum ring with radius $R = 2$, potential strength $V_0 = 1$, and varying number of particles N. Points indicate the exact energy for each interaction while the corresponding lines indicate the unbroken-symmetry Hartree-Fock energy. Figure adapted from [25].

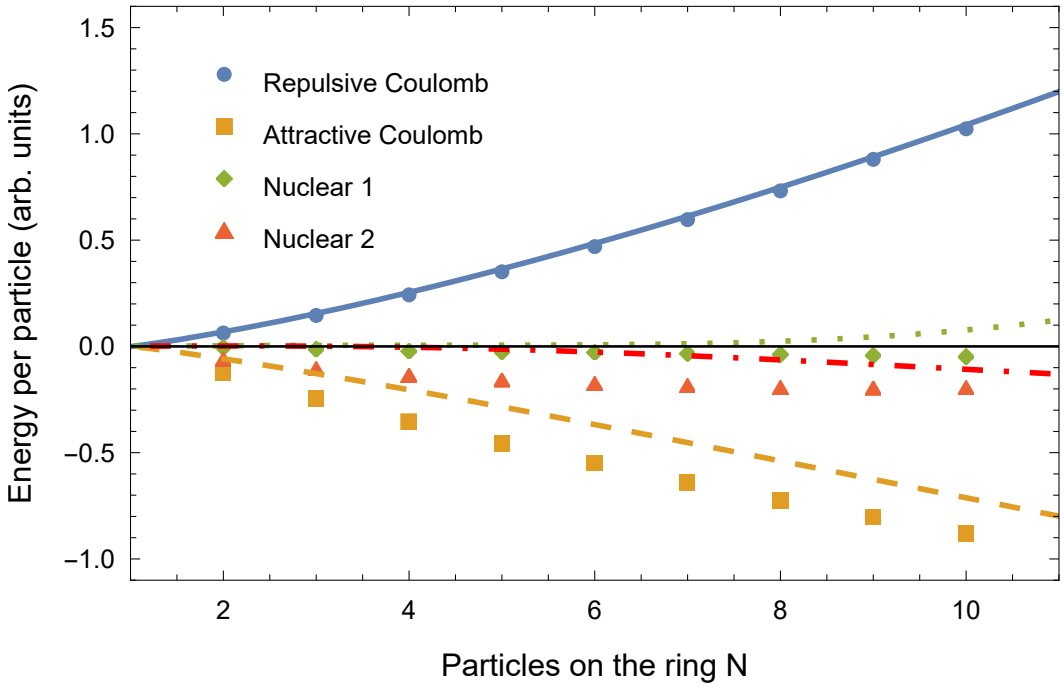

Figure 2.4: Energy per particle for a quantum ring with radius $R = 5$, potential strength $V_0 = 1$, and varying number of particles N. Points indicate the exact energy for each interaction while the corresponding lines indicate the unbroken-symmetry Hartree-Fock energy. Figure adapted from [25].

ground state of a quantum ring. They varied a range of systems parameters including the number of particles on the ring, the radius of the ring and the interaction potential between the particles to understand under what conditions the Hartree-Fock method produced a good approximation to the true ground state. The quantum Monte Carlo methods they used consisted of variational Monte Carlo [28] to produce an optimised trial wave function which was then fed into diffusion Monte Carlo [28] for further optimisation. Both methods were implemented in the CASINO program (Monte **CA**rlo **SI**mulation of electro**N** trajectory in s**O**lids) [29] while the Hartree-Fock energies were calculated analytically. Due to the larger variational space which included correlations between the particles, the quantum Monte Carlo methods always produced an equal to or lower approximate ground state energy per particle than the unbroken symmetry Hartree-Fock method, which generally indicates a better approximation to the ground state[2]. As such, the results of the quantum Monte Carlo methods were considered to be equal to the exact ground state for the purposes of benchmarking the Hartree-Fock method. For the rest of this section, I will refer to the quantum Monte Carlo results as the exact ground state energy per particle of the system.

The interactions investigated in this paper are the same as outlined in the previous section, with $V_0 = 1$. For reference they were: a repulsive Coulomb interaction $V_{C+}(r_{\alpha\beta}) = \frac{1}{r_{\alpha\beta}}$, an attractive 'Coulomb' interaction $V_{C-}(r_{\alpha\beta}) = -\frac{1}{r_{\alpha\beta}}$, and two model nuclear interactions, $V_{N1}(r_{\alpha\beta}) = \frac{1}{r_{\alpha\beta}}(100e^{-2r_{\alpha\beta}} - 64e^{-1.5r_{\alpha\beta}})$ and $V_{N2}(r_{\alpha\beta}) = \frac{1}{r_{\alpha\beta}}(12e^{-2r_{\alpha\beta}} - 8e^{-r_{\alpha\beta}})$, the first one having a larger 'hard-core' repulsion than the second. The paper also investigates a repulsive Yukawa interaction potential, $\frac{1}{r_{\alpha\beta}}e^{-ar_{\alpha\beta}}$, with variable range a, however, since I do not cover this interaction in this thesis, I will omit those results here.

First, I will outline the main results for 5 particles on a ring of varying radius which is shown in figure (2.2). The repulsive Coulomb interaction energy per particle decreased monotonically with increasing ring size and at all radii the unbroken symmetry Hartree-Fock method gave a great approximation for the ground state energy. All the interactions with attractive components (V_{C-}, V_{N1} and V_{N2}) had the Hartree-Fock ground state energy per particle go to 0 for large R, while the exact solution went to a constant negative value. This is because the rotational symmetry makes it such that the particles get further and further apart on average in the Hartree-Fock method as the ring radius is increased and thus stop interacting. In the exact solution on a sufficiently large ring, the particles are able to correlate their positions to 'bunch together' and so form a self-bound system on the ring which has a constant negative energy. In this self-bound system, the particle sit at some equilibrium distance from each other that depends on the interaction potential. For these large ring radii ($R > 5$), changing the size of the ring barely affects this self bound system and so the energy goes to a constant value. All four interactions had their ground state energy per particle go to infinity as $R \to 0$. For the attractive Coulomb interaction this was due to Pauli exclusion forcing the particles to have a higher kinetic energy as they became closer together, while for the two nuclear interactions and the

[2]This is due to the variational principle of quantum mechanics which will be discussed at the start of the next chapter.

repulsive Coulomb, this was a combination of Pauli exclusion-increased kinetic energy and the diverging potential energy. In this limit, the Hartree-Fock method performed well for the attractive and repulsive Coulomb and Nuclear 2 interactions but was significantly different for the Nuclear 1 interaction. This was again due to spatial correlation between the particles. For the Nuclear 1 interaction exact ground state, the particles could localise their positions to be as far away from each other as possible to minimise their potential energy. Localisation in position increases the kinetic energy of the wave function, so it is only present in the exact ground state if the decrease in potential energy is larger than the kinetic energy increase. This is the case for the stronger 'hard-core' repulsion of the Nuclear 1 interaction but not for the weaker Nuclear 2 or repulsive and attractive Coulomb interactions. Thus, since the unbroken symmetry Hartree-Fock cannot localise the position of its particles, it performs poorly for the Nuclear 1 interactions but well for the rest of the interactions.

Next, I will outline the results on a ring of radius $R = 2$ with varying numbers of particles on the ring, from $N = 2$ to $N = 10$ which is shown in figure (2.3). The energy of the system with the repulsive Coulomb interaction increases almost linearly with the number of particles on the ring while for the attractive Coulomb case it decreases almost linearly. This can be understood by considering the infinite range of the Coulomb interaction. N particles on the ring have $\frac{N}{2}(N-1)$ interactions, all with approximately equal strength due to the small size of the ring. As a result, the total potential energy approximately scales with N^2, so the energy per particle scales with N, hence the linear dependence. The deviation from this linear dependence comes again from the Pauli exclusion principle which increases the kinetic energy per particles as the particles get packed closer together. On this smaller ring, the Hartree-Fock method gives a good approximation for both Coulomb cases as not much localisation is present in the exact ground state. For the nuclear interactions in the exact case, the energy per particle initially decreases as more particles are added, as the particles sit at distances from each other where their respective potentials are attractive. As more particles are added and the ring fills up, the particles are forced to be at distances where the potential is repulsive and the energy per particle increases again. Again, the Hartree-Fock method is able to give a good approximation for all N for the Nuclear 2 interaction which does not induce much spatial correlation, but fails for the Nuclear 1 interaction. As N increases, the particles in the exact ground state become more strongly localised to minimise the increasingly repulsive potential and so the Hartree-Fock method gives a worse approximation with increasing N for the Nuclear 1 case.

Finally, I will outline the results for a ring of radius $R = 5$ with varying numbers of particles which is shown in figure (2.4). This was largely similar to the $R = 2$ case with a few changes. For the cases with attractive components to the potential (V_{C-}, V_{N1} and V_{N2}), the Hartree-Fock method gives a significantly worse ground state energy for the same reason as outlined in the R-varying results. Similar to the $R = 2$ case, the attractive Coulomb has a linear decrease with increasing number of particles, however now the two nuclear interactions go to a constant negative energy per particle with increasing N. The difference in this behaviour can be understood by considering the range of the

interaction. As mentioned in the previous $R = 2$ case, the infinite range of the attractive Coulomb potential means that the total potential energy scales with N^2 so the energy per particle scales with N. For the finite range[3] nuclear interactions on a larger ring, however, each particle only interacts significantly with its nearest neighbours, so the number of interactions and thus the total potential energy scales linearly with N, resulting in the observed constant dependence for the energy per particle.

To summarise these results, the Hartree-Fock with unbroken symmetry gave good approximations for the repulsive Coulomb interaction for all cases. It also gave good approximations for the attractive Coulomb and Nuclear 2 interactions in small systems but was not able to reproduce the 'self-bound' feature for these interactions in large systems due to its lack of correlations. It also was not able to approximate the localisation of particles in small systems with the Nuclear 1 interaction, giving a poor estimate of the ground state energy per particle in this case as well. The inability of the Hartree-Fock method with unbroken symmetry to adequately describe these systems motivates the investigation of symmetry breaking and symmetry restoration of the Hartree-Fock states to try and account for the missing correlations in this method. These methods will be explored in this thesis and a description of them along with details on how they were implemented can be found in the next chapter. Before this, I will first discuss higher dimensional ringiums and their importance for properly benchmarking approximate methods.

2.5 Extension to higher dimensions

While useful as a starting point, a major limitation of the quantum ring is its one-dimensional nature. There are only a few quantum systems which can be approximated by the one-dimensional quantum ring and all of them are quasi one-dimensional, that is, the rings have some small finite width. The properties of the ground state may change significantly with the dimension of the system, so this motivates the investigation of higher dimensions[4]. Fortunately, the simplicity of a quantum ring system can be extended to higher dimensions. Instead of particles being constrained to be on the edge of a circle, higher dimensional spheriums are quantum systems in which particles are constrained to be on the $\mathcal{D}$-dimensional surface of a $(\mathcal{D}+1)$-dimensional hypersphere. The $\mathcal{D} = 1$ case is the familiar quantum ring (also referred to as a ringium in the literature), the $\mathcal{D} = 2$ case is called a spherium (particles constrained to be on the surface of a sphere), and the $\mathcal{D} = 3$ case, a glomium (particles constrained to be on the surface of a 4-D hypersphere).

Loos and Gill have investigated the ground state of two-electron spheriums for $\mathcal{D}$ equal to 1 through to 8 [30]. They were able to analytically find exact ground state wave functions and energies for these systems. One important property of the ground state that they

[3]Here I consider the $\frac{1}{r_{\alpha\beta}}$ dependence of the Coloumb potential to be infinite range and the $\frac{e^{-ar_{\alpha\beta}}}{r_{\alpha\beta}}$ dependence of the nuclear interactions to be finitely ranged. In reality, both potentials have some non-zero value at any large R, however the exponential factor of the nuclear case means the potential goes to 0 far more rapidly than for the Coulomb case.

[4]Note that this will not be done in this thesis. This section is included to further motivate the use of the one dimensional quantum ring as a starting point for further investigations.

calculated was the correlation energy. This energy is defined as the difference between the unbroken symmetry Hartree-Fock ground state energy (which does not include correlations) and the exact ground state energy. It can be thought of as a measure of the importance of correlations in the ground state with a larger correlation energy implying more significant correlations. They found that for two electrons (with the repulsive Coulomb interaction), the correlation energy was moderate for $\mathcal{D} = 1$, at its largest for $\mathcal{D} = 2$, moderate again for $\mathcal{D} = 3$, then monotonically decreasing for larger $\mathcal{D}$. Their results suggest that the effectiveness of approximate methods are likely to have a significant dependence on the dimensionality of the system. As an extension to the work done in this thesis, one could check if this same dependence on dimensionality holds for systems with more particles and other interaction potentials. Loos and Gill also compare the ground state energy of two electrons on a $\mathcal{D}$-spherium to other more realistic models of three-dimensional two-electron systems, the Hooke's law atom and the helium-like ion. In the limit that the radius of these systems goes to 0, the Hooke's Law atom ground state energy approaches -0.0497 a.u. [31] while the energy of the helium-like ion approaches -0.0467 a.u.[32]. Of all $\mathcal{D}$-spheriums, they found that $\mathcal{D} = 3$ had the most similar ground state energy of -0.0476 a.u., leading them to conclude that this system was the most similar to real three-dimensional systems. Again, as an extension to this thesis, one could check if this is the case for other interaction potentials and with more particles.

I have now established some background for the quantum ring system that I will be investigating in this thesis. In the next chapter, I will outline the methods use to investigate the ground state of the quantum ring along with the details of their numerical implementation.

Chapter 3

Many-Body Methods and their Numerical Implementations

3.1 Variational principle background

Two of the methods used in this thesis make use of the variational principle so I will discuss it here before elaborating on these methods.

Any valid many-body state, $|\Psi\rangle$, that exists in the N-particle Hilbert space can be represented as a superposition of energy eigenstates of the system, $\{|E_0\rangle, |E_1\rangle, |E_2\rangle ...\}$, where $|E_0\rangle$ is the ground state of the system,

$$|\Psi\rangle = \left(\sum_i |E_i\rangle\langle E_i| \right) |\Psi\rangle = \sum_i \langle E_i|\Psi\rangle \, |E_i\rangle, \tag{3.1}$$

which has an energy expectation value

$$\langle\Psi|\hat{H}|\Psi\rangle = \sum_i |\langle E_i|\Psi\rangle|^2 \, E_i. \tag{3.2}$$

Given that, by its definition, $E_0 \leq E_i$, it follows that

$$\langle\Psi|\hat{H}|\Psi\rangle = \sum_i |\langle E_i|\Psi\rangle|^2 \, E_i \geq \sum_i |\langle E_i|\Psi\rangle|^2 \, E_0 = E_0 \sum_i |\langle E_i|\Psi\rangle|^2 = E_0, \tag{3.3}$$

that is, the energy expectation value is always bounded from below by the ground state energy. The variational method is based on the fact that, given a trial many-body state which depends on some parameters, we can get better and better approximations to the true ground state of the system by minimising the energy of the trial state. Additionally, whatever energy we find for the trial state, this will always be an upper bound for the true ground state energy of the system.

The minimisation of the total energy of the system can be viewed as the simultaneous minimisation of the system's potential and kinetic energies which often have opposite effects on the system's spatial distribution of particles. In the position basis, the kinetic energy involves the second derivative of the wave function so, qualitatively, wave func-

tions with sharper peaks have higher kinetic energies than flatter wave functions. Thus, minimising the kinetic energy amounts to de-localising the particles such that their probability of being found at some position is closer to being the same everywhere on the ring. On the other hand, in many cases (including systems with Coulomb and Yukawa potentials), minimising the potential energy of the system has the opposite effect; it tends to localise the position of the particles so that they are more likely to be found in regions of low potential energy. The ground state is found when the perfect mixture of localised and de-localised particles has been reached. In this state, the potential energy could be reduced further by localising the particles more, but this would result in a larger increase in kinetic energy and the same can be said of attempting to minimise the kinetic energy further.

3.2 Hartree-Fock method with unbroken and broken symmetries

3.2.1 Theoretical background

We previously discussed the use of the variational principle to find the ground state. In most systems, the variational space is far too large to search fully, so approximate methods seek to restrict the space to get closer to the true ground state in a given amount of time. The Hartree-Fock approximation [2], significantly restricts the variational space by only considering uncorrelated single-particle states. For a system of identical fermions, this can be represented as a Slater determinant of single-particle states

$$|\Psi\rangle = \frac{1}{N!}\begin{vmatrix} |1:\psi_1\rangle & |2:\psi_1\rangle & \cdots & |N:\psi_1\rangle \\ |1:\psi_2\rangle & |2:\psi_2\rangle & \cdots & |N:\psi_2\rangle \\ \vdots & \vdots & \ddots & \vdots \\ |1:\psi_N\rangle & |2:\psi_N\rangle & \cdots & |N:\psi_N\rangle \end{vmatrix}, \tag{3.4}$$

where $|\alpha:\psi_\beta\rangle$ denotes particle α in the single-particle state $|\psi_\beta\rangle$. Taking a Slater determinant of these states ensures that the many-body wave function changes sign when two particles are exchanged, which is required for a system of identical fermions. Under the Hartree-Fock approximation, we now seek to find the N single-particle states which correspond to the lowest energy Slater determinant, which we call the Hartree-Fock ground state. Using the variational principle, it is possible to show that these single-particle states are solutions to the eigenvalue equation

$$\hat{h}|\psi_\alpha\rangle = \epsilon_\alpha|\psi_\alpha\rangle, \tag{3.5}$$

with the N lowest values of ϵ_α, where $\hat{h}$ is a one-body operator known as the Hartree-Fock single-particle Hamiltonian and is itself a function of the single-particle states. This operator effectively averages all the two-body interactions in the system, transforming the N-body problem to N, non-linear one-body problems. Solving equation (3.5) requires the elements of the Hartree-Fock Hamiltonian in a given basis, which I will label as

$\{|\phi_1\rangle, |\phi_2\rangle, ..., |\phi_k\rangle\}$, using Latin characters to label basis states. These elements can be easily found by taking the functional derivative of the energy expectation value with respect to the density matrix

$$h_{ij} = \langle\phi_i|\hat{h}|\phi_j\rangle = \frac{\delta\langle\Psi|\hat{H}|\Psi\rangle}{\delta\rho_{ji}}, \tag{3.6}$$

where the density matrix is

$$\rho_{ji} = \langle\phi_j|\hat{\rho}|\phi_i\rangle = \sum_{\alpha=1}^{N}\langle\phi_j|\psi_\alpha\rangle\langle\psi_\alpha|\phi_i\rangle, \tag{3.7}$$

and contains all of the same information as the single-particles states for a system of independent particles. Since the Hartree-Fock Hamiltonian depends on the many-body state $|\Psi\rangle$ (or equivalently on the one-body density matrix ρ), equation (3.5) is non-linear and so cannot be solved by simply diagonalising $\hat{h}$.

There are several numerical methods for solving equation (3.5). The original method put forth by Hartree [1] is a fixed-point iteration algorithm. In its simplest form, it involves making a reasonable guess for the Hartree-Fock Hamiltonian, diagonalising the matrix for that Hamiltonian to find its N lowest energy single-particle eigenstates, then calculating a new guess for the Hamiltonian from those N lowest states. This process is then repeated until the single-particle states used to calculate the Hartree-Fock Hamiltonian are also its N lowest energy eigenstates. The method is not guaranteed to converge for all choices of initial Hamiltonian and unfortunately, depending on the size of the basis used, it can involve the diagonalisation of large matrices which requires a large amount of computational effort.

An alternative method which does not require the diagonalisation of large matrices is the imaginary time-step method [33]. We start with the N time-dependent Hartree-Fock equations which govern the time evolution of the single-particle states under the Hartree-Fock approximation (and are analogous to the time-dependent Schrödinger equation with the system's actual Hamiltonian, $\hat{H}$),

$$i\frac{d}{dt}|\psi_\alpha(t)\rangle = \hat{h}(t)|\psi_\alpha(t)\rangle. \tag{3.8}$$

In the limit of a short time-step dt, we can evolve each state as

$$|\psi_\alpha(t+dt)\rangle = e^{-idt\,\hat{h}(t+\frac{dt}{2})}|\psi_\alpha(t)\rangle. \tag{3.9}$$

where the operator $e^{-idt\,\hat{h}(t+\frac{dt}{2})}$ is both unitary, which ensures that the single-particle states remain orthonormal, and also conserves the energy of the many-body system. If dt is replaced with $-id\tau$ (an imaginary time step), the operator $e^{-d\tau\,\hat{h}(\tau)}$ now decreases the single-particle energy of each state. This can be seen by expanding each $|\psi_i(\tau)\rangle$ in

the basis of the eigenstates of $\hat{h}(\tau)$, which I write as $\{|\varepsilon_0\rangle, |\varepsilon_1\rangle, |\varepsilon_2\rangle, ...\}$,

$$e^{-d\tau\,\hat{h}(t)}|\psi_\alpha(\tau)\rangle = e^{-d\tau\,\hat{h}(\tau)}\sum_i c_{\alpha i}|\varepsilon_i\rangle = \sum_i c_{\alpha i}\,e^{-d\tau\,\varepsilon_i}\,|\varepsilon_i\rangle. \tag{3.10}$$

The elements of the superposition with greater single-particle energies, ε_i, decay faster in imaginary time than the states with lower single-particle energies, resulting in a lower energy for the whole state. The operation is no longer unitary, however, so to recover N orthonormal single-particle states after applying the operator, we need to apply a procedure such as the Gram-Schmidt process.

All that remains is to find the evolution operator $e^{-d\tau\,\hat{h}(\tau)}$ in the given basis. We first need the energy expectation value of the Slater determinant. For a system Hamiltonian comprised of one-body kinetic energy operators, $\hat{T}_\alpha$, one-body external potential operators, $\hat{V}_\alpha^{\text{ext}}$ [1], and two-body interaction potential operators, $\hat{V}^{\text{int}}(\alpha,\beta)$, the energy expectation value of a Slater determinant is given by the Slater-Condon rules [34],

$$\langle\Psi|\hat{H}|\Psi\rangle = \sum_{\alpha=1}^{N}\langle\psi_\alpha|\hat{T}_\alpha|\psi_\alpha\rangle + \sum_{\alpha=1}^{N}\langle\psi_\alpha|\hat{V}_\alpha^{\text{ext}}|\psi_\alpha\rangle \tag{3.11}$$

$$+\frac{1}{2}\sum_{\alpha=1}^{N}\sum_{\beta=1}^{N}\langle 1:\psi_\alpha, 2:\psi_\beta|\hat{V}^{\text{int}}(1,2)\Big(|1:\psi_\alpha, 2:\psi_\beta\rangle - |1:\psi_\beta, 2:\psi_\alpha\rangle\Big). \tag{3.12}$$

In a given basis, this becomes

$$\langle\Psi|\hat{H}|\Psi\rangle = \sum_{i,j=1}^{K}\rho_{ji}T_{ij} + \sum_{i,j=1}^{K}\rho_{ji}V_{ij}^{\text{ext.}} + \frac{1}{2}\sum_{i,j,k,l=1}^{K}(\rho_{ki}\rho_{lj} - \rho_{kj}\rho_{li})V_{ijkl}^{\text{int}}, \tag{3.13}$$

where I use the usual notation for the matrix representation of an operator, $O_{ij} = \langle\phi_i|\hat{O}|\phi_j\rangle$ and $O_{ijkl} = \langle 1:\phi_i, 2:\phi_j|\hat{O}(1,2)|1:\phi_k, 2:\phi_l\rangle$. Then the Hartree-Fock Hamiltonian in this basis is

$$h[\rho]_{mn} = \frac{\delta\langle\Psi|\hat{H}|\Psi\rangle}{\delta\rho_{nm}} = T_{mn} + V_{mn}^{\text{ext}} + \sum_{i,j=1}^{K}\rho_{ji}(V_{imjn}^{\text{int}} - V_{imnj}^{\text{int}}), \tag{3.14}$$

and the evolution operator can be approximated by expanding the matrix exponential to first order in $d\tau$ (in the limit of small $d\tau$) as

$$(e^{-d\tau\,\hat{h}})_{mn} \approx \delta_{mn} - d\tau\,h[\rho]_{mn} \tag{3.15}$$

$$= \delta_{mn} - d\tau\,\frac{\delta\langle\Psi|\hat{H}|\Psi\rangle}{\delta\rho_{nm}} \tag{3.16}$$

$$= \delta_{mn} - d\tau\left(T_{mn} + V_{mn}^{\text{ext}} + \sum_{i,j=1}^{K}\rho_{ji}(V_{imjn}^{\text{int}} - V_{imnj}^{\text{int}})\right), \tag{3.17}$$

[1] Although the true Hamiltonian for my ring system does not include any external potentials, I have included it here for use later in breaking the rotational symmetry of the Slater determinant.

Symmetries in the Hartee-Fock approximation

The system Hamiltonian has certain symmetries, that is, there are certain operations which commute with the Hamiltonian and leave the energy of the ground state unchanged. The phase of the many-body wave function is one such symmetry. We can multiply the many-body state by a complex phase $e^{i\lambda}$ without changing its energy, since the constant $e^{i\lambda}$ commutes with the Hamiltonian.

The symmetry my project focuses on is the rotational symmetry of the ring system. Since the interaction potential only depends on the distance between the particles and not their exact position on the ring, rotating the system by some angle θ', does not change the energy of the system and so we would expect the ground state to also be rotationally symmetric. However, constricting the Hartree-Fock many-body state to be rotationally symmetric can result in a higher energy than if the symmetry is allowed to be broken. This can be understood through the variational principle. By allowing broken symmetry solutions in the Hartree-Fock method, we enlarge the variational space in which we are looking and so find an equal to or lower energy Hartree-Fock ground state energy.

In the ring system, the rotationally symmetric Hartree-Fock ground state is simply comprised of the N lowest single-particle kinetic energy eigenstates of the ring [25]. For an odd number of particles, the angular position wave functions of these eigenstates are[2]

$$\frac{1}{\sqrt{2\pi}}, \frac{\sin(\theta)}{\sqrt{\pi}}, \frac{\cos(\theta)}{\sqrt{\pi}}, \frac{\sin(2\theta)}{\sqrt{\pi}}, \frac{\cos(2\theta)}{\sqrt{\pi}}, ..., \frac{\sin((N-1)\theta/2)}{\sqrt{\pi}}, \frac{\cos((N-1)\theta/2)}{\sqrt{\pi}}, \quad (3.18)$$

while for an even number of particles they are

$$\frac{\sin(\theta/2)}{\sqrt{\pi}}, \frac{\cos(\theta/2)}{\sqrt{\pi}}, \frac{\sin(3\theta/2)}{\sqrt{\pi}}, \frac{\cos(3\theta/2)}{\sqrt{\pi}}, ..., \frac{\sin((N-1)\theta/2)}{\sqrt{\pi}}, \frac{\cos((N-1)\theta/2)}{\sqrt{\pi}}. \quad (3.19)$$

The reason that the ground state is made up of kinetic energy eigenstates is due to the system's inability to localise its particles thanks to the rotational symmetry (particles being more likely to be found at one point on the ring than another would break the rotational symmetry of the system). As discussed at the end of the previous section, localisation of particle position is what allows optimisation of the potential energy of the system. Without this freedom, only the kinetic energy can be minimised and so the lowest possible energy state is comprised of the lowest kinetic energy eigenstates. The true ground state of the system gets around this constraint through the correlation between its particles' positions. Instead of optimising the potential energy by localising the absolute position of particles, the particles localise to some degree in their relative positions which lowers the potential energy without breaking the rotational symmetry.

[2]This set of real orthonormal wave functions were adapted from the set of complex wave functions given in [25] by taking complex, linear combinations wave functions which were degenerate in energy. Working with real wave functions allowed for a simpler numerical implementation of the method.

3.2.2 Numerical implementation

The previous section discussed the background theory for the Hartree-Fock method with preserved and broken symmetries. In this section, I will discuss the details behind my implementation of the method by outlining and attempting to justify the choices that were made.

First, I needed to decide the single-particle basis to work in. There were a number of viable options that could have been chosen; the only strict requirements were that the basis states should be orthonormal and span enough of the Hilbert space to accurately capture the physics of the system. I chose the kinetic energy eigenstates as my basis to make the evaluation of the kinetic energy of the system easy to implement. Additionally, representing the rotationally symmetric ground state, which I used as the initial state for the imaginary time-step method, was also easy in this basis as it was comprised of the N lowest kinetic energy eigenstates. The accuracy of this basis could be controlled with a single parameter K, being the number of kinetic energy eigenstates used and in the limit of $K \to \infty$, the basis would span the whole Hilbert space of the quantum ring. It may be useful to consider how K influences the resolution of the angular wave function, that is, if instead I used the position basis for the ring, what position step size dx would be induced by the finiteness of K? The highest kinetic energy eigenstate would have a wave function $\frac{1}{\sqrt{\pi}}\sin\left(\frac{K\theta}{2}\right)$ or $\frac{1}{\sqrt{\pi}}\cos\left(\frac{(K-1)\theta}{2}\right)$ so the minimum wavelength that could be represented would be around $\frac{4\pi R}{K}$. If we assume that this minimum wavelength is approximately the angular resolution of the method, then we can approximate the position resolution as $dx \approx \frac{4\pi R}{K}$. This dependence on the ring radius R is important to keep in mind for larger rings which need a larger K to achieve the same accuracy for a fixed size system.

Figure (3.1) shows the dependence of the broken-symmetry energy on the choice of K for the Nuclear 1 interaction with strength $V_0 = 1$ on a ring of radius $R = 2$ with $N = 4$ particles. In this case, increasing K beyond 20 does not bring significant improvement to the Hartree-Fock ground state energy. As a result, $K = 20$ was used for all results with $R \leq 2$. Problems were found for larger rings, the $R = 5$ and $R = 10$ results. In some cases, the results were not able converge with increasing K, for $K \leq 35$. An example of this can be seen in figure (3.2), which shows the broken-symmetry energy for an $N = 4$ particle ring of radius $R = 10$ and the Nuclear 1 potential with strength $V_0 = 2.5$. Unfortunately, I was not able to increase K beyond 35 due to computational constraints, so I omitted the results that did not converge in the next chapter. The majority of the computational effort was spent on calculating the potential energy matrix of equation (3.14),

$$V_{ijkl}^{\text{int diff}} = V_{ijkl}^{\text{int}} - V_{ijlk}^{\text{int}} \tag{3.20}$$

$$= \langle 1:\phi_i, 2:\phi_j|\hat{V}^{\text{int}}(1,2)\Big(|1:\phi_k, 2:\phi_l\rangle - |1:\phi_l, 2:\phi_k\rangle\Big) \tag{3.21}$$

$$= \int_0^{2\pi} d\theta_1 \int_0^{2\pi} d\theta_2\, \phi_i(\theta_1)\phi_j(\theta_2)V^{\text{int}}(\theta_1,\theta_2)\Big(\phi_k(\theta_1)\phi_l(\theta_2) - \phi_l(\theta_1)\phi_k(\theta_2)\Big). \tag{3.22}$$

Each index of $V_{ijkl}^{\text{int diff}}$ contributed a factor of K to the time required to calculate this

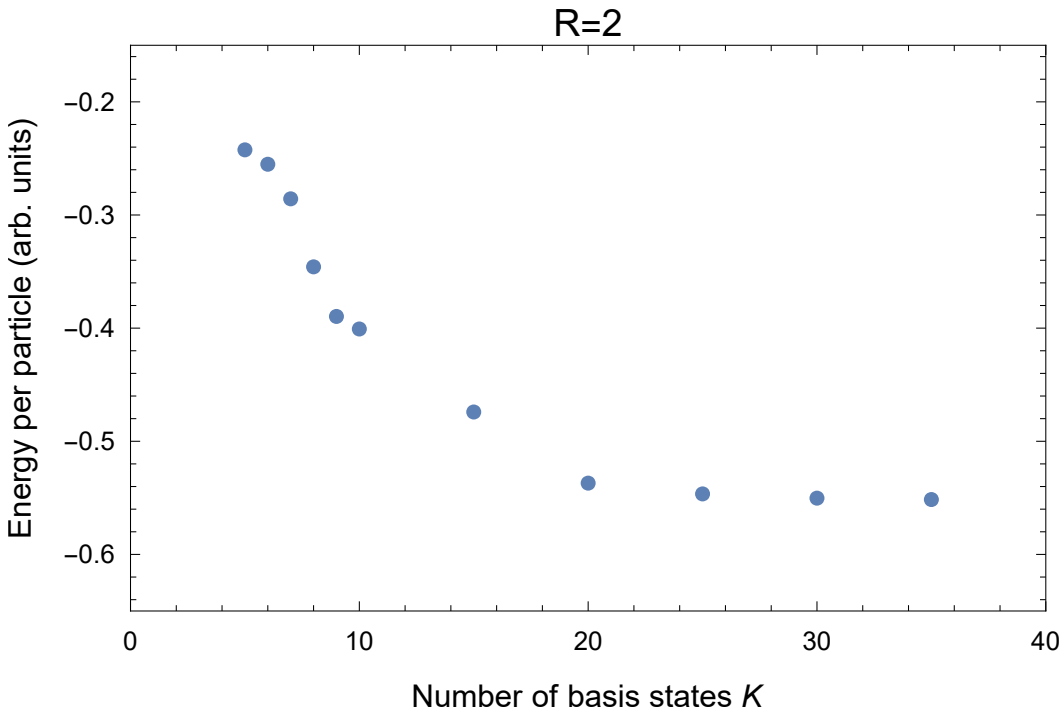

Figure 3.1: Dependence of energy per particle on the number of single-particle basis states used in the Hartree-Fock symmetry breaking method for $N = 4$ particles on a ring of radius $R = 2$, interacting with the Nuclear 1 interaction of strength $V_0 = 2.5$.

matrix. Additionally, I computed the integrals numerically on a 2D grid, where the number of grid points were chosen to capture the details of the fastest oscillating basis wave function ϕ and so the time taken for each integral could be proportional to as high a factor as K^2. Thus the total time required for this method was approximately proportional to K^6 which severely restricted the choice of K [3].

The next decision I made was on the size of the imaginary time-step, $d\tau$. The choice was an important one because smaller values of $d\tau$ were more likely to decrease the energy of the Slater determinant, but would also result in a slower convergence, so a balance had to be found between the speed and stability of the method. The important factor for this consideration was the degree to which the evolution operator $e^{-d\tau\,\hat{h}(t)}$ changed the single-particle states, which depends on the size of $d\tau$ and $\hat{h}$. Thus, to decide an appropriate value for $d\tau$, I assumed $\hat{h}$ was on the order of the unbroken Hartree-Fock ground state energy of the system, E_0^{unbroken}, and set $d\tau = \frac{10^{-2}}{E_0^{\text{unbroken}}}$. By doing it this way (as opposed to setting some arbitrarily low $d\tau$ for all my results), I made it such that the method would still converge at a reasonable speed whatever the energy scale of the system while remaining stable. Figure (3.3) shows that this method could converge across a range of energy scales without dramatically increasing the number of time steps required.

[3] I was able to cut the total time down by a factor of eight using several symmetry arguments for the matrix $V_{ijkl}^{\text{int diff}}$, however this did not change the overall scaling dependence on K

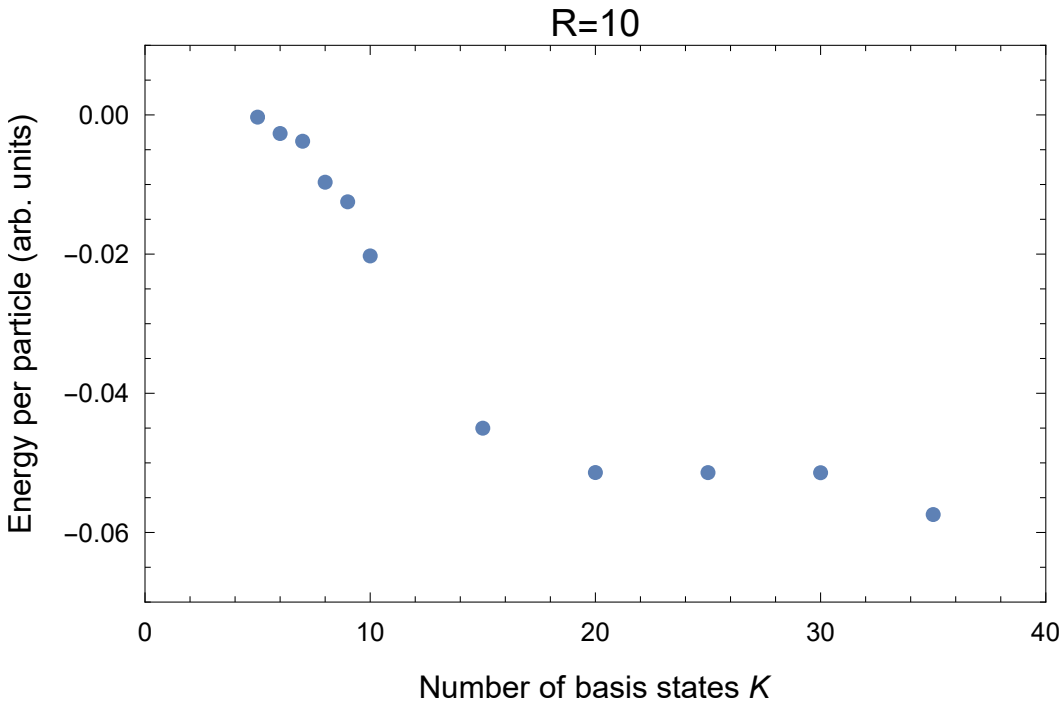

Figure 3.2: The same as figure (3.1) for a ring of radius $R = 10$.

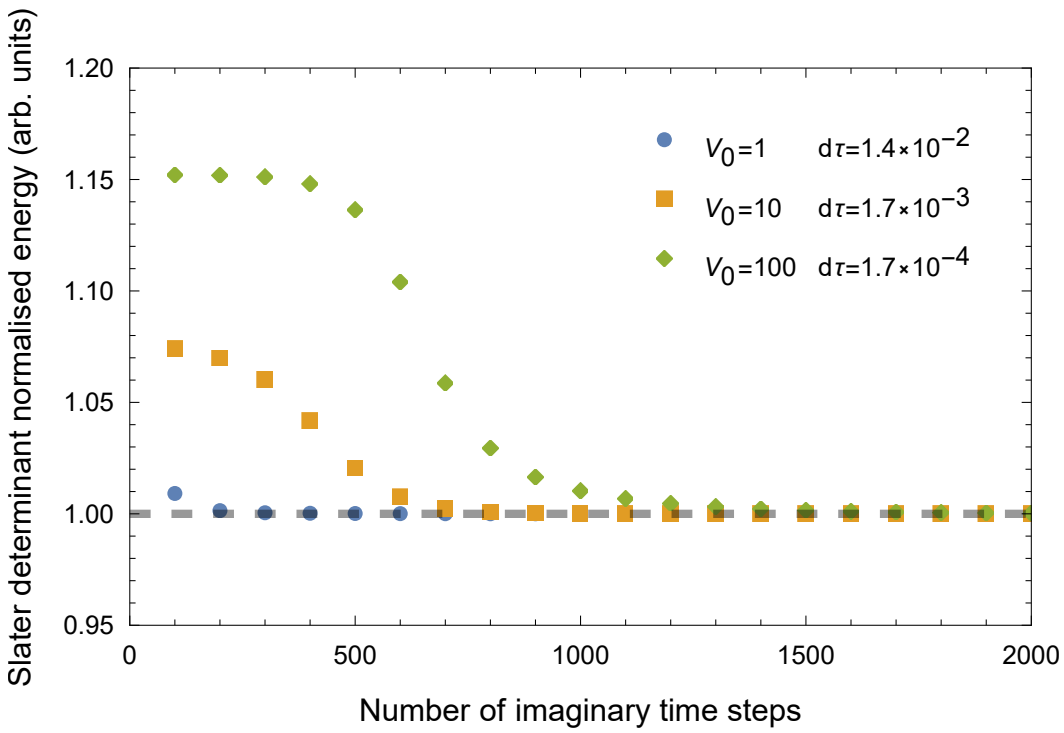

Figure 3.3: Energy per particle for the Hartree-Fock state over imaginary time for $N = 4$ particles on a ring of radius $R = 2$ with the Coulomb interaction of varying strengths V_0. The energy was normalised by the final energies of the states which were 0.7, 5.5 and 49.9 arbitrary units for $V_0 = 1$, $V_0 = 10$ and $V_0 = 100$, respectively.

The next decision concerned how to promote symmetry breaking in the method. For all the results, the state was initialised in the symmetry unbroken ground state, as I knew that this state had a relatively low energy (at least relative to other unbroken symmetry states). If I evolved this state in imaginary time, eventually numerical errors would spontaneously break the rotational symmetry of the state allowing for its evolution to the broken symmetry Hartree-Fock ground state. However, waiting for this numerical symmetry breaking was often a slow process and it was difficult to know whether symmetry breaking would occur at all, that is, whether or not the unbroken symmetry state was also the lowest energy state in the broken symmetry variational space. To speed up the process and to ensure that symmetry broken states were at least being explored, I introduced an external potential to break the symmetry of the Hartree-Fock Hamiltonian. I would evolve the Slater determinant under this external potential (as well as with the two-body interaction potential) for several time-steps, then turn off the potential and evolve for longer without it so that it did not influence the final ground state. For all of my results, I used the somewhat arbitrarily chosen external potential

$$V^{\text{ext}}(\theta) = 10(\theta - \pi)^4 - 10(\theta - \pi)^3 - 100(\theta - \pi)^2. \tag{3.23}$$

I chose this function to be asymmetrical on either side of $\theta = \pi$ just in case maintaining this symmetry would result in a higher energy ground state. From experimentation with a few different potentials, I found that the exact form did not have a large impact on the convergence time of the method or the energy of the converged state. Additionally, the actual evolution in imaginary time step was far quicker than the calculation of $V_{ijkl}^{\text{int diff}}$ so I did not invest much time in optimising this step. For the application of this method to other systems, it may be more important to choose a good $V^{\text{ext}}(\theta)$ that guides the single-particle states quickly into the broken symmetry ground state.

Finally, I will discuss how I could check the validity of my results. Analytical expressions for the unbroken symmetry energy had already been found in [25] for each of the interaction potentials in this thesis. By comparing my results to these, I was reassured that I had initialised the unbroken symmetry state correctly and that I was evaluating the energy of a Slater determinant correctly. Next, to check the validity of the broken symmetry Hartree-Fock ground state, I compared its energy to the unbroken symmetry Hartree-Fock ground state energy as well as the variational Monte Carlo ground state energy (which will be discussed in a later chapter). Given that the unbroken symmetry Hartree-Fock state was found in a smaller variational space and the variational Monte Carlo ground state was found in a larger variational space, the variational principle guarantees that the broken symmetry energy should be less than or equal to the unbroken symmetry energy and greater than or equal to the variational Monte Carlo energy[4]. The next check was to calculate and plot the angular particle density around the ring of the resulting many-body wave function to see if it matched expectations. This density is given by the diagonal elements of the one-body density matrix in the angular position

[4]Unfortunately, if the broken symmetry energy is less than the variational Monte Carlo energy, this check does not tell us which method has failed.

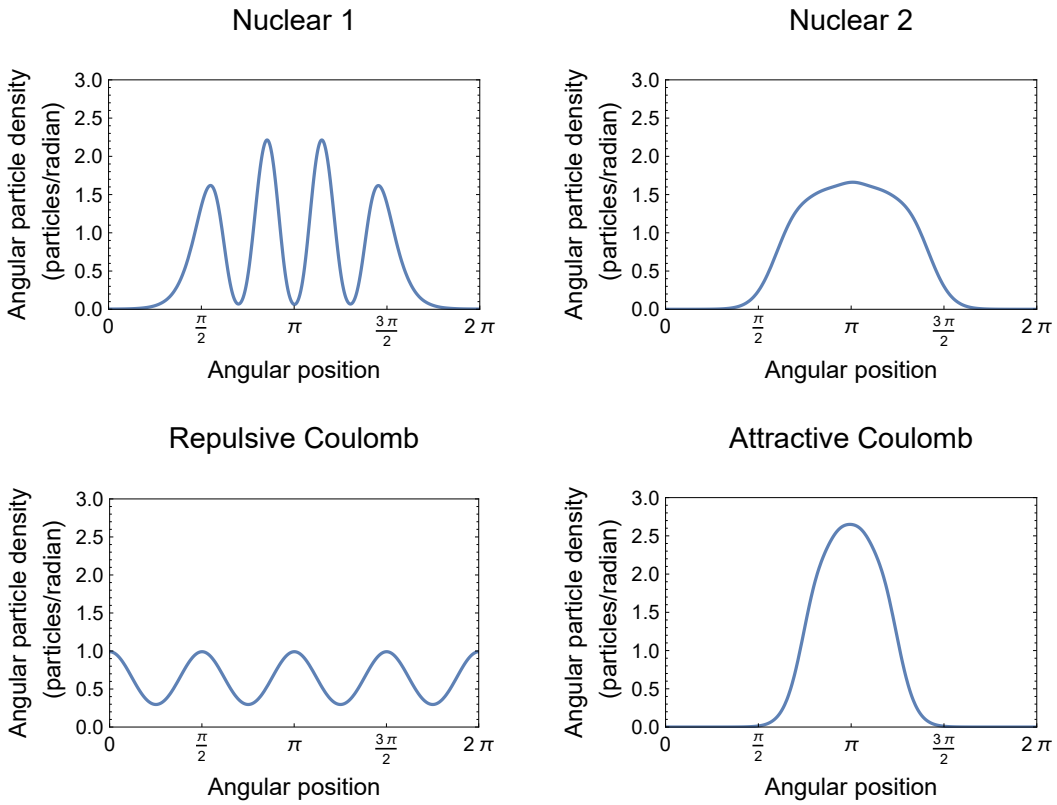

Figure 3.4: Angular particle densities of the broken-symmetry Hartree-Fock ground state for $N = 4$ particles on a ring of radius $R = 2$ with potential strength $V_0 = 2.5$.

basis

$$\rho(\theta) = \langle\theta|\hat{\rho}|\theta\rangle = \sum_{\alpha=1}^{N} |\psi_\alpha(\theta)|^2. \tag{3.24}$$

Firstly, for no symmetry breaking, I would expect a flat density function, that is, equal probability of finding a particle at any point of the ring, since this is the only function which has the required rotational symmetry. If symmetry does occur, i.e. when the energy of the state after the imaginary time evolution is lower than the unbroken symmetry energy, then the shape of the density function should depend on the potential interaction. For Coulomb repulsion, the particles should be as far away from each other as possible in their lowest energy state, so I would expect N equally-spaced peaks in the density function. For attractive interactions, the particles will collapse together into a single peak localised at some point on the ring. For the two nuclear interactions, the form of the density plot should depend on the radius of the ring. In smaller rings where the particles are all forced to be close together, I would expect a similar density function as the Coulomb repulsion case as only the repulsive part of their interaction potentials is being probed. On larger rings, particles would be classically expected to sit at fixed distances away from each other at the minimum of their interaction potential, so I would expect a density plot to show some fixed size system localised at one region of the ring.

I found that the density plots produced from my results, shown in figure (3.4), matched these expectations and this, along with convergence of the energy with respect to the number of basis states, K, and the imaginary time, τ, provided good evidence that the results were valid.

After performing this method, I am left with many-body independent-particle states without rotational symmetry. However, the true ground state of the system exists in the space with rotational symmetry. Later in this chapter, I will outline a symmetry restoration method which will find the projection of these broken-symmetry states into the space of rotationally symmetric states (which are no longer required to be independent-particle states) which is hoped to produce a state even closer to the exact ground state. First though, I will cover the variational Monte Carlo method used to find a better approximation to the exact ground state, since it involves an algorithm that I also use in the symmetry restoration method.

3.3 Variational Monte Carlo

3.3.1 Theoretical background

In the previous method, I restricted the variational space in which I was searching for the ground state, to independent-particle many-body states. In the variational Monte Carlo method, I explore a larger variational space that has been found to give much better approximations to the true ground state [24, 25]. The method revolves around a trial ground state $|\Psi_{\text{vmc}}(\boldsymbol{a})\rangle$, which depends on several parameters, a_1, a_2, ..., a_J. Thanks to the variational principle discussed earlier, we can find an approximation to the true ground state of the system by minimising the expectation energy of the trial state with respect to its parameters [28].

Unlike the previous method with its simpler independent-particle state, evaluating the energy of this trial state cannot be performed analytically in general. This is because the expectation energy of the trial state is given by a high dimensional integral of the trial wave function $\Psi_{\text{vmc}}(\boldsymbol{\theta}, \boldsymbol{a})$,

$$\langle \Psi_{\text{vmc}}(\boldsymbol{a})|\hat{H}|\Psi_{\text{vmc}}(\boldsymbol{a})\rangle = \frac{\int d\boldsymbol{\theta}\, \Psi^*_{\text{vmc}}(\boldsymbol{\theta}, \boldsymbol{a}) H \Psi_{\text{vmc}}(\boldsymbol{\theta}, \boldsymbol{a})}{\int d\boldsymbol{\theta}\, \Psi^*_{\text{vmc}}(\boldsymbol{\theta}, \boldsymbol{a}) \Psi_{\text{vmc}}(\boldsymbol{\theta}, \boldsymbol{a})}, \tag{3.25}$$

where the integration is over the position of each of the particles on the ring, $d\theta_1$, $d\theta_2$, ..., $d\theta_N$. In the variational Monte Carlo method, this integral is evaluated numerically using Monte Carlo integration. To perform this integration, I first write equation (3.25) as:

$$\langle \Psi_{\text{vmc}}(\boldsymbol{a})|\hat{H}|\Psi_{\text{vmc}}(\boldsymbol{a})\rangle = \int d\boldsymbol{\theta} P(\boldsymbol{\theta}, \boldsymbol{a}) E_L(\boldsymbol{\theta}, \boldsymbol{a}) \tag{3.26}$$

where $P(\boldsymbol{\theta}, \boldsymbol{a}) = \frac{|\Psi_{\text{vmc}}(\boldsymbol{\theta}, \boldsymbol{a})|^2}{\int d\boldsymbol{\theta} |\Psi_{\text{vmc}}(\boldsymbol{\theta}, \boldsymbol{a})|^2}$ and $E_L(\boldsymbol{\theta}, \boldsymbol{a}) = \frac{H\Psi_{\text{vmc}}(\boldsymbol{\theta}, \boldsymbol{a})}{\Psi_{\text{vmc}}(\boldsymbol{\theta}, \boldsymbol{a})}$. I then treat $P(\boldsymbol{\theta}, \boldsymbol{a})$ as a proba-

bility distribution[5] and $E_L(\boldsymbol{\theta}, \boldsymbol{a})$ as the local energy of the wave function, which can be thought of as the energy of the state for a particular configuration of particle positions θ_1, θ_2, ..., θ_N. In this form, equation (3.25) is a continuous weighted average of the local energies of configurations with the weights given by the probability of finding the system in those configurations.

The simplest numerical method for approximating this average would involve taking a discrete weighted average of local energies at regular intervals in the integration space (which is equivalent to the trapezoidal rule for numerical integration). That is, for the set of points $\boldsymbol{\theta}_i$ in the integration space:

$$\langle \Psi_{\text{vmc}}(\boldsymbol{a}) | \hat{H} | \Psi_{\text{vmc}}(\boldsymbol{a}) \rangle \approx \frac{V}{n_s} \sum_{i=1}^{n_s} P(\boldsymbol{\theta}_i, \boldsymbol{a}) E_L(\boldsymbol{\theta}_i, \boldsymbol{a}) \tag{3.27}$$

where n_s is the number of samples in the set and $V = (2\pi)^N$ is the volume of the integration space. Using regular intervals has several disadvantages. Firstly, estimating the error of this method is difficult without knowing much about the properties of the function being integrated. And secondly, the number of sample points needed to achieve a given level of accuracy increases rapidly with the dimension of the integral, so the method requires too much computational time for a large number of particles. If the interval size between each sample point is kept fixed, then the number of sample points increases exponentially with the dimension of the integral.

Instead, Monte Carlo integration involves random sampling of the configuration space, where the configurations to average are chosen through some random process. Its advantage is that it gives a statistical uncertainty in the final result, giving an indication of how close the result is to the true expectation energy of the trial wave function with a given set of parameters. Additionally, Monte Carlo integration scales much better with the dimension of the integral; typically it has polynomial rather than exponential scaling with the number of particles [28]. Finally, Monte Carlo integration can easily be run in parallel on multiple computer cores to reduce the time needed to get a result. Each core can work separately on finding the local energy of different samples and only needs to communicate with the other cores to update the average across all the samples.

The Metropolis algorithm

There are several stochastic methods of sampling that could be used in Monte Carlo integration. The simplest would be to sample randomly from a uniform distribution over the integration space. This would converge to the true average energy of the wave function given enough samples, however there are methods of reducing the uncertainty in the result faster (that is, with less samples) which include stratified, importance and sequential sampling.

The issue with uniform random sampling is that many of the samples will be in regions of low probability (i.e. have relatively small $P(\boldsymbol{\theta}_i, \boldsymbol{a})$), meaning they do not contribute

[5] This can be done since the function is strictly positive and normalised, $\int d\boldsymbol{\theta} P(\boldsymbol{\theta}, \boldsymbol{a}) = 1$.

significantly to the overall average. In this project, I used the Metropolis algorithm [35], a method of sequential sampling which uses the previous sample to stochastically produce the next one. Rather than choosing samples randomly and weighting their local energies with $P(\boldsymbol{\theta}_i, \boldsymbol{a})$ in the average, the Metropolis algorithm instead chooses samples with a probability proportional to $P(\boldsymbol{\theta}_i, \boldsymbol{a})$ and then weights them evenly in the average. In this way, a larger proportion of the sampled configurations contribute significantly to the average, resulting in a faster convergence to the true expectation energy. To accomplish this, a new configuration is generated in each step by subjecting the previous configuration to a small jump in the position of one of its particles. Then the probabilities of finding the new and old states are compared. If the new state is more likely, i.e. $P(\boldsymbol{\theta}_{\text{new}}, \boldsymbol{a}) > P(\boldsymbol{\theta}_{\text{old}}, \boldsymbol{a})$, then the jump is accepted. If it is less likely then the jump is accepted with the probability $\frac{P(\boldsymbol{\theta}_{\text{new}}, \boldsymbol{a})}{P(\boldsymbol{\theta}_{\text{old}}, \boldsymbol{a})}$ or rejected with the probability of $1 - \frac{P(\boldsymbol{\theta}_{\text{new}}, \boldsymbol{a})}{P(\boldsymbol{\theta}_{\text{old}}, \boldsymbol{a})}$. Each accepted configuration in the sequence has its local energy computed and included in the average and if a jump is rejected, the energy of the old configuration is included in the average again. In this way, the sequence of samples is drawn randomly from the probability distribution, $P(\boldsymbol{\theta}_i, \boldsymbol{a})$, so that the local energies can then be weighted evenly when calculating the average energy. Another advantage of the Metropolis algorithm is that it is no longer necessary to calculate the normalisation factor, $\frac{1}{\int d\boldsymbol{\theta} |\Psi_{\text{vmc}}(\boldsymbol{\theta}, \boldsymbol{a})|^2}$, since we only ever need the ratio of two probabilities $\frac{P(\boldsymbol{\theta}_{\text{new}}, \boldsymbol{a})}{P(\boldsymbol{\theta}_{\text{old}}, \boldsymbol{a})}$. Thus, we only ever need to do one Monte Carlo integration to find the energy of the state rather than two[6]. Finally, it is worth noting that the Metropolis algorithm also requires a 'thermalising' period for the first part of its sequential sampling. In this period, the local energy of the samples is not included in the overall average so as to avoid the choice of initial configuration from influencing the final average. For instance, you could choose a highly improbable configuration with a very large local energy as your first sample, which would unfairly raise the final average energy.

The average distance between the particles for this method was also calculated using the Metropolis algorithm, simply replacing $E_L(\boldsymbol{\theta}_i, \boldsymbol{a})$ with $\frac{2}{N(N-1)} \sum_{\alpha<\beta}^{N} r_{\alpha\beta}(\theta_\alpha, \theta_\beta)$.

Uncertainty in the final result

As mentioned previously, one of the advantages of Monte Carlo integration when compared to other numerical integration methods is that it gives a statistical uncertainty in its final result, which indicates how good of an approximation the discrete sampling is to the continuous integral. For random uncorrelated samples, this uncertainty is simply the unbiased standard error in the mean,

$$\sigma_{E_L} = \sqrt{\frac{\sum_{i=1}^{n_s} (E_L(\boldsymbol{\theta}_i, \boldsymbol{a}) - \langle E_L(\boldsymbol{a}) \rangle)^2}{n_s(n_s - 1)}}. \tag{3.28}$$

[6]That is, one Monte Carlo integration for the numerator of equation (3.25) and one for the denominator.

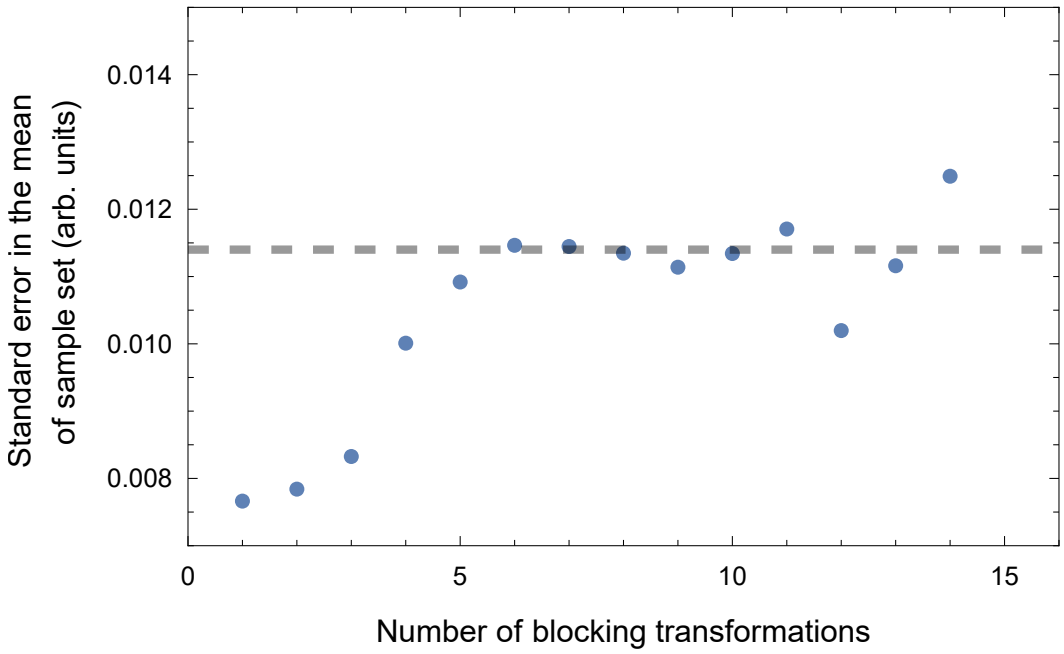

Figure 3.5: Demonstrating the use of the blocking transformation in estimating the true statistical error in a set of correlated samples.

However, the Metropolis algorithm with sequential sampling gives correlated samples which require a more careful treatment. The blocking method gives an estimate of the statistical error of correlated samples [36]. The method involves successive transformations of the set $\{E_{L\,1}, E_{L\,2}, ..., E_{L\,n_s}\}$, to a set half as large, $\{E'_{L\,1}, E'_{L\,2}, ..., E'_{L\,\frac{n_s}{2}}\}$, by averaging adjacent samples $E'_{L\,i} = \frac{1}{2}(E_{L\,i} + E_{L\,i+1})$. After each blocking transformation, the standard error in the mean (equation (3.28)) of the new set is calculated. These values then converge to the true statistical error of the original set as shown in figure (3.5)[7]. In this case, a naive calculation of the error in the mean would give a statistical error of 0.008, while the true statistical error is actually larger at around 0.011.

Choice of trial wave function

The choice of trial wave function is an important consideration for the method. The function needs to be as flexible as possible to find a good approximation to the ground state while also depending on as few parameters as possible to reduce the computational time required to find their optimal values. The balancing between these two factors can be improved by ensuring the trial wave function shares important properties with the true wave function as outlined in the previous chapter. For identical fermions, we know the position wave function should be antisymmetric upon the exchange of any two particles, should be continuous everywhere in the configuration space, and should have continuous bounded derivatives everywhere except at singular points of the interaction potential. Additionally, to ensure the local energy does not diverge at these points, there was a

[7]The method eventually breaks down after too many blocking transformations as information is lost.

condition on the second derivative of the wave function,

$$\left.\frac{\partial^2\Psi}{\partial r_{\alpha\beta}^2}\right|_{r_{\alpha\beta}\to 0} = \left.\frac{V_1}{r_{\alpha\beta}}\Psi\right|_{r_{\alpha\beta}\to 0} \tag{3.29}$$

which was derived in appendix B.

The Jastrow wave function [37] has shown to be a compact and accurate approximation to the many body wave function for interacting fermions [38]. It consists of a Slater determinant of single-particle wave functions multiplied by a Jastrow correlation factor which consists of the product of positive functions of the inter-particle distances, $r_{\alpha\beta}$,

$$\Psi_{\text{vmc}}(\theta_1, \theta_2, ..., \theta_n, \boldsymbol{a}) = \begin{vmatrix} \phi_1(\theta_1) & \phi_1(\theta_2) & \cdots & \phi_1(\theta_n) \\ \phi_2(\theta_1) & \phi_2(\theta_2) & \cdots & \phi_2(\theta_n) \\ \vdots & \vdots & \ddots & \vdots \\ \phi_n(\theta_1) & \phi_n(\theta_2) & \cdots & \phi_n(\theta_n) \end{vmatrix} \prod_{\alpha<\beta}^{N} f(r_{\alpha\beta}, \boldsymbol{a}). \tag{3.30}$$

The Slater determinant part of the trial wave function ensures that it is antisymmetric under the exchange of two particles, while the Jastrow factor allows for correlations between the particles' positions by increasing or decreasing the magnitude of the wave function depending on the distance between the particles. In this method, I keep the Slater determinant fixed and just optimise the correlation factor whose functions depend on the parameters that will be optimised.

3.3.2 Numerical implementation

As mentioned in the previous chapter, Bray and Simenel [25] used the previously developed CASINO program to obtain their quantum Monte Carlo results. The issue with the CASINO program was that it was not clear how to implement higher dimensional spheriums which was a core goal for future research. Thus, in this project, the decision was made to develop a new variational Monte Carlo simulation from scratch which would be easier to modify to include spheriums. As I did for the previous method, in this section I will outline and attempt to justify the choices that were made in this numerical implementation of the variational Monte Carlo method.

The first major choice was on the form of the trial wave function which consisted of a Slater determinant of single-particle wave functions and a Jastrow correlation factor. Initially, I chose the single-particle wave functions and Jastrow correlation factor to be the same as Bray and Simenel's [25]. The single-particle wave functions were the kinetic energy eigenstates whose Slater determinant was the unbroken symmetry Hartree-Fock ground state discussed in the previous section. The wave functions of these states were, for an odd number of particles,

$$\frac{1}{\sqrt{2\pi}}, \frac{\sin(\theta)}{\sqrt{\pi}}, \frac{\cos(\theta)}{\sqrt{\pi}}, \frac{\sin(2\theta)}{\sqrt{\pi}}, \frac{\cos(2\theta)}{\sqrt{\pi}}, ..., \frac{\sin((N-1)\theta/2)}{\sqrt{\pi}}, \frac{\cos((N-1)\theta/2)}{\sqrt{\pi}}, \tag{3.31}$$

and for an even number of particles,

$$\frac{\sin(\theta/2)}{\sqrt{\pi}}, \frac{\cos(\theta/2)}{\sqrt{\pi}}, \frac{\sin(3\theta/2)}{\sqrt{\pi}}, \frac{\cos(3\theta/2)}{\sqrt{\pi}}, ..., \frac{\sin((N-1)\theta/2)}{\sqrt{\pi}}, \frac{\cos((N-1)\theta/2)}{\sqrt{\pi}}. \tag{3.32}$$

The advantage of using these states as a starting point (before introducing correlations with the Jastrow factor) is that they are already relatively low in energy and their Slater determinant is rotationally symmetric. Additionally, we know that these states can reproduce the exact ground state when there is no interaction between the particles (so long as the Jastrow factor can be equal to 1). Another advantage of this particular Slater determinant of single-particle states is that it can be evaluated rapidly by comparing it to the Vandermonde determinant which is done in appendix C. This gives

$$\begin{vmatrix} \phi_1(\theta_1) & \phi_1(\theta_2) & \cdots & \phi_1(\theta_n) \\ \phi_2(\theta_1) & \phi_2(\theta_2) & \cdots & \phi_2(\theta_n) \\ \vdots & \vdots & \ddots & \vdots \\ \phi_n(\theta_1) & \phi_n(\theta_2) & \cdots & \phi_n(\theta_n) \end{vmatrix} \propto \prod_{\alpha<\beta}^{N} \sin\left(\frac{\theta_i - \theta_j}{2}\right) \propto \prod_{\alpha<\beta}^{N} r^*_{\alpha\beta} \tag{3.33}$$

where $r^*_{\alpha\beta} = 2R\sin\left(\frac{\theta_\alpha - \theta_\beta}{2}\right)$ is the signed inter-particle distance which is allowed to be positive or negative. The constants in front of this term are not important as normalisation of the wave function is dealt with by the Metropolis algorithm. Generally, the determinant consists of the sum of $N!$ terms each of which is the product of N single-particle wave functions. Instead, the determinant can be calculated as the product of $\frac{N}{2}(N-1)$ functions which can be evaluated much faster, particularly for larger N. I used this Slater determinant of single-particle wave functions for all variational Monte Carlo results in this thesis.

I initially used the same Jastrow factor as Bray and Simenel [25],

$$\prod_{\alpha<\beta}^{N} f(r_{\alpha\beta}, \boldsymbol{a}) = \exp\left(\sum_{\alpha<\beta}^{N} (r_{\alpha\beta} - L_c)^3 \Theta(L_c - r_{\alpha\beta}) \sum_{k=0}^{5} a_k r^k_{\alpha\beta}\right), \tag{3.34}$$

where a_k are the parameters of the trial wave function, Θ is the Heaviside step function and L_c is a parameter which controls the maximum distance over which two particles can correlate their positions. The Jastrow factor was first given in [38], and was developed for use in both finite systems and infinite periodic systems, hence the need for a cut-off length, L_c. Since the quantum ring was finite and I wanted all the particles to be able to be correlated, I simply set $L_c = \pi R$, which is larger than the diameter of the ring. In this form, the condition on the second derivative of the ring which prevents divergence in the local energy becomes a condition on the relation between two of the wave functions parameters

$$a_0 = \frac{L_c}{3}\left(a_1 + \frac{V_1}{2L_c^3}\right) \tag{3.35}$$

and the derivation can be found in appendix D.

The bounds of the parameters a_1 through to a_5 were another important consideration for the numerical implementation of the method. A smaller parameter space took less time to search and could result in a more finely optimised wave function in a given amount of time, however, the smaller the parameter space was, the more likely it was that it would not include the best possible parameter set and so could lead to a worse approximation to the ground state. For this Jastrow factor, I chose the bounds such that the maximum magnitude of each term, $a_k(r_{\alpha\beta}-L_c)^3 r_{\alpha\beta}^k$ (over all possible $r_{\alpha\beta}$ and a_k within the bounds), was approximately the same, equal to 10. This was to allow each parameter of the trial wave function to have roughly equal ability to change the shape of the wave function; if one term was significantly smaller than the others then there would be no sense in trying to optimise that parameter as it would have little effect on the overall wave function. This was especially true thanks to the exponential function which further obscured small changes in its polynomial argument. The choice of the bounds of a_1 also factored in the a_1 dependence of the a_0 term such that the maximum magnitude of $(a_0 + a_1 r_{\alpha\beta})(r_{\alpha\beta} - L_c)^3$ was roughly the same as the other terms.

The difficulty in using the aforementioned Jastrow factor arose when trying to increase the strength of the interaction potential, V_0[8]. Since the strength of V_0 factored into the magnitude of the a_0 term (since $V_1 \propto V_0$), larger values of V_0 resulted in tighter parameter bounds for a_1 using the current method of choosing parameter bounds. I could mitigate this by increasing the maximum allowed magnitude for any of the terms, however this resulted in larger parameter bounds and slower optimisation of the other parameters. To resolve this issue, I relaxed the condition on the second derivative of the wave function and used a simpler Jastrow function with only four free parameters,

$$\prod_{\alpha<\beta}^{N} f(r_{\alpha\beta}, \boldsymbol{a}) = \exp\left(\sum_{\alpha<\beta}^{N}\sum_{k=1}^{4} a_k r_{\alpha\beta}^k\right). \tag{3.36}$$

I chose to use a simpler form because the original Jastrow function had been engineered to have particular behaviours at the cut-off distance L_c [38], which were not important on the finite quantum ring. I chose to decrease the number of parameters because I noticed that in most runs, a_5 was not being optimised and so I assumed it was not necessary to achieve a good approximation to the ground state. In this new form, the second derivative condition would give $a_1 = \frac{V_1}{2}$ (shown in appendix D), although I still allowed a_1 to vary. My assumption was that so long as $\frac{V_1}{2}$ was within the bounds of a_1, the optimisation process itself would decide if the second derivative condition was necessary for finding the best ground state approximation in this variational space.

Figure (3.6) shows that for $N = 2$ particles on a $R = 2$ radius ring, interacting via Nuclear 1 of strength $V_0 = 5$, this new Jastrow factor was able to achieve a much better approximation to the ground state energy in shorter amount of time. Indeed, the more complicated Jastrow function was not able to converge to the same ground state energy even when run for more than seven times as long as the simpler Jastrow function. Ad-

[8]I wanted to increase V_0 to display the rotational symmetry breaking in the previous Hartree-Fock method. Low values of V_0 resulted in no symmetry breaking.

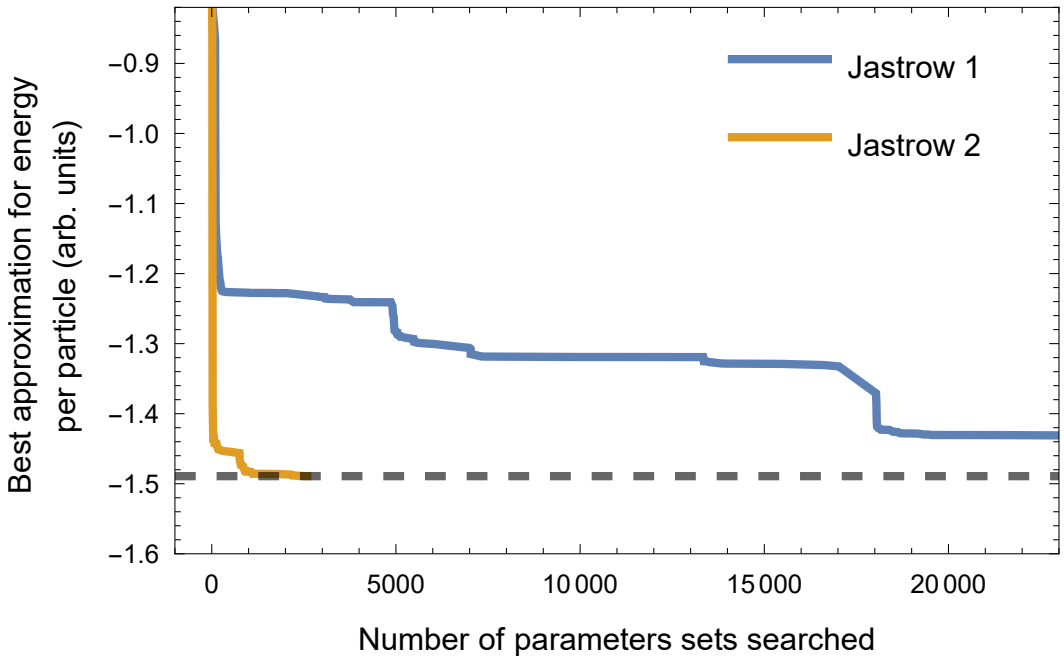

Figure 3.6: A comparison of the two Jastrow functions used in the trial wave function of the variational Monte Carlo method. Jastrow 1 had a more complicated form and included the second derivative condition to prevent local energy divergence while Jastrow 2 had a simpler form and was not required to satisfy this condition.

ditionally, the optimal set of parameters had $a_1 = 6.3$ rather than $a_1 = 90$ as required to prevent the divergence of the kinetic energy. The reason that this condition was not necessary was likely due to the Pauli-exclusion between the fermions and the Metropolis algorithm. The Pauli-exclusion (which comes from the antisymmetry of the trial wave function, which is built-in to the Slater determinant) ensures that the trial wave function goes to zero as two particles approach one another. The Metropolis algorithm ensures that these configurations with low probability are rarely sampled and so the diverging local energy does not contribute significantly to the average energy calculated by the Monte Carlo integration. Given that the new simpler Jastrow factor gave better approximations to the ground state, I decided to use it for all the remaining variational Monte Carlo results.

The next major decision concerned the exact method of optimisation. A number of different optimisation routines exists each with their own advantages and disadvantages for particular problems. In order to quickly test a range of routines and find a suitable one for my project, I used the NLopt non-linear optimisation package [39], which is an open-source library containing a range of different optimisation routines. Aside from having many different routines, NLopt also had extensive program documentation and worked examples online which made it easier to implement in my own code. In figure (3.7), I compare the convergence of several different routines included in the package (the details of each routine can be found on the NLopt website). I chose the DIRECT (DIviding RECTangles) algorithm proposed by Jones, Perttunen and Stuckman in 1993 [40]. This

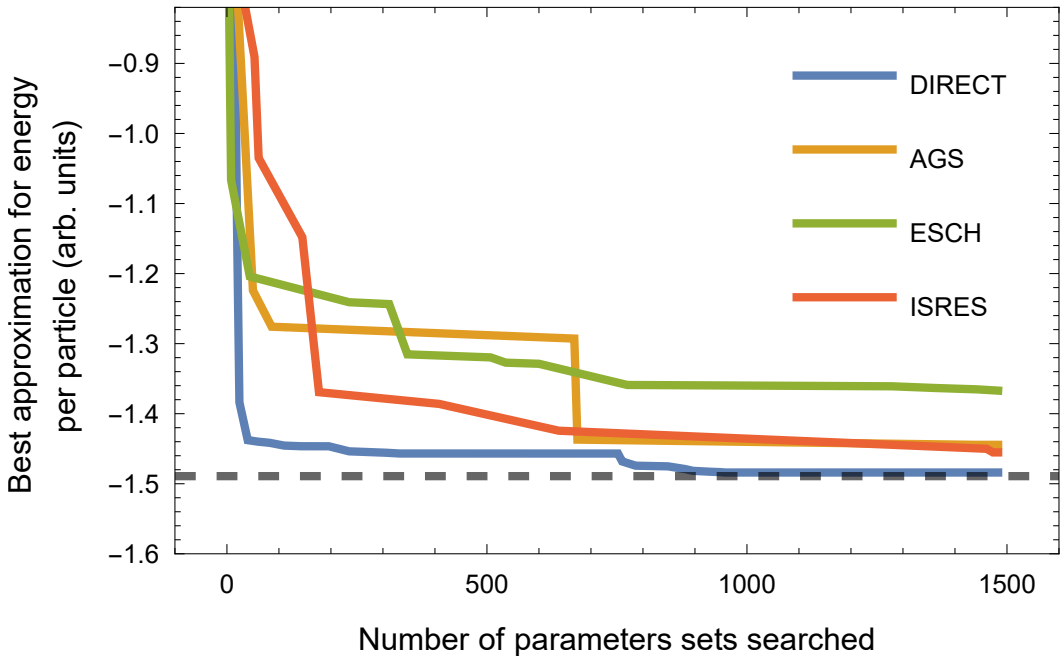

Figure 3.7: A comparison of several of the optimisation routines available from NLopt. The DIRECT routine converges faster to a lower energy per particle than the other routines.

algorithm deterministically searches for extremes of a function by recursively dividing the function domain into smaller and smaller hyperrectangles. The function value at the centre-point of each hyperrectangle is evaluated before the next hyperrectangle to divide is chosen. The decision of which hyperectangle to divide next is based on both the size of the hyperrectangle (with larger hyperrectangles being more likely to contain the function's minimum or maximum) and the function value at the centre of the hyperrectangle (with lower or higher function values being more likely to be close to the minimum or maximum, respectively). In this way, the algorithm balances the global search for the extreme (by searching larger hyperectangles first) and the local search, (by searching hyperrectangles with more extreme centre-point function values).

The next decision concerned how I would parallelise the program to decrease the time taken for it to run. I decided to have each parallel core of the Gadi supercomputer run one instance of the Metropolis algorithm with different random starting configurations. I chose the thermalising period for each instance of the algorithm to be 1000 samples long (that is, the first 1000 samples in the sequence were not included in the average) as I found that this was more than long enough to prevent the initial choice of configuration from influencing the result. I had the program run in parallel on 48 cores and stopped when 10^5 samples (across all the cores) had been included in the average. This number of samples was chosen because it decreased the uncertainty in the final energy to less than 1% of the result. This was generally far smaller than the difference in energies between each of the methods explored in this project so the choice provided a good balance between accuracy and computational time. In later plots, the error bars on the variational Monte Carlo data points typically appear as a single horizontal line due to

the small size of the uncertainty (rather than two horizontal lines for the upper and lower bounds for the result). It is important to remember that these error bars are simply the error in the expectation energy of the trial wave function and give no indication of how close the result is to the true ground state energy of the system.

The final decision concerned the nature of the random jumps used in the Metropolis algorithm. Smaller jumps meant the jump was less likely to be rejected by the algorithm but made the sampling take longer to explore the full configuration space which is required for a valid result (0 to 2π for each of θ_1, θ_2 etc.). Conversely, larger jumps reached further into the configuration space but were more likely to be rejected by the algorithm and not included in the final average. I chose to sample the random jump sizes from a Gaussian probability distribution and I found a distribution with standard deviation of 0.7 radians gave a jump acceptance rate of 50% which seemed like a good balance between the speed and accuracy of the method.

Many of the parameters and choices outlined in this section could have been investigated and optimised further to improve the efficiency of the variational Monte Carlo method. However, since my project focuses on the relative accuracy of the methods outlined in this chapter, the speed of the method was only improved to the point where the method was viable before I moved on to the next task. This is why some of the decisions made in this section are somewhat arbitrary.

Finally, the validity of this implementation of the variational Monte Carlo method was assessed by comparing the results to both the quantum Monte Carlo results found using the CASINO program by Bray and Simenel [25] and the analytical results found by Loos and Gill [23] which is shown table (3.1). The comparison shows that the implementation of the variational Monte Carlo method is able to give the exact ground state energy (within its statistical uncertainty) and performs significantly better than the Hartree-Fock method with unbroken rotational symmetry. In addition, the variational Monte Carlo method was also able to reproduce the results of the CASINO program, leading to the conclusion that this implementation of the method is valid.

3.4 Symmetry restoration of the broken symmetry Hartree-Fock ground state

3.4.1 Theoretical background

Earlier in this chapter, we discussed finding a Hartree-Fock ground state with broken rotational symmetry,

$$|\Psi_{bs}\rangle = \begin{vmatrix} |1:\psi_1\rangle & |1:\psi_2\rangle & \cdots & |1:\psi_n\rangle \\ |2:\psi_1\rangle & |2:\psi_2\rangle & \cdots & |2:\psi_n\rangle \\ \vdots & \vdots & \ddots & \vdots \\ |n:\psi_1\rangle & |n:\psi_2\rangle & \cdots & |n:\psi_n\rangle \end{vmatrix}, \tag{3.37}$$

Ring radius (arb. units)	Exact energy (arb. units)	Variational Monte Carlo (arb. units)	Hartree Fock (arb. units)
$1/2$	$9/4 = 2.2500$	2.2503 ± 0.0008	2.2732
$\sqrt{3/2}$	$2/3 = 0.66667$	0.66661 ± 0.00016	0.68646
$\sqrt{\frac{3}{4}(7+\sqrt{33})}$	$\frac{25}{96}(7-\sqrt{33}) = 0.32694$	0.32695 ± 0.00006	0.34352
$\sqrt{23/2}$	$9/46 = 0.19565$	0.19562 ± 0.00003	0.20947

Table 3.1: Exact, variational Monte Carlo and unbroken rotational symmetry Hartree-Fock ground state energies for a quantum ring with $N = 2$ particles and a repulsive Coulomb interaction of strength $V_0 = 1$. The broken-symmetry and restored-symmetry Hartree-Fock methods gave the same energies as the unbroken-symmetry Hartree-Fock in this case.

with single-particle states, $|\psi_i\rangle$, that have been optimised to give the lowest possible energy in this variational space. We now want a projector operator, $\hat{P} = \hat{P}^2$, that will restore the rotational symmetry of this broken symmetry state. For restoring the rotational symmetry of a one-dimensional ring, the relevant operator is a projection onto a state of well defined total angular momentum, M, in the direction normal to the plane of the ring which I call the z-direction [11]:

$$\hat{P} = \frac{1}{2\pi}\int_0^{2\pi} d\theta' \, e^{-i\theta'(\hat{J}_z - M)}. \tag{3.38}$$

The total angular momentum operator is a combination of spin, $\hat{S}_z$, and orbital angular momentum, $\hat{L}_z$, operators which act on each single-particle state separately:

$$\hat{J}_z = \hat{L}_z + \hat{S}_z = \sum_\alpha^N \left(\hat{L}_{z\,\alpha} + \hat{S}_{z\,\alpha}\right) \tag{3.39}$$

Firstly, we want to know how the rotation operator $\hat{R}(\theta') = e^{-i\theta'(\hat{J}_z - M)}$ acts on the wave function. Recall that in this work, all the single-particle states are considered to have the same spin in the z-direction, spin up. Then the action of the spin part of the rotation on a single-particle state is

$$e^{-i\theta'(\hat{S}_{z\,\alpha})}|\psi_\alpha\rangle = \exp\left(-i\theta'\frac{1}{2}\begin{pmatrix}1 & 0\\ 0 & -1\end{pmatrix}\right)\begin{bmatrix}1\\0\end{bmatrix} = \begin{bmatrix}e^{-\frac{i\theta'}{2}}\\0\end{bmatrix} = e^{-\frac{i\theta'}{2}}|\psi_\alpha\rangle. \tag{3.40}$$

We see that the spin operator does not change the spin of the single-particle state; it just adds a phase, $e^{-\frac{i\theta'}{2}}$, that depends on the size of the angle rotated. For N single-particles states, all spin up, the spin part of the rotation operator $e^{-i\theta'\sum_\alpha(\hat{S}_{z\,\alpha})}$ gives an overall phase of $e^{-\frac{i\theta' N}{2}}$.

The orbital angular momentum part of the rotation operator rotates angular position

eigenstates as

$$e^{-i\theta'\hat{L}_z}|\theta\rangle = |\theta+\theta'\rangle. \tag{3.41}$$

Its action on a single-particle state simply rotates its angular position wave function

$$e^{-i\theta'\hat{L}_z}{}_\alpha\left(\int_0^{2\pi} d\theta\,\psi_\alpha(\theta)\,|\theta\rangle\right) = \int_0^{2\pi} d\theta\,\psi_\alpha(\theta)\,|\theta+\theta'\rangle = \int_0^{2\pi} d\theta\,\psi_\alpha(\theta-\theta')\,|\theta\rangle. \tag{3.42}$$

We are now ready to find the energy of the symmetry restored state, $|\Psi_{sr}\rangle = \hat{P}|\Psi_{bs}\rangle$

$$E_{sr} = \frac{\langle\Psi_{sr}|\hat{H}|\Psi_{sr}\rangle}{\langle\Psi_{sr}|\Psi_{sr}\rangle} = \frac{\langle\Psi_{bs}|\hat{P}^\dagger\hat{H}\hat{P}|\Psi_{bs}\rangle}{\langle\Psi_{bs}|\hat{P}^\dagger\hat{P}|\Psi_{bs}\rangle} \tag{3.43}$$

$$= \frac{1}{4\pi^2\langle\Psi_{bs}|\hat{P}^\dagger\hat{P}|\Psi_{bs}\rangle}\int_0^{2\pi} d\theta''\int_0^{2\pi} d\theta'\,\langle\Psi_{bs}|e^{+i\theta''(\hat{J}_z^\dagger-M)}\hat{H}e^{-i\theta'(\hat{J}_z-M)}|\Psi_{bs}\rangle. \tag{3.44}$$

Since $\hat{J}$ corresponds to a real observable it must be a Hermitian operator, $\hat{J}^\dagger = \hat{J}$, and we also know it commutes with the Hamiltonian of the system, $\hat{H}$. This allows us to combine the first exponential operator with the second,

$$E_{sr} = \frac{1}{4\pi^2\langle\Psi_{bs}|\hat{P}^\dagger\hat{P}|\Psi_{bs}\rangle}\int_0^{2\pi} d\theta''\int_0^{2\pi} d\theta'\,\langle\Psi_{bs}|\hat{H}e^{-i(\theta'-\theta'')(\hat{J}_z-M)}|\Psi_{bs}\rangle \tag{3.45}$$

With a change of variables, $\varphi = \theta' - \theta''$ and $\varphi' = \theta' + \theta''$ and integrating over φ', the energy becomes:

$$E_{sr} = \frac{1}{2\pi\langle\Psi_{bs}|\hat{P}^\dagger\hat{P}|\Psi_{bs}\rangle}\int_{-2\pi}^{2\pi} d\varphi\,\langle\Psi_{bs}|\hat{H}e^{-i\varphi(\hat{J}_z-M)}|\Psi_{bs}\rangle \tag{3.46}$$

A similar line of reasoning can be used on the denominator to get

$$E_{sr} = \frac{\int_{-2\pi}^{2\pi} d\varphi\,\langle\Psi_{bs}|\hat{H}e^{-i\varphi(\hat{J}_z-M)}|\Psi_{bs}\rangle}{\int_{-2\pi}^{2\pi} d\varphi\,\langle\Psi_{bs}|e^{-i\varphi(\hat{J}_z-M)}|\Psi_{bs}\rangle}. \tag{3.47}$$

Working in the angular position basis, where $|\Psi_{bs}\rangle = \int_0^{2\pi} d\boldsymbol{\theta}\,\Psi_{bs}(\boldsymbol{\theta})|1:\theta_1, 2:\theta_2, ..., n:\theta_n\rangle$ (using $\int d\boldsymbol{\theta}$ to indicate N integrals over $d\theta_1$, $d\theta_2$, ... , $d\theta_n$) and

$$\Psi_{bs}(\boldsymbol{\theta}) = \begin{vmatrix} \psi_1(\theta_1) & \psi_2(\theta_1) & \cdots & \psi_n(\theta_1) \\ \psi_1(\theta_2) & \psi_2(\theta_2) & \cdots & \psi_n(\theta_2) \\ \vdots & \vdots & \ddots & \vdots \\ \psi_1(\theta_n) & \psi_2(\theta_n) & \cdots & \psi_n(\theta_n) \end{vmatrix}, \tag{3.48}$$

the energy is

$$E_{sr} = \frac{\int_{-2\pi}^{2\pi} d\varphi\int_0^{2\pi} d\boldsymbol{\theta}\,\Psi_{bs}(\boldsymbol{\theta},0)\hat{H}\Psi_{bs}(\boldsymbol{\theta},\varphi)e^{-i\varphi(\frac{N}{2}-M)}}{\int_{-2\pi}^{2\pi} d\varphi\int_0^{2\pi} d\boldsymbol{\theta}\,\Psi_{bs}(\boldsymbol{\theta},0)\Psi_{bs}(\boldsymbol{\theta},\varphi)e^{-i\varphi(\frac{N}{2}-M)}}, \tag{3.49}$$

where $\Psi_{bs}(\boldsymbol{\theta},\varphi) = \Psi_{bs}(\theta_1-\varphi, \theta_2-\varphi, ..., \theta_N-\varphi)$. A question remains of what value M should be, that is what state of total angular momentum should the method project onto?

Central interaction potentials which depend only on the distance between particles (like the ones studied in this thesis) have ground states with zero orbital angular momentum [41]. Thus, the total angular momentum of the ground state is comprised entirely of the spin of the particles, so we should choose $M = N\frac{1}{2}$ which means the phase factor is $e^{-i\varphi(\frac{N}{2}-M)} = 1$.

A rotation of 2π around the ring does not change the total wave function[9], so we can pull out a factor of 2 by changing the bounds of integration for φ to 0 to 2π. Doing this for the numerator and denominator cancels these factors of 2. Finally, in the position basis, the Hamiltonian is

$$\hat{H}\Psi_{bs}(\boldsymbol{\theta},\varphi) = \Psi_{bs}(\boldsymbol{\theta},\varphi)\left(\frac{-1}{2R^2\Psi_{bs}(\boldsymbol{\theta},\varphi)}\sum_{\alpha=1}^{N}\frac{\partial^2\Psi_{bs}(\boldsymbol{\theta},\varphi)}{\partial\theta_\alpha^2} + \sum_{\alpha<\beta}^{N} V(\theta_\alpha,\theta_\beta)\right), \tag{3.50}$$

which gives a final energy of:

$$E_{sr} = \int_0^{2\pi} d\varphi\, d\boldsymbol{\theta}\, \frac{\Psi_{bs}(\boldsymbol{\theta},0)\Psi_{bs}(\boldsymbol{\theta},\varphi)}{\int_0^{2\pi} d\varphi\, d\boldsymbol{\theta}\, \Psi_{bs}(\boldsymbol{\theta},0)\Psi_{bs}(\boldsymbol{\theta},\varphi)} \left(\frac{-1}{2R^2\Psi_{bs}(\boldsymbol{\theta},\varphi)}\sum_{\alpha=1}^{N}\frac{\partial^2\Psi_{bs}(\boldsymbol{\theta},\varphi)}{\partial\theta_\alpha^2} + \sum_{\alpha<\beta}^{N} V(\theta_\alpha,\theta_\beta)\right). \tag{3.51}$$

As in the variational Monte Carlo method, this integral is too complicated to evaluate analytically so I used numerical Monte Carlo integration with the Metropolis algorithm once again. In a similar way to the variational Monte Carlo, I consider the sampling distribution to be

$$P(\boldsymbol{\theta},\varphi) = \frac{|\Psi_{bs}(\boldsymbol{\theta},0)\Psi_{bs}(\boldsymbol{\theta},\varphi)|}{\int_0^{2\pi} d\varphi\, d\boldsymbol{\theta}\, \Psi_{bs}(\boldsymbol{\theta},0)\Psi_{bs}(\boldsymbol{\theta},\varphi)} \tag{3.52}$$

and the function which we are taking a continuously weighted average of is

$$f(\boldsymbol{\theta},\varphi) = \text{sign}\left(\Psi_{bs}(\boldsymbol{\theta},0)\Psi_{bs}(\boldsymbol{\theta},\theta')\right)\left(\frac{-1}{2R^2\Psi_{bs}(\boldsymbol{\theta},\varphi)}\sum_{\alpha=1}^{N}\frac{\partial^2\Psi_{bs}(\boldsymbol{\theta},\varphi)}{\partial\theta_\alpha^2} + \sum_{\alpha<\beta}^{N} V(\theta_\alpha,\theta_\beta)\right). \tag{3.53}$$

Then the expectation energy is given by the integral

$$E_{sr} = \int_0^{2\pi} d\varphi\, d\boldsymbol{\theta}\, P(\boldsymbol{\theta},\varphi) f(\boldsymbol{\theta},\varphi) \tag{3.54}$$

which is approximated by the discrete sum

$$E_{sr} \approx \frac{1}{n_s}\sum_{i=1}^{n_s} f(\boldsymbol{\theta}_i,\varphi_i) \tag{3.55}$$

[9]This can be seen by considering the kinetic energy basis states used in the Hartree-Fock broken symmetry section. For an odd number of particles, the basis states 1, $\sin(k\theta)$ or $\cos(k\theta)$ for k an integer, do not change with $\theta \to \theta + 2\pi$. For an even number of particles, when k is a half integer, the single-particle states do change sign with $\theta \to \theta + 2\pi$, but since the total wave function involves products of an even number of these states, the total wave function does not change sign.

where the samples $\{\theta_i, \varphi_i\}$ are chosen sequentially using the Metropolis algorithm which I describe in the previous section. As mentioned in that section, a major advantage of the Metropolis algorithm is that there is no need to calculate the normalisation factor as each new configuration in the sequence, $\boldsymbol{\theta}_{new}, \varphi_{new}$, is accepted with probability $P(\boldsymbol{\theta}_{new}, \varphi_{new})/P(\boldsymbol{\theta}_{old}, \varphi_{old})$ which does not depend on the denominator of P.

As in the variational Monte Carlo method, to calculate the expectation value for the average distance between particles I simply replace $f(\boldsymbol{\theta}, \varphi)$ with $\text{sign}\left(\Psi_{bs}(\boldsymbol{\theta}, 0)\Psi_{bs}(\boldsymbol{\theta}, \theta')\right)\left(\frac{2}{N(N-1)}\sum_{\alpha<\beta}^{N} r_{\alpha\beta}(\theta_\alpha, \theta_\beta)\right)$ in the Metropolis algorithm.

3.4.2 Numerical implementation

The decisions made for this method were largely kept the same as for the variational Monte Carlo method to save time. In this section, I will quickly recount the decisions made as well as what was changed.

The Metropolis algorithm involved 10^6 samples, sequentially found across 48 parallel cores of the Gadi supercomputer. Each core first ran a thermalising period of 10^3 samples which were not included in the final average. The random jumps used in the Metropolis algorithm were kept the same, randomly sampled from a Gaussian distribution with a standard deviation of 0.7 radians.

Unlike the variational Monte Carlo method which had a compact wave function whose derivatives could be found analytically, the wave function in this method was generally very complicated. It involved the determinant of N single-particle wave functions, each of which consisted of the linear combination of up to 35 basis wave functions so an analytical expression for the second derivative would have been difficult to calculate. Instead, I used a finite difference formula to calculate the second derivative,

$$\frac{\partial^2 \Psi}{\partial \theta_\alpha^2} \approx \frac{\Psi(\theta_\alpha + \Delta\theta) - 2\Psi(\theta_\alpha) + \Psi(\theta_\alpha - \Delta\theta)}{\Delta\theta^2}, \tag{3.56}$$

where the terms on the right hand side vary the θ_α coordinate and keep all other coordinates fixed. Using this method to find the kinetic energy required a choice of the finite difference angle $\Delta\theta$. In figure (3.8), I compare the local kinetic energy of a variational Monte Carlo ground state (the $N = 4$ particle, $R = 2$ radius with Coulomb interactions of strength $V_0 = 5$, of an arbitrary configuration $\theta_1 = 0.1$, $\theta_2 = 2$, $\theta_3 = 3$, and $\theta_4 = 4$), calculated using the finite difference formula to the same kinetic energy found analytically. The finite difference formula seems to be the most reliably accurate at around $\Delta\theta = 10{-}3$, though down to 10^{-5} and up to 0.01 would likely also be sufficiently accurate (that is, the error in the kinetic energy would still remain much smaller than the statistical error of the Monte Carlo integration). Similar comparisons with other system parameters, also indicated that 10^{-3} radians was also highly accurate in these cases. As a result, I set $\Delta\theta = 10^{-3}$ radians for this method.

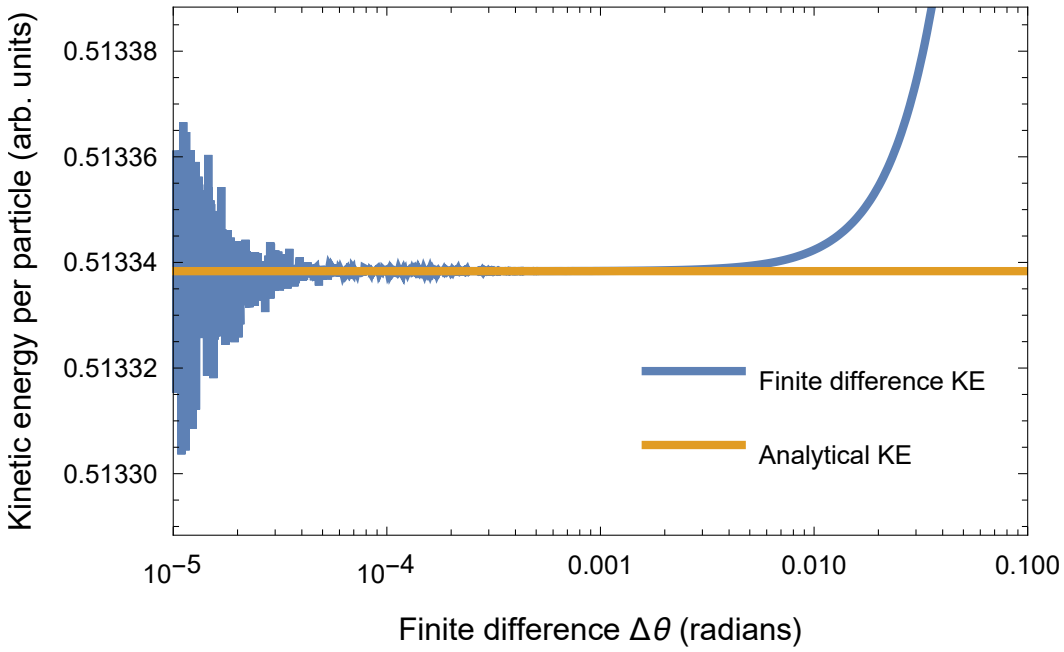

Figure 3.8: Local kinetic energy per particle of a variational Monte Carlo ground state as calculated by the finite difference formula and analytically.

Chapter 4

Results and Discussion

The aim of this thesis was to benchmark the broken-symmetry Hartree-Fock (BSHF) and the restored-symmetry Hartree-Fock (RSHF) methods by comparing them to unbroken-symmetry Hartree-Fock (USHF) and the variational Monte Carlo (VMC) methods. To do this, I searched the parameter space of the quantum ring with the four different interaction potentials: the repulsive Coulomb, attractive Coulomb, Nuclear 1 and Nuclear 2 potentials. For each of these potentials I varied the number of particles on the ring, the size of the ring and the strength of the interaction potential to understand under what conditions the extensions to the Hartree-Fock method were worth implementing.

4.1 Radius dependence

4.1.1 Repulsive Coulomb Interaction

Figure (4.1) shows the effect of varying the ring radius on the energy per particle for the repulsive Coulomb interaction. All methods show decreasing energy with increasing radius as a result of the potential energy decreasing as the particles become further apart. Across all radii, the USHF method already performs well; it differs from the VMC method by less than 3% for all radii and the difference decreases with increasing R. At low radii, $R < 2$, no symmetry breaking occurs (that is, the USHF ground state is also the lowest energy state of the BSHF variational space), so the BSHF and RSHF methods give the same energy as the USHF. At larger radii, symmetry breaking does occur and brings small improvements to the energy per particle. The density plot of the BSHF result, figure (4.2)[1], shows four equally spaced peaks spread out over the entire ring for $R = 2$, 5, and 10. It can be seen that the degree of correlation between the particles (that is, their deviation from a flat density) increases with the ring size. This is because on larger rings, the wave functions are not required to be as steep to achieve a given degree of localisation, resulting in a smaller kinetic energy cost for a given amount of localisation. For all radii, the RSHF method gives a similar result to the BSHF method, bringing only small improvements to the ground state energy.

[1]For the R-varying density plots, I show the distance-around-the-ring linear density to compare densities on rings of different sizes. All other density plots are given as the angular density.

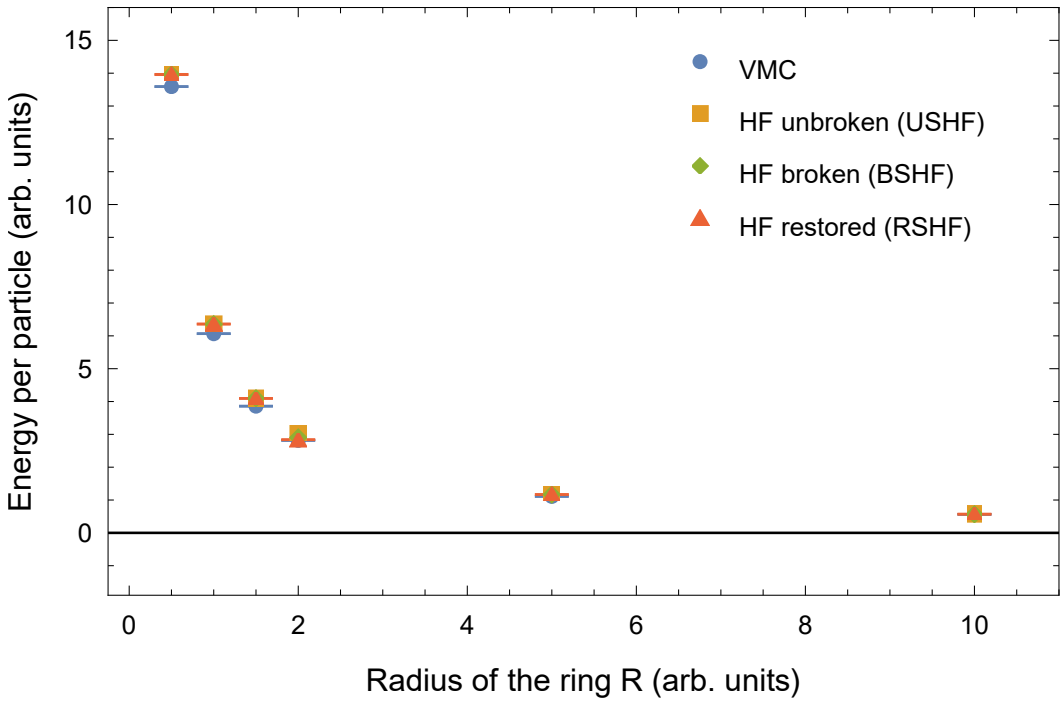

Figure 4.1: Energy per particle for a quantum ring with repulsive Coulomb interactions of strength $V_0 = 5$, $N = 4$ particles, and varying radii of the ring, R.

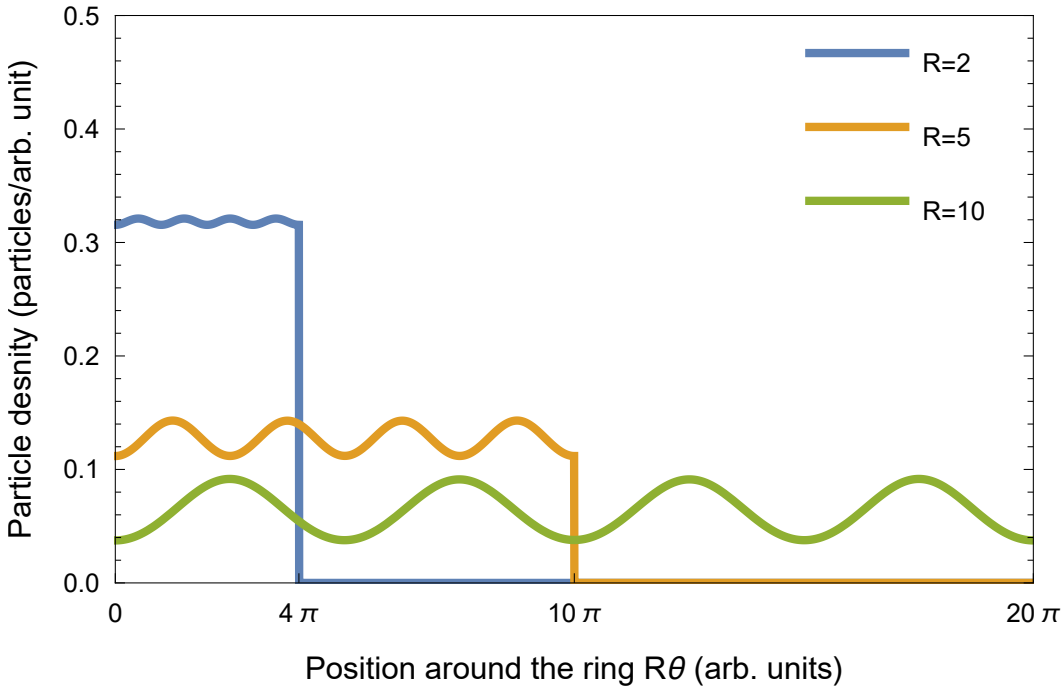

Figure 4.2: Linear particle densities of the BSHF ground state with the Coulomb repulsive interaction of strength $V_0 = 5$ and $N = 4$ particles.

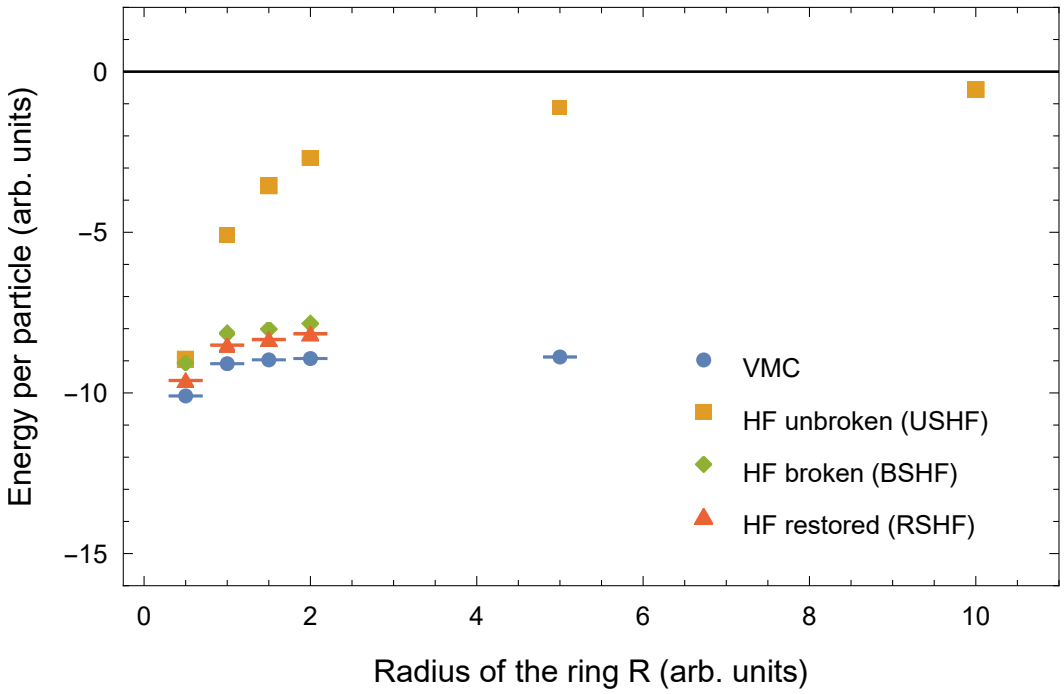

Figure 4.3: Energy per particle for a quantum ring with attractive Coulomb interactions of strength $V_0 = 5$, $N = 4$ particles, and varying radii of the ring, R. The $R = 5$ and $R = 10$ results for the BSHF and RSHF methods as well as the $R = 10$ result for the VMC method did not converge.

4.1.2 Attractive Coulomb Interaction

Figure (4.3) shows the radius dependence of the energy per particle for the attractive Coulomb interaction. Over the range of radii studied, the energy per particle is negative for all methods and rises to a constant value as the radius increases for the VMC, BSHF and RSHF methods while the USHF decreases to 0. The difference between the BSHF and RSHF results and the VMC result remains approximately constant with R which leads to both methods accounting for a larger portion of the correlation energy (the difference in energy between the uncorrelated USHF ground state and the VMC result with correlations) as the radius increases and the correlation energy grows. The RSHF brings a small improvement to the BSHF across all radii but still fails to account for all of the missing correlation energy in the BSHF method.

The constant dependence with radius at larger R of the VMC, BSHF and RSHF energies is a result of correlations in the particles' positions which either localise the absolute position of particles to one region of the ring in the BSHF method or localise the relative positions of particles to be in the same region in the case of the VMC and RSHF methods. This 'bunching' of particles can be seen in figure (4.4) which shows the angular particle density for $R = 2$ case of the BSHF state (with $N = 4$ particles and interaction strength $V_0 = 5$). The density shows that all four particles are most likely to be found around $\theta = \pi$, and have close to zero probability of being found elsewhere. In this case, the system of particles in now self-bound by its own internal forces (as opposed to being

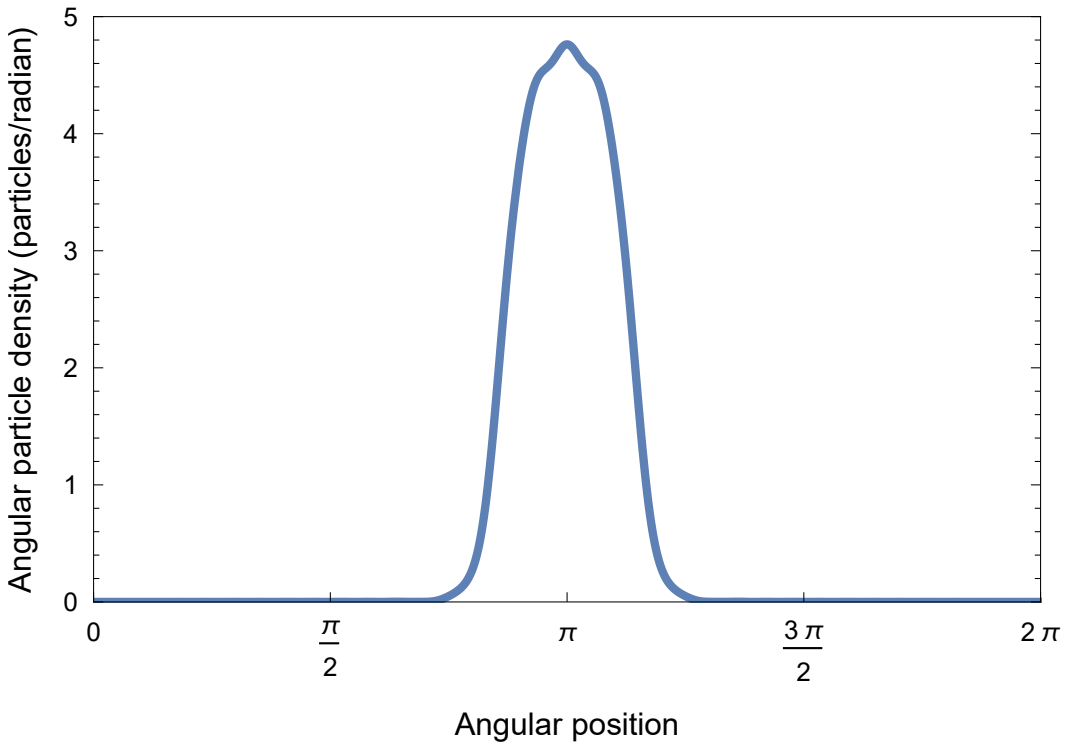

Figure 4.4: Angular particle density of the BSHF ground state with the attractive Coulomb interaction of strength $V_0 = 5$, on a ring with radius $R = 10$, and $N = 4$ particles.

bound by the limited size of the ring) and so further increases to the size of the ring have little effect on the properties of the system such as the energy per particle. Small changes in the energy are observed for $R > 1$ due to the curvature of the ring changing the through-the-ring distance between particles. As R increases, this curvature effect should vanish as the ring locally becomes a straight line.

When comparing to the results of Bray and Simenel [25], which are discussed in Chapter 2, I noticed that there is a minimum in the energy per particle at $R = 1$ for the attractive Coulomb interaction and the energy rises as the radius decreases to 0, which is not present in figure (4.4). This behaviour is expected to occur as the positive kinetic energy of the system scales with $\frac{1}{R^2}$ as $R \to 0$ while the negative potential energy scales with $\frac{1}{R}$. The minimum for the result in this thesis was likely shifted to a lower radius value by the increase in potential strength from $V_0 = 1$ in [25] to $V_0 = 5$ and is thus not present in the range of radii investigated in figure (4.4). In any case, the USHF method gave an excellent approximation to the exact ground state at low radii in [25], so the BSHF and RSHF would have brought little to no improvement here.

4.1.3 'Nuclear 1' Interaction

Figure (4.5) shows the energy per particle for the Nuclear 1 interaction. All methods have the energy go to infinity as $R \to 0$ before decreasing to some minimum negative energy per particle then increasing again. In a similar way to the previous interaction,

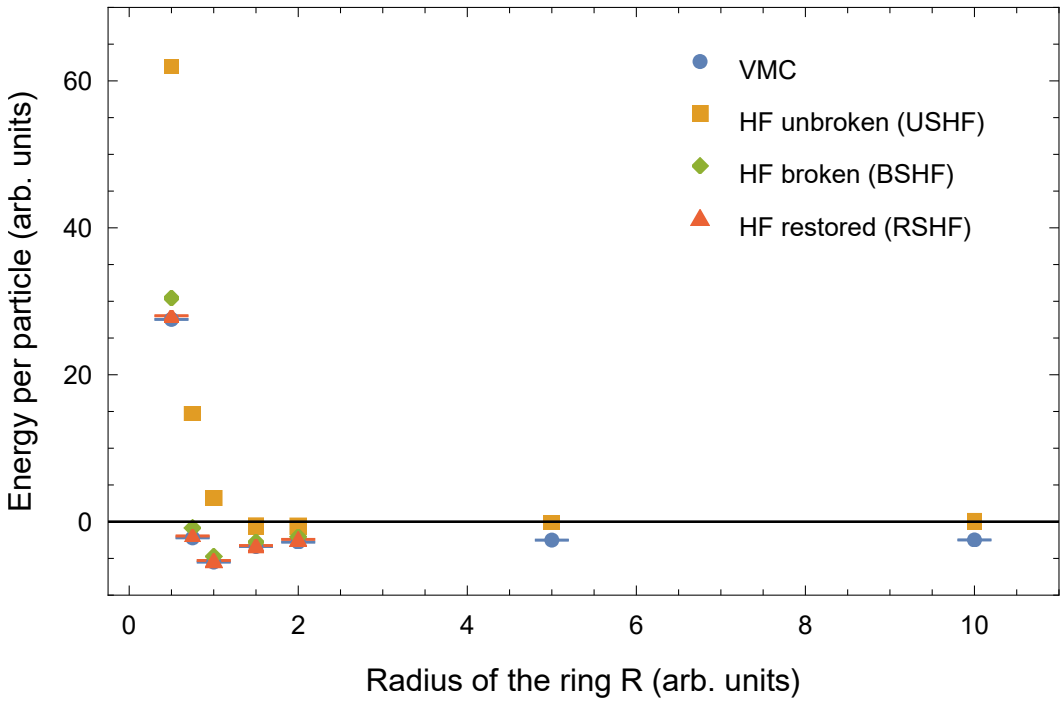

Figure 4.5: Energy per particle for a quantum ring with Nuclear 1 interactions of strength $V_0 = 5$, $N = 4$ particles, and varying radii of the ring, R. The BSHF and RSHF methods for $R = 5$ and $R = 10$ did not converge.

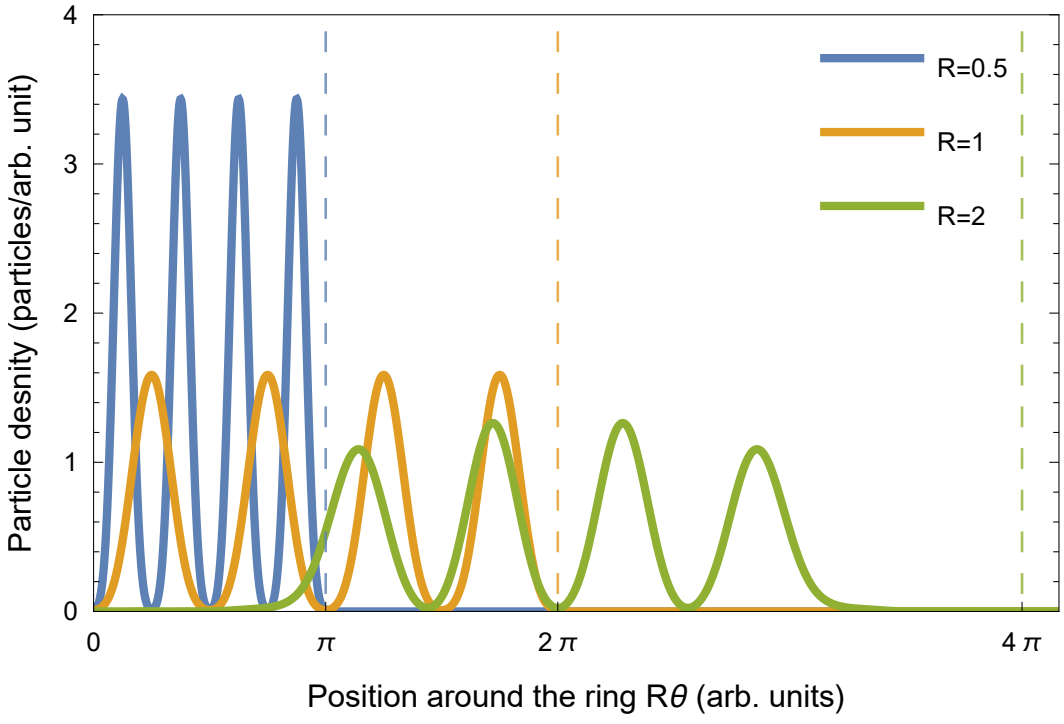

Figure 4.6: Linear particle density of the BSHF ground state with the Nuclear 1 interaction of strength $V_0 = 5$ and $N = 4$ particles. The vertical lines indicate the size of the ring in each case.

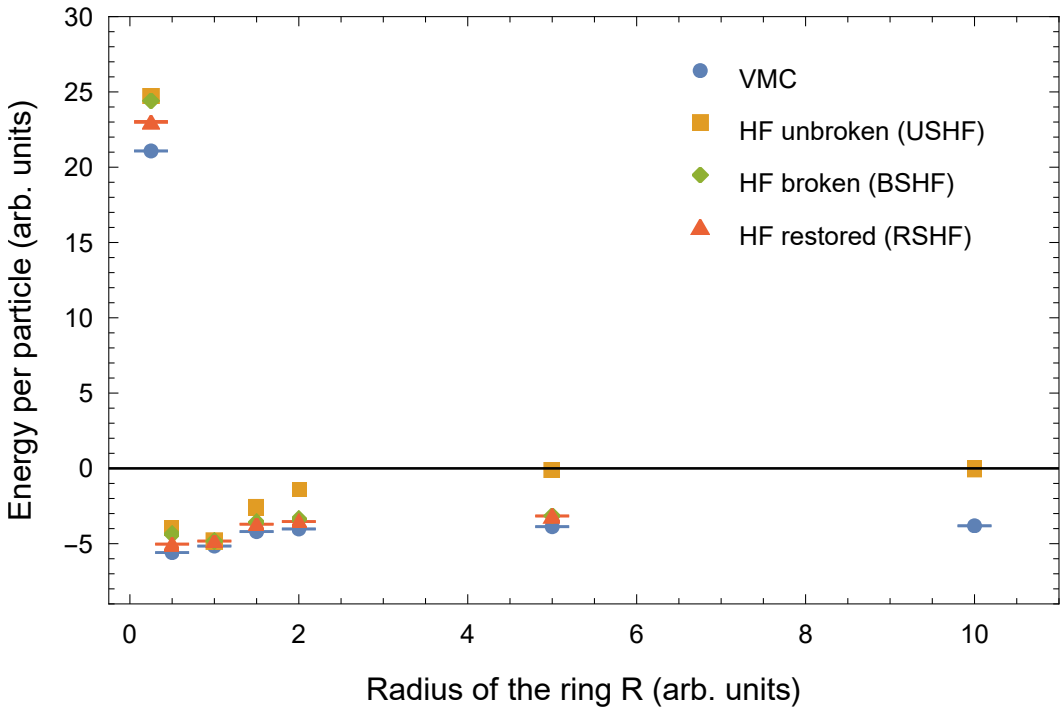

Figure 4.7: Energy per particle for a quantum ring with Nuclear 2 interactions of strength $V_0 = 5$, $N = 4$ particles, and varying radii of the ring, R. The BSHF and RSHF methods for $R = 10$ did not converge.

the USHF method goes to 0 as $R \to \infty$ since the particles are not able to correlate their positions and get further away from each other as the radius increases. Like for the attractive Coulomb interaction, the VMC result converges to a negative value as the radius increases. The BSHF method is able to account for a large portion of the correlation energy, particularly at small radii. For $R = 0.5$, for example, it accounts for 92% of the correlation energy, making it a significant improvement to the USHF method. The RSHF performs even better, accounting for 6% of the remaining correlation energy, making it almost as good as the VMC method in this case.

The density plot in figure (4.6) shows two different types of correlation between particles. At lower radii, the particles localise their positions in a similar way to the repulsive Coulomb case, with four peaks spread out evenly on the ring in order to minimise the hard-core repulsion of the Nuclear 1 potential. As the radius increases to the $R = 2$ case, the particles localise to one region of the ring in a similar way to the attractive Coulomb case, due to the attractive component of Nuclear 1. Unlike the attractive Coulomb case, however, the self-bound system does not exhibit a single peak. Instead it consists of four spread out peaks within the self-bound system which is a result of the strong hard-core repulsion of the interaction potential. This hard-core component induces a significant potential energy 'cost' when particles are too close together, even in the self-bound system which is characterised by the attraction between particles.

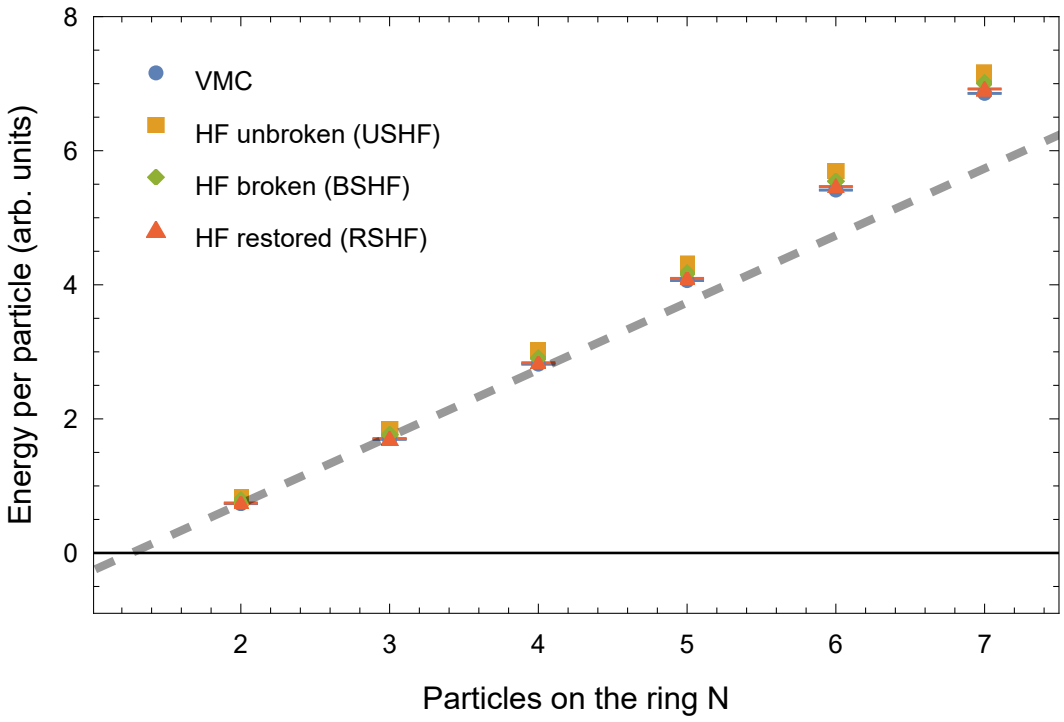

Figure 4.8: Energy per particle for a quantum ring with repulsive Coulomb interactions of strength $V_0 = 5$, radius $R = 2$, and varying numbers of particles on the ring, N. The dashed line is included to show the deviation from a linear dependence.

4.1.4 'Nuclear 2' Interaction

Figure (4.7) demonstrates the radius dependence for the Nuclear 2 interaction. The results are similar to the Nuclear 1 case with a few changes. Most notably, the USHF result performs much better at smaller radii with this interaction than for Nuclear 1 due to the smaller hard-core repulsion leading to less correlation in the exact ground state. As a result, the BSHF and RSHF give less of an improvement for these ring sizes than they did for Nuclear 1. For smaller radii, when the particles mainly repel each other, the RSHF method is able to improve significantly on the BSHF method while for larger radii it gives the same energy. Another change is that the minimum in the energy has shifted to smaller radii (compared to Nuclear 1) which is a result of the smaller classical equilibrium distance for Nuclear 2.

4.2 Number of particles dependence

4.2.1 Repulsive Coulomb Interaction

Figure (4.8) shows the dependence of the energy per particle on the number of particles on the ring for the repulsive Coulomb interaction with $R = 2$ and $V_0 = 5$. The energy per particle increases monotonically with the number of particles for all four methods. The effectiveness of both the BSHF and RSHF methods remains approximately constant with

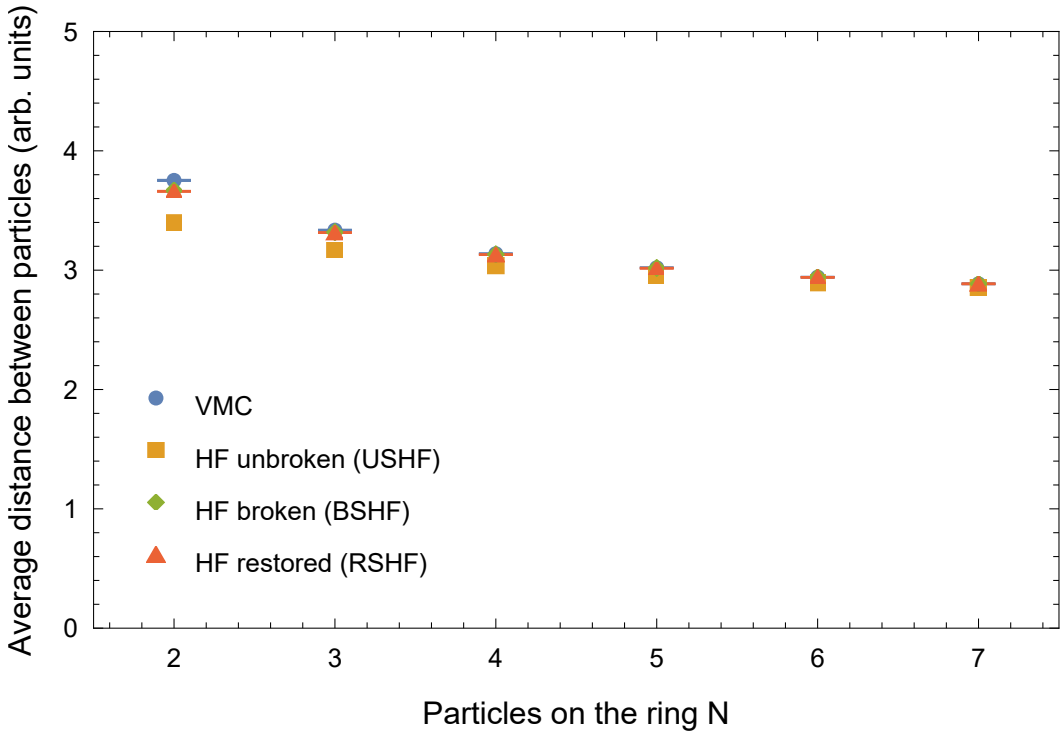

Figure 4.9: Average distance between particles for a quantum ring with repulsive Coulomb interactions of strength $V_0 = 5$, radius $R = 2$ and varying numbers of particles on the ring, N.

N. The BSHF method accounts from between 40% and 50% of the correlation energy while the RSHF gives a significant improvement of between 80% and 90% for all numbers of particles investigated. Both methods do not give significant absolute improvement to the energy because the USHF method already gives a good approximation to the VMC ground state energy.

Figure (4.9) shows the average distance between particles for the repulsive Coulomb interaction. Each of the methods has the highest average distance for $N = 2$ particles but this decreases to a constant value at larger number of particles. The greatest disagreement between the methods is also at lower number of particles, with the VMC result having the larger average distance and the USHF having the lowest. For this interaction, a larger average distance is an indication of greater correlation in particle position which allows particles to be further away from each other on average in order to lower the system's potential energy.

The approximately linear dependence of the energy per particle for each method can be explained by considering the number of pairwise interactions in the system. A system with N particles has $\frac{N}{2}(N-1)$ total interactions between pairs of particles. Since the range of the Coulomb interaction is much larger than the radius of the ring, each of these interactions contributes an approximately equal amount of potential energy to the system. Thus the total potential energy scales approximately with $N(N-1)$ and the potential energy per particle scales with $N-1$. The deviation from this linear dependence comes partly from a small increase in potential energy due to particles getting closer together

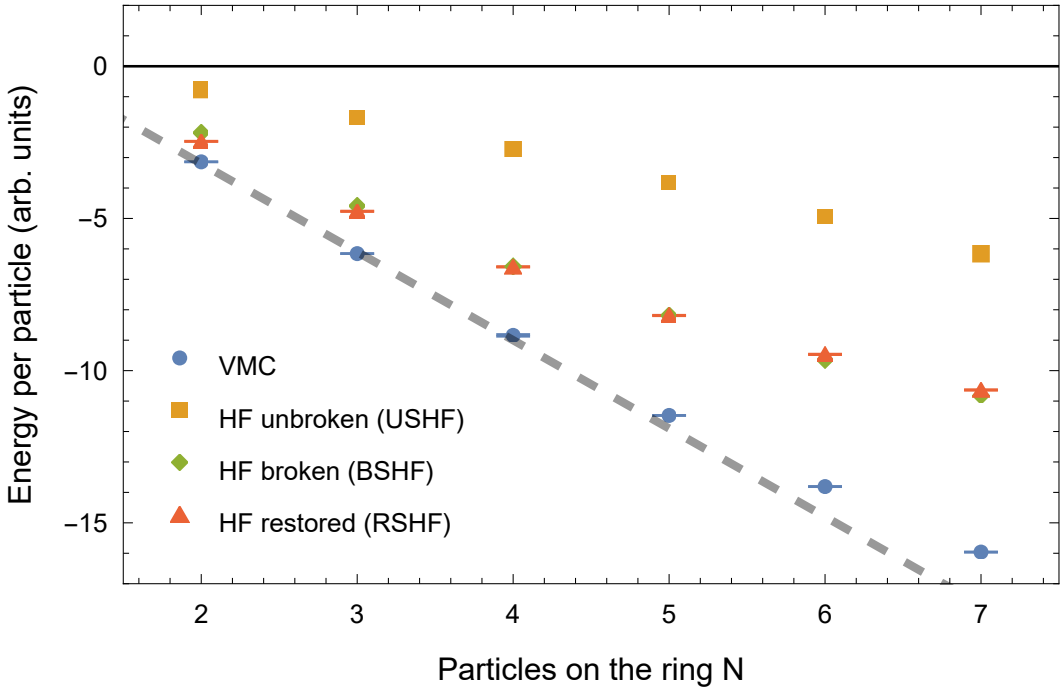

Figure 4.10: Energy per particle for a quantum ring with attractive Coulomb interactions of strength $V_0 = 5$, radius $R = 2$, and varying numbers of particles on the ring, N. The dashed line is included to show the deviation from a linear dependence.

on average (as shown in figure (4.9)) and partly from the kinetic energy per particle contribution to the total energy. As particles get closer together (as a result of more particles being added to the finite size ring), the Pauli exclusion principle increases their kinetic energy. This is supported by considering the kinetic energy per particle for the USHF method. For $N = 2$ it is 0.03 arbitrary units while for $N = 7$, it has risen to 0.5 arbitrary units.

4.2.2 Attractive Coulomb Interaction

Figure (4.10) demonstrates the particle number dependence for the attractive Coulomb interaction. For each method, the energy per particle decreases with the number of particles. Over all particle numbers, the BSHF and RSHF give similar results with the RSHF performing slightly better for $N \leq 5$ and slightly worse for $N > 5$. Both methods account for a greater portion of the correlation energy for a smaller number of particles and this portion decreases with increasing N.

The average distance between particles is shown in figure (4.9). The VMC, BSHF and RSHF methods have a low average distance between particles which increases with increasing N, while the USHF has a higher average distance and decreases with N. The increase of average distance in the methods with correlation is again due to localisation of particles to one region of the ring. As more particles are added to this region, it grows larger which may be due to the Pauli exclusion principle 'pushing' the particles away from each other. As the region grows, particles within the region get further apart on average.

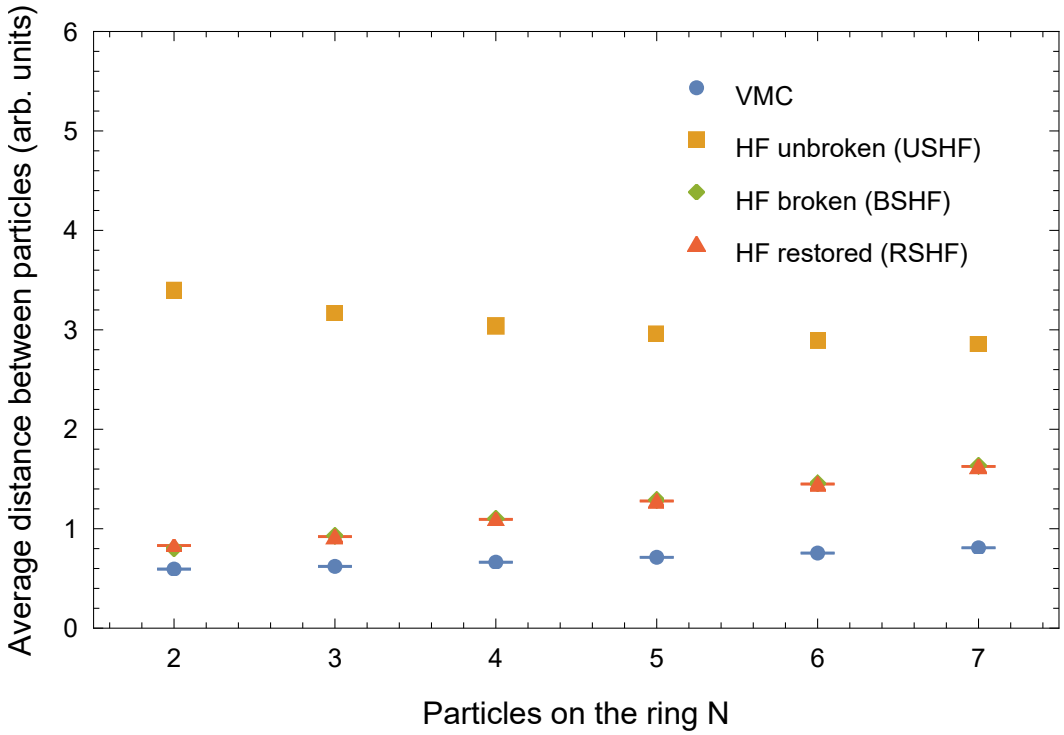

Figure 4.11: Average distance between particles for a quantum ring with attractive Coulomb interactions of strength $V_0 = 5$, radius $R = 2$ and varying numbers of particles on the ring, N.

Without the correlation in particle positions, the USHF average distance decreases with more particles in the same way as the repulsive Coulomb case.

The approximately linear dependence of the energy per particle on N can be explained in a similar way to the repulsive Coulomb case, since the range of the interaction is still much larger than the size of ring. The cause of the small positive deviation from linear dependence is also probably due to the Pauli exclusion principle like the repulsive Coulomb case.

4.2.3 'Nuclear 1' Interaction

Figure (4.12) shows the particle number dependence for the Nuclear 1 interaction. For the VMC, BSHF and RSHF methods, the energy per particle decreases almost linearly with the number of particles while the USHF method initially decreases to a negative minimum then increases with N. The N-dependence of the USHF method can be explained by considering the Nuclear 1 interaction potential. With a small number of uncorrelated particles on the ring, they mostly can be found at distances from each other where the interaction potential is negative. As more particles are added and they get closer together on average, they begin to experience more of the hard-core repulsion component of the interaction potential and so the energy per particle increases. The approximate linear decrease of the VMC, BSHF and RSHF methods is likely for the same reason as the Coulomb cases. The range of Nuclear 1 interaction is still large enough for all particles

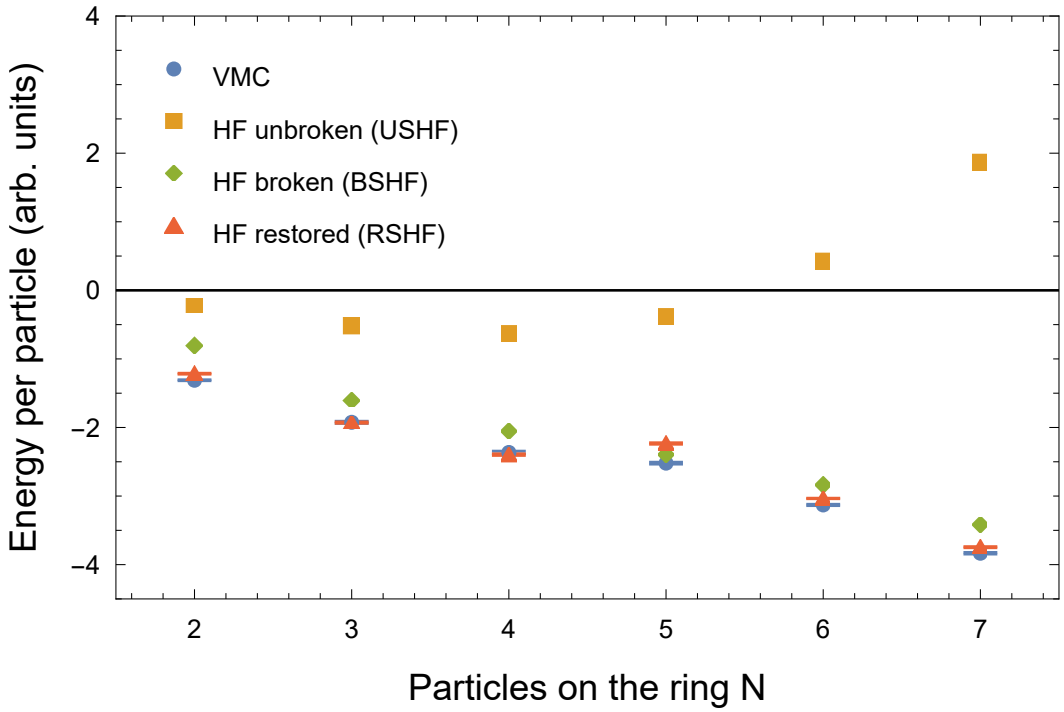

Figure 4.12: Energy per particle for a quantum ring with Nuclear 1 interactions of strength $V_0 = 5$, radius $R = 2$, and varying numbers of particles on the ring, N.

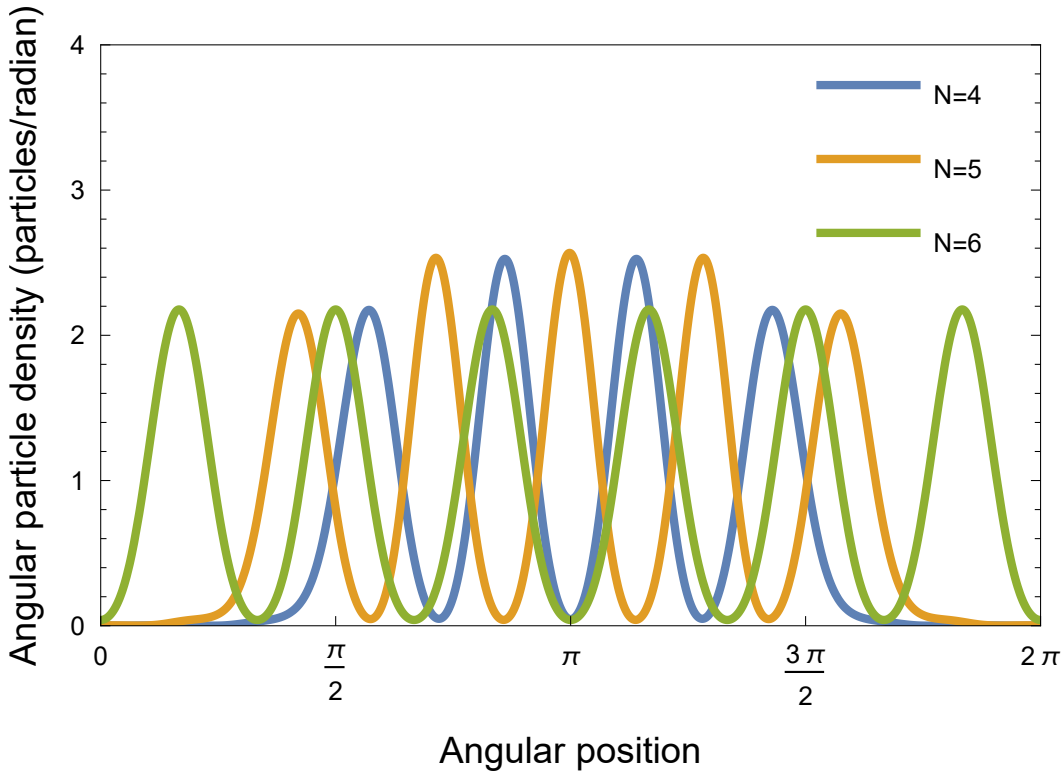

Figure 4.13: Angular particle densities of the BSHF ground state with the Nuclear 1 interaction of strength $V_0 = 5$ and radius $R = 2$.

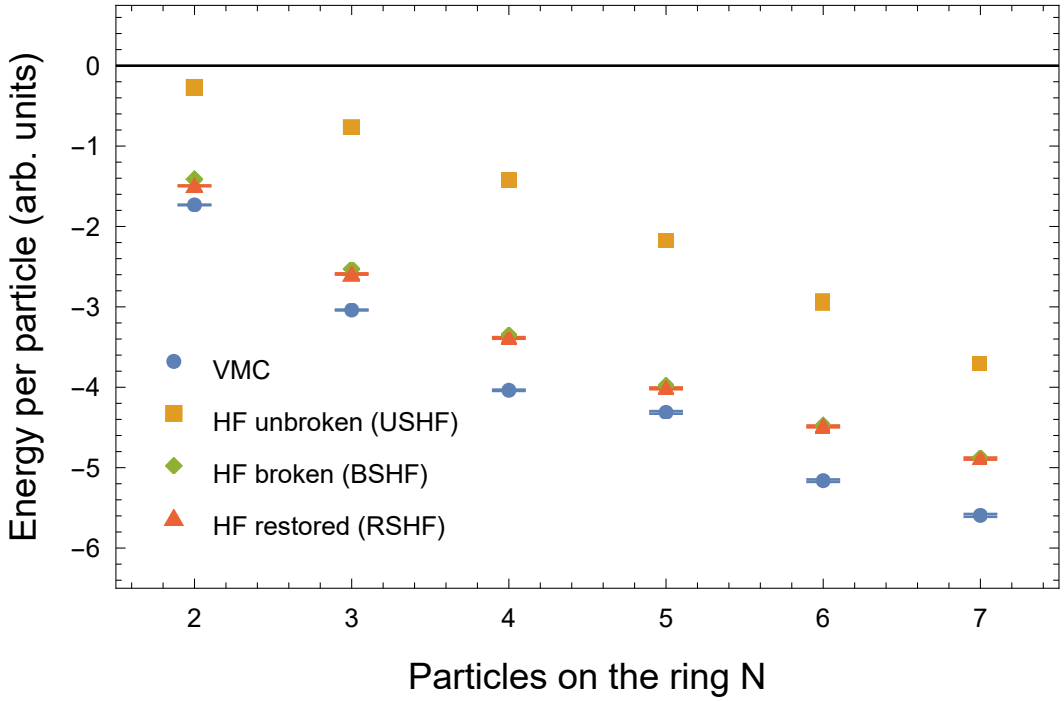

Figure 4.14: Energy per particle for a quantum ring with Nuclear 2 interactions of strength $V_0 = 5$, radius $R = 2$, and varying numbers of particles on the ring, N.

on the ring to interact with each other, thus, the total potential energy scales with $N(N-1)$. Due to the correlation between the particles, they are likely to be found at distances where the interaction is attractive, thus we see a linear decrease in the energy per particle.

In the same way as the radius-varying case, both the BSHF and RSHF methods perform very well for this interaction and are able to account for most of the correlation energy for all numbers of particles. The RSHF performs the best, accounting for almost all of the remaining correlation energy that the BSHF method missed. The only result which does not follow this pattern is the $N = 5$ data point. The VMC, BSHF and RSHF energies per particle for $N = 5$ also do not follow the general trend of the other N values. This may be a result of the methods not properly converging here or may be due to some transition in the ground state. Figure (4.13) shows that for the BSHF method, the transition between particles spread over the entire ring at higher N, and particles bunching together on a region of the ring at lower N, occurs between $N = 5$ and $N = 6$. It may be that around this point, the methods oscillate between the two types of wave functions which are similar in energy, hence taking longer to converge.

4.2.4 'Nuclear 2' Interaction

Figure (4.14) shows the particle number dependence for the Nuclear 2 interaction. In several ways it is similar to both the attractive Coulomb and Nuclear 1 interactions, with an approximately linear decrease in energy per particle for all the methods due to the

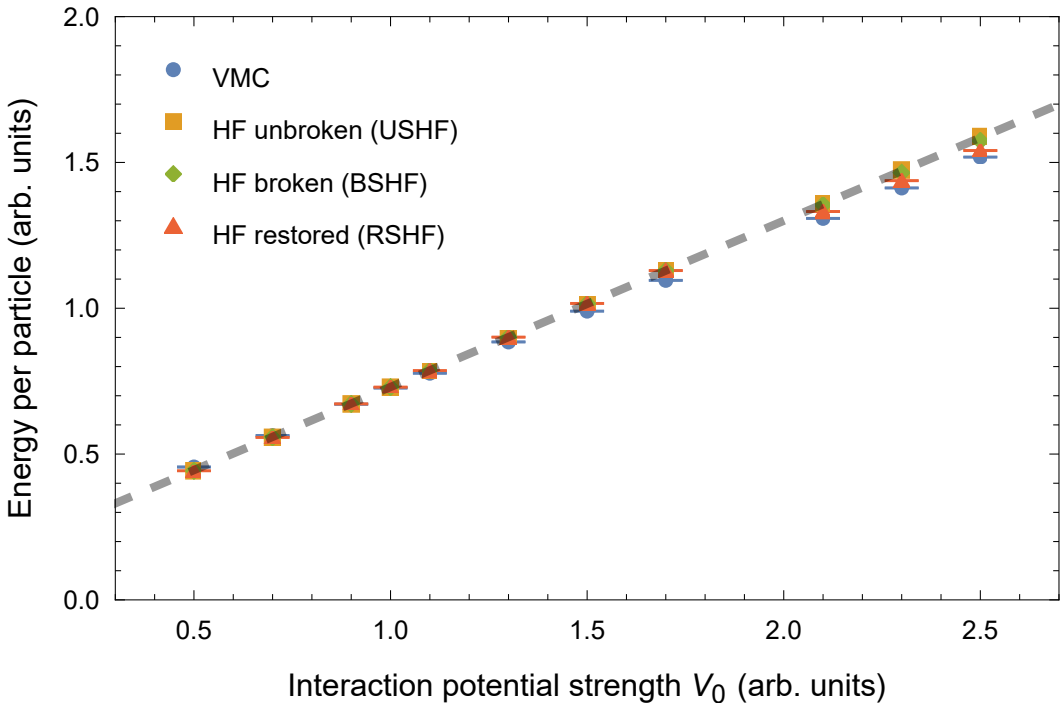

Figure 4.15: Energy per particle for a quantum ring with repulsive Coulomb interactions, radius $R = 2$, $N = 4$ particles and varying strength of the interaction potential V_0. The dashed line is included to show the linear dependence of the USHF method.

attractive component of the Nuclear 2 potential and the small size of the ring. Unlike the Nuclear 1 case, the USHF method does not increase in energy under the range of N investigated which is likely due to the weaker and shorter ranged hard-core repulsion of Nuclear 2 compared to Nuclear 1. The BSHF and RSHF methods performed well across a range of N values and were able to account for between 60% and 90% of the correlation energy. Like the attractive Coulomb case, the RSHF method performed a few percent better than the BSHF method for $N = 2$ and $N = 3$ particles but gave effectively the same energy for larger N.

4.3 Interaction potential strength dependence

4.3.1 Repulsive Coulomb Interaction

Figure (4.15) shows the V_0 dependence for the repulsive Coulomb interaction. The USHF has a linear dependence on V_0 since its kinetic energy per particle is constant and its potential energy is directly proportional to V_0. In the other three methods at larger V_0 values, the potential energy contribution is slightly reduced by localising the particle positions. This increases the kinetic energy per particle, so it is only when the potential is stronger that localisation lowers the ground state energy. The transition between localised and de-localised is indicated by the energy per particle falling below the USHF energy. For the VMC method this occurs at around $V_0 = 1$, while BSHF and RSHF

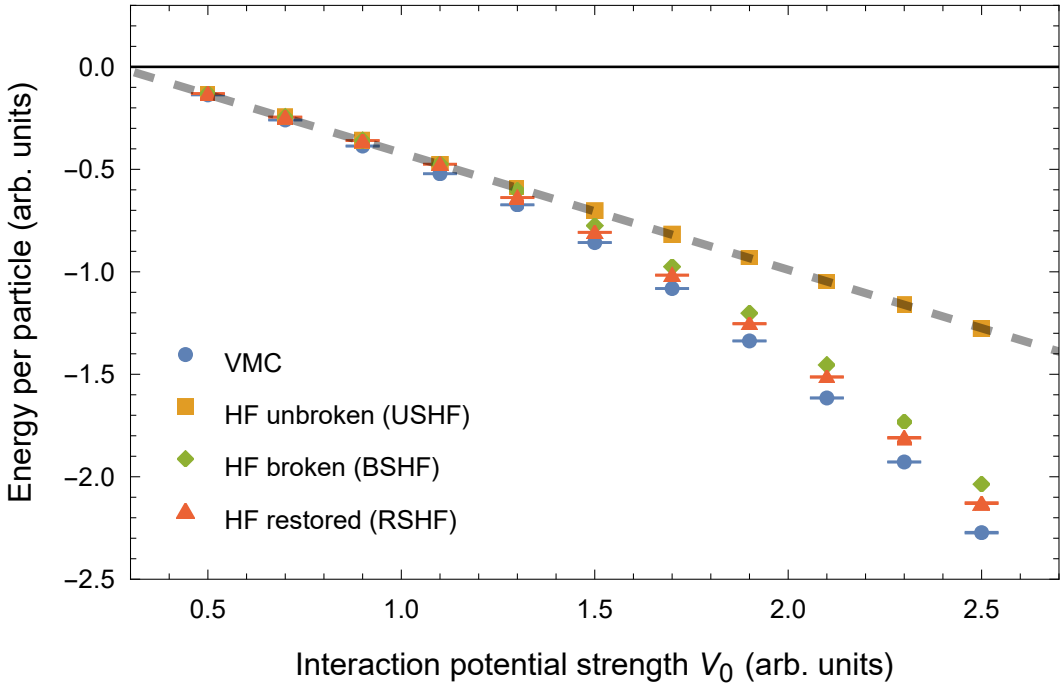

Figure 4.16: Energy per particle for a quantum ring with attractive Coulomb interactions, radius $R = 2$, $N = 4$ particles and varying strength of the interaction potential V_0. The dashed line is included to show the linear dependence of the USHF method.

transition occurs around $V_0 = 1.7$. Once the symmetry breaking has occurred in the BSHF method, the RSHF method begins to perform significantly better than the BSHF method. At $V_0 = 1.7$, the BSHF accounts for 0.6% of the correlation energy while the RSHF gives 3%. At $V_0 = 2.5$, the BSHF accounts for 20% while the RSHF gives 68% of the correlation energy.

4.3.2 Attractive Coulomb Interaction

Figure (4.16) shows the potential strength dependence for the attractive Coulomb interaction. As with the repulsive Coulomb case, the wave function of the USHF method does not vary with V_0, so its kinetic energy remains constant. Since its potential energy is proportional to V_0, its total energy per particle has a linear dependence. Also similar to the repulsive Coulomb case, the VMC, BSHF and RSHF fall below the USHF energy at particular values of V_0. For the VMC method this occurs around $V_0 = 0.7$ while for the BSHF and RSHF it occurs at $V_0 = 1.3$. This additional binding energy is again likely due to the localisation of particles positions to one region of the ring. It cannot occur at lower values of V_0 because the kinetic energy 'cost' of localisation is larger than the potential energy decrease.

Both the BSHF and RSHF perform reasonably well for $V_0 > 1.3$, accounting for a greater percentage of the correlation energy as the VMC method deviates further from the USHF energy. The RSHF still performs slightly better than the BSHF, giving an improvement of around -0.05 arbitrary units of energy per particle across the range of V_0 studied and

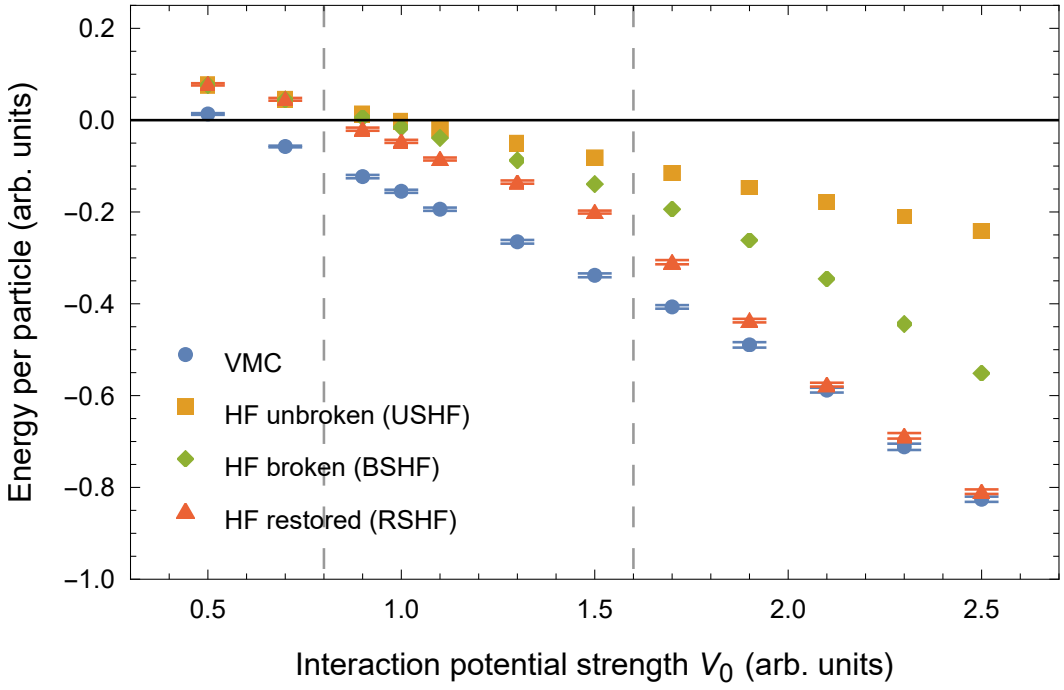

Figure 4.17: Energy per particle for a quantum ring with Nuclear 1 interactions, radius $R = 2$, $N = 4$ particles and varying strength of the interaction potential V_0. The vertical dashed lines indicate the phase transitions for the BSHF and RSHF methods.

the magnitude of the improvement slowly increases with V_0.

4.3.3 'Nuclear 1' Interaction

Figure (4.17) shows the V_0 dependence for the Nuclear 1 interaction. Once again the USHF method has a linear dependence for the same reasons as the other interactions. For small V_0, the energy per particle is positive due to the dominance of kinetic energy. As V_0 increases, the attractive component of Nuclear 1 potential energy takes over and the energy becomes negative. The other methods also show a steady decrease in energy, however, with the gradient changing at different regions of V_0.

Figure (4.18) shows the angular particle density for the BSHF result with the Nuclear 1 interaction and different values for V_0. For $V_0 < 0.8$, the density is flat, between $V_0 = 0.8$ and $V_0 = 1.6$, the density shows four equally spaced peaks spread out over the whole ring, and for $V_0 > 1.6$, the density shows bunching of the particles on one region of the ring. These differing behaviours can be considered as phases of the BSHF and RSHF ground states and the values $V_0 \approx 0.8$ and $V_0 \approx 1.6$, the phase transitions.

Figure (4.19) shows the average distance between particles as a function of V_0 which allows for the exploration of these phase transitions in more detail. For $V_0 < 0.8$, the BSHF and RSHF average distance match the USHF average distance which remains constant as its wave function does not change with V_0. For $0.8 < V_0 < 1.6$, the average distance increases with V_0. This indicates that the potential energy is being minimised

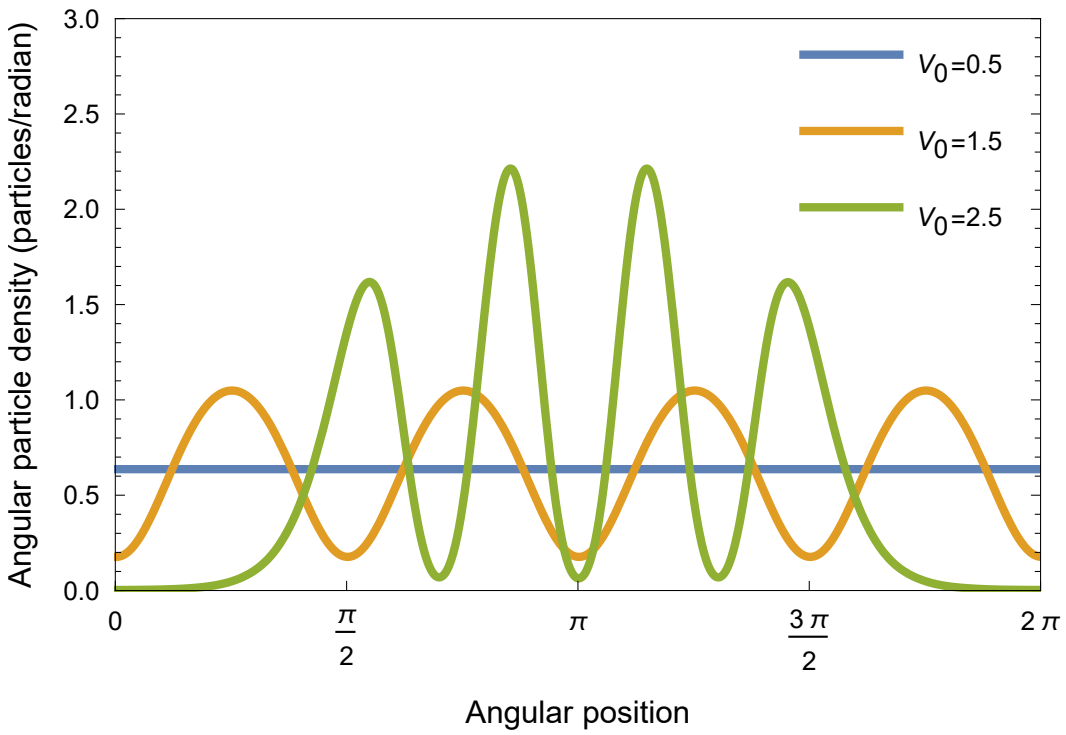

Figure 4.18: Angular particle densities of the BSHF ground state with the Nuclear 1 interaction, radius $R = 2$ and $N = 4$ particles.

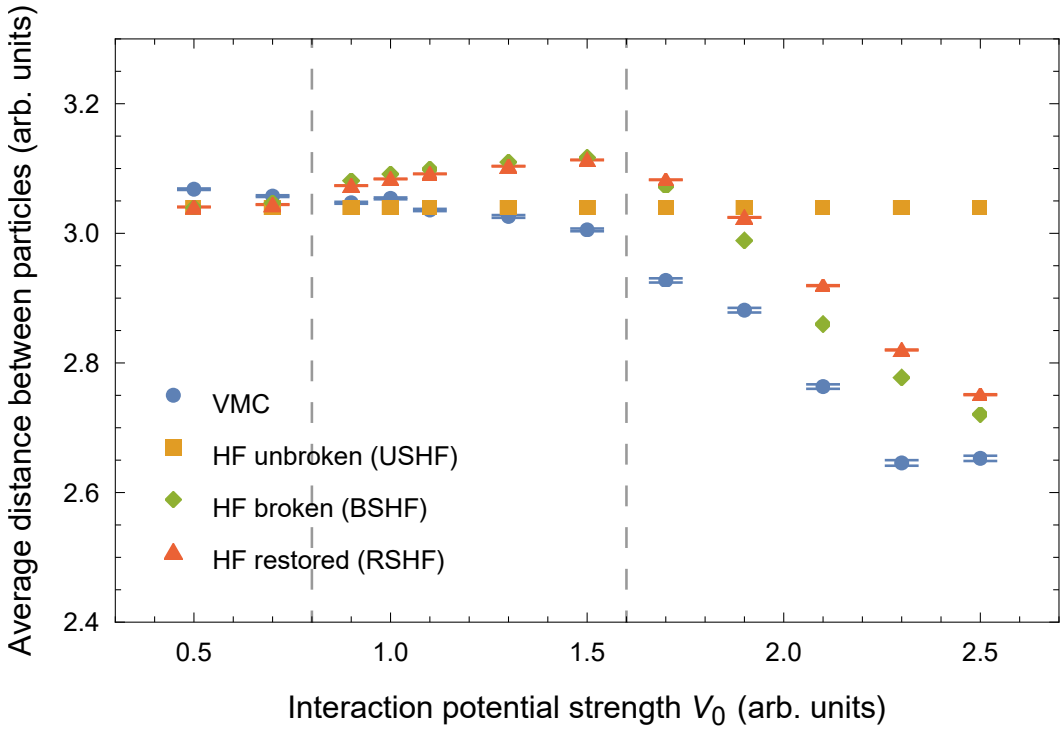

Figure 4.19: Average distance between particles for a quantum ring with the Nuclear 1 interaction, radius $R = 2$, $N = 4$ particles and varying strength of the potential, V_0. The vertical dashed lines indicate the phase transitions for the BSHF and RSHF methods.

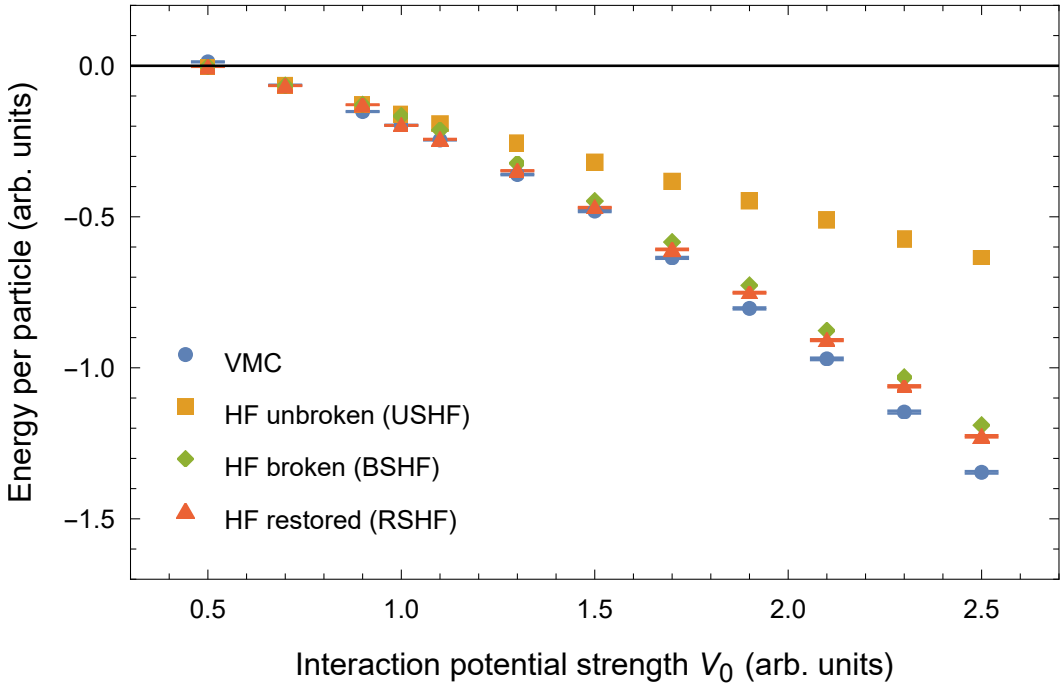

Figure 4.20: Energy per particle for a quantum ring with Nuclear 2 interactions, radius $R = 2$, $N = 4$ particles and varying strength of the interaction potential V_0.

by particles spreading out on the ring, with a higher V_0 allowing for more localisation and hence a higher average distance between particles. For $V_0 > 1.6$, the average distance for the BSHF and RSHF methods decreases with increasing V_0, suggesting that the potential energy is being minimised by particles bunching together. The higher the value of V_0, the more tightly the particle wave functions are able to bunch and the smaller the average distance between particles. Given that the average distance between particles for the VMC method decreases across the whole range of V_0 investigated, this suggests that bunching is probably the dominant form of spatial correlation between particles and the method does not exhibit a phase transition in this range.

Returning to figure (4.17), we see that the performance of the BSHF and RSHF methods changes significantly between phases. Clearly, they perform the worst when no symmetry is broken in the first phase. In the second phase, the BSHF method accounts for a maximum of 22% of the correlation energy while the RSHF reaches a maximum of 46%. In the third phase, both methods significantly improve, with the BSHF reaching up to 53% at $V_0 = 2.5$ and the RSHF reaching 97%. The improvement can be explained by considering the significant difference in the systems modelled by the VMC versus the Hartree-Fock methods. For $V_0 < 1.6$, the VMC method is modelling a system of bunched particles while the BSHF and RSHF methods are modelling spread out particles. It is not until V_0 is increased past 1.6 that the systems predicted by the methods become more similar and the energies improve.

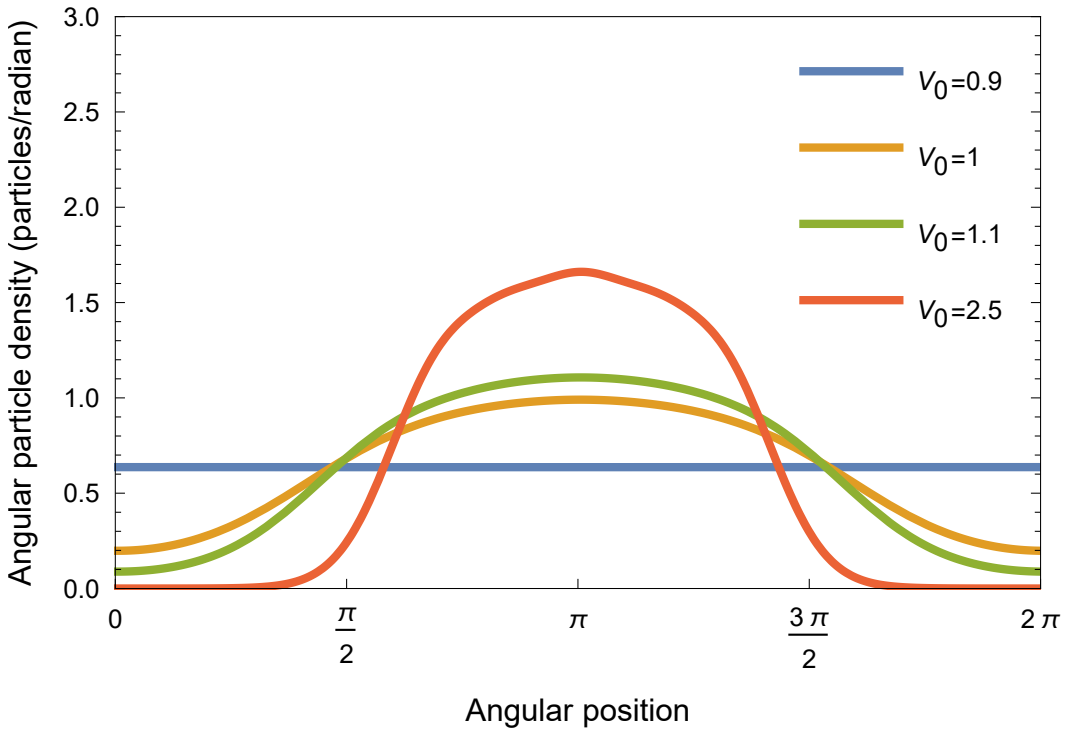

Figure 4.21: Angular particle density of the BSHF ground state with the Nuclear 2 interaction, radius $R = 2$ and $N = 4$ particles.

4.3.4 'Nuclear 2' Interaction

Finally, figure (4.20) shows the V_0 dependence for the Nuclear 2 interaction. Like the previous interactions, the USHF energy has a linear dependence. There is also a clear phase transition from no localisation to bunching for the other three methods as is evident by their energies falling below the USHF energy. For this interaction, both the BSHF and RSHF methods perform well for all $V_0 > 1$, with the RSHF only giving a small improvement to the BSHF method.

The angular particle densities for the BSHF method in figure (4.21) show a flat density for $V_0 < 1$ indicating no rotational symmetry breaking has occurred. For $V_0 > 1$, the angular densities consist of a single peak localised to one region of the ring, unlike the self-bound system of Nuclear 1 (for $V_0 > 1.6$) which had a group of four peaks. The difference is likely to be a result of the weaker hard-core repulsion of Nuclear 2 which is not strong enough to make the particles spread out within the self-bound system. As a result, only one phase transition is observed for this case.

4.4 BSHF and RSHF discussion

In this section, I will summarise the effectiveness of the BSHF and RSHF methods together in the different regions of the parameter space before discussing the regions where the RSHF method significantly improves on the BSHF result.

4.4.1 Absolute improvement to the USHF method

Generally, the two methods seem to give little absolute improvement in energy per particle in weakly repulsive systems. These included the repulsive Coulomb interaction for all N, R, and V_0 as well as the two nuclear interactions when V_0 was small. It is likely this was due to little correlation in particle positions in the true ground state and the correlations that were present did not significantly reduce the energy per particle compared to the USHF method. The methods also gave little improvement in the moderate potential strength Nuclear 1 interaction which was a result of their wave functions optimising in a different way to the VMC ground state. The BSHF and RSHF methods optimised their potential energy by having the particles spread out on the ring while the VMC method optimised by having the particles bunch together.

The two methods gave a much larger improvement with attractive potentials where the particles formed self bound systems. These systems included the attractive Coulomb potential at all R, N and V_0 and the two nuclear potentials at larger R and stronger V_0. In these cases, the USHF wave function without particle localisation was a particularly bad approximation to the true wave function, so it is not surprising that the symmetry breaking and restoration were able to improve on it. In additions to these systems, the methods gave a large improvement in the case of the Nuclear 1 interaction on small radii. In this case, the repulsion between particles was strong, resulting in a high potential energy for the USHF state and hence a large improvement in energy from the particles spreading out on the ring.

4.4.2 Relative improvements of the RSHF to the BSHF method

The RSHF method typically gave a significant relative improvement (greater than 30% of the correlation energy) to the BSHF method in repulsive systems in the cases where the symmetry was broken. These included the repulsive Coulomb systems for larger V_0 and N and the two nuclear interactions at smaller values for R. This suggests that the RSHF method may have use in modelling real, many-fermion systems in which the particles repel each other and are externally bound.

The RSHF method performed relatively worse in attractive systems (the attractive Coulomb and Nuclear 2 systems), typically only improving on the BSHF method by a few percent. In these systems, the BSHF state had particles bunched together on one region of the ring. This suggest that the symmetry restoration operation applied to the position of the bunch on the ring does not significantly affect the energy of the resultant state.

An exception to this poor relative performance in attractive systems was the Nuclear 1 interaction at larger V_0 values whose BSHF density function exhibited two types of spatial correlation between the particles: bunching on one region of the ring to maximise the attractive component of the potential and spreading out within the bunch to minimise the hard-core repulsive component. It may be that RSHF method is able to more effectively incorporate both types of correlation at once, thus improving significantly on the BSHF

method. In this project, the double nature of the correlations was found unintentionally. To further explore the effectiveness of the RSHF method when applied to systems with multiple types of correlations, I could try breaking other symmetries of a quantum ring (such as the phase of the wave function) along with breaking rotational symmetry. By comparing the improvement brought by the RSHF to the BSHF method for when one symmetry was broken and restored, to when two symmetries are broken and restored, I could test if the amazing performance of the RSHF for the Nuclear 1 interaction was a result of the multiple types of correlations in the BSHF ground state.

Chapter 5

Conclusion

Approximate methods are commonly used to find solutions to the quantum many-body problem for real systems and their accuracy in these systems is an important consideration in their use. In this thesis, I used the ground state of the quantum ring model to benchmark the Hartree-Fock method with broken and restored rotational symmetry. By varying the radius of the ring, the number of particles on the ring and the strength and type of interaction between the particles, I was able to gain a comprehensive understanding of the effectiveness of each method in different electronic and nuclear-like systems.

I found that rotational symmetry breaking in the Hartree-Fock method brought little improvement to weakly repulsive systems where the spatial correlations between particles were low. As the strength of the interaction increased, so did the strength of correlations and the relative effectiveness of symmetry breaking. This suggests that interaction strength is an important consideration for the use of symmetry breaking in mean-field methods for repulsive systems. For all repulsive systems, symmetry restoration was able to improve upon the symmetry-broken solution. Thus, if high accuracy is required in these systems, implementing a rotational symmetry restoration is likely to be worth doing.

In contrast, I found that symmetry breaking was vital in almost all attractive systems provided the ring was large enough for the particles to form a self-bound system. Despite its significant improvement to the symmetry-unbroken Hartree-Fock method, there were still many systems in which the approximation to the true ground state remained poor, suggesting that rotational symmetry breaking alone is likely not able to account for all of the correlations induced by an attractive interaction. In general, the restoration of symmetry in these systems provided little if any improvements at low numbers of particles. The small size of the improvements achieved through symmetry restoration relative to the difference in energy to the true ground state suggests that symmetry restoration might be unnecessary for improving the energy of the ground state. As mentioned in the introduction, having states with well-defined quantum numbers (such as the total angular momentum after rotational symmetry restoration) can often be important for the calculation of observables such as transition amplitudes, so rotational symmetry restoration still has some use in these systems.

Finally, for the Nuclear 1 interaction which was characterised by a stronger repulsive

core, I found that the symmetry restoration performed extremely well relative to the symmetry broken method at stronger potentials strengths. In this regime, the breaking of the rotational symmetry resulted in two types of spatial correlation: so-called 'bunching' of the particle wave functions at one region of the ring forming a self-bound system and 'spreading-out' of the particles within the self-bound system. The rotational symmetry restoration applied to the first correlation type would have restored the symmetry of the position of the centre of mass of the self bound-system while the symmetry restoration applied to the second correlation type would have restored the symmetry of the position of the particles within the self-bound system. It was thought that the application of the rotational symmetry restoration to both correlation types at the same time was what led to the observed significant improvement, though more testing with different symmetries is required to confirm this.

A major caveat to the above conclusions lies in the dimensionality of the system. We already discussed how the dimensionality can significantly affect the correlation energy for a many-electron spherium in Chapter 2 [30], so it would be natural to assume that dimensionality would also change the effectiveness of the approximate methods. Thus, the main direction for further research is to extend this study to higher dimensional quantum rings, in particular $\mathcal{D} = 3$-dimensional glomium which was shown by Loos and Gill [30] to be the most similar to more realistic models of three-dimensional systems.

In this work, I only investigated and compared ground state energies, which were the easiest to find and made comparison between methods straightforward. However, this only provides a limited picture of the effectiveness of approximate methods which are often used to find higher energy states and the transition energies between them. It may be that the effectiveness of each method depends on the energy eigenstate being approximated. Thus, future work can compare more energies levels as predicted by each approximate method to obtain a more complete picture.

Finally, there are other symmetries to be broken in real systems and several of these could be explored in the quantum ring. In particular, the system was invariant under changes to the complex phase of the ground state wave function. This is known as a U(1) gauge symmetry and results in a conserved number of particles on the ring. Breaking this symmetry allows for the incorporation of pairing correlations between particles which is a key component of the Hartree-Fock-Bogliobov method. Since most modern implementations of the Hartree-Fock method use this extension, it would valuable to benchmark it on a quantum ring.

Constant local energy of energy eigenstates

One of the properties of the ground state (and indeed any energy eigenstate of a quantum system) is that its local energy, which can be interpreted as the energy of a particular configuration of particle coordinates, is equal to the energy of that eigenstate,

$$E_L(\boldsymbol{\theta}) = \frac{H\Psi_i(\boldsymbol{\theta})}{\Psi_i(\boldsymbol{\theta})} = E_i, \tag{A.1}$$

where H is the Hamiltonian of the system in the given coordinate basis and $\Psi_i(\boldsymbol{\theta})$ is the energy eigenstate's wave function with energy E_i. To show this, I start with the time-independent Schrödinger equation,

$$\hat{H}|\Psi_i\rangle = E_i|\Psi_i\rangle, \tag{A.2}$$

and contract both sides with an arbitrary position eigenstate $|\boldsymbol{\theta}\rangle$,

$$\langle\boldsymbol{\theta}|\hat{H}|\Psi_i\rangle = \langle\boldsymbol{\theta}|E_i|\Psi_i\rangle. \tag{A.3}$$

I recognise the wave function as $\Psi_i(\boldsymbol{\theta}) = \langle\boldsymbol{\theta}|\Psi_i\rangle$ and insert the identity operator $\hat{1} = \int d\boldsymbol{\theta'}\, |\boldsymbol{\theta'}\rangle\langle\boldsymbol{\theta'}|$ to get

$$\langle\boldsymbol{\theta}|\hat{H}\left(\int d\boldsymbol{\theta'}\, |\boldsymbol{\theta'}\rangle\langle\boldsymbol{\theta'}|\right)|\Psi_i\rangle = E_i\Psi_i(\boldsymbol{\theta}). \tag{A.4}$$

Then $\langle\boldsymbol{\theta'}|\Psi_i\rangle = \Psi_i(\boldsymbol{\theta'})$ and $\langle\boldsymbol{\theta}|\hat{H}|\boldsymbol{\theta'}\rangle = \delta(\boldsymbol{\theta'} - \boldsymbol{\theta})H$, where H is now in the position basis. This gives

$$\int d\boldsymbol{\theta'}\, \delta(\boldsymbol{\theta'} - \boldsymbol{\theta})H\Psi_i(\boldsymbol{\theta'}) = E_i\Psi_i(\boldsymbol{\theta}), \tag{A.5}$$

$$H\Psi_i(\boldsymbol{\theta}) = E_i\Psi_i(\boldsymbol{\theta}), \tag{A.6}$$

and finally,

$$E_L(\boldsymbol{\theta}) = \frac{H\Psi_i(\boldsymbol{\theta})}{\Psi_i(\boldsymbol{\theta})} = E_i \tag{A.7}$$

for $\Psi_i(\boldsymbol{\theta}) \neq 0$.

Condition to prevent divergence of local energy

I want to find some condition on the trial ground state wave function which prevents the local energy, $E_L(\boldsymbol{\theta}) = \Psi(\boldsymbol{\theta})^{-1} H \Psi(\boldsymbol{\theta})$, from diverging at Coulomb-like singular points in the potential. By Coulomb-like, I mean the interaction potential becomes proportional to $1/r_{\alpha\beta}$ in the limit of $r_{\alpha\beta} \to 0$, that is, when particles α and β approach one another.

The local energy is comprised of kinetic and potential components:

$$E_L(\boldsymbol{\theta}) = \frac{H\Psi(\boldsymbol{\theta})}{\Psi(\boldsymbol{\theta})} = -\frac{1}{2\Psi R^2} \sum_{\alpha=1}^{N} \frac{\partial^2 \Psi}{\partial \theta_\alpha^2} + \sum_{\alpha<\beta}^{N} V(r_{\alpha\beta}), \tag{B.1}$$

where $r_{\alpha\beta} = 2R \left| \sin\left(\frac{\theta_\alpha - \theta_\beta}{2}\right) \right|$. We are interested in two-body interaction potentials which diverge as $\frac{V_1}{r_{\alpha\beta}}$ as $r_{\alpha\beta} \to 0$. For the local energy to not diverge, we need a component of the kinetic energy of the wave function to diverge to the opposite extreme, that is, it needs to go to $-\frac{V_1}{r_{\alpha\beta}}$ as $r_{\alpha\beta} \to 0$.

I assume that the wave function depends only on the distances between the particles and not directly on the positions of the particles (which is the case for the trial wave functions used in the variational Monte Carlo method in this thesis), so $\Psi(r_{12}, r_{13}, ..., r_{1n}, ..., r_{(n-1)n})$. The derivatives of the wave function are

$$\frac{\partial \Psi}{\partial \theta_\alpha} = \sum_{\beta \neq \alpha}^{N} \frac{\partial r_{\alpha\beta}}{\partial \theta_\alpha} \frac{\partial \Psi}{\partial r_{\alpha\beta}}, \tag{B.2}$$

$$\frac{\partial^2 \Psi}{\partial \theta_\alpha^2} = \sum_{\beta \neq \alpha}^{N} \left(\frac{\partial^2 r_{\alpha\beta}}{\partial \theta_\alpha^2} \frac{\partial \Psi}{\partial r_{\alpha\beta}} + \left(\frac{\partial r_{\alpha\beta}}{\partial \theta_\alpha} \right)^2 \frac{\partial^2 \Psi}{\partial r_{\alpha\beta}^2} + \frac{\partial r_{\alpha\beta}}{\partial \theta_\alpha} \sum_{\substack{\gamma \neq \alpha \\ \gamma \neq \beta}} \frac{\partial r_{\alpha\gamma}}{\partial \theta_\alpha} \frac{\partial^2 \Psi}{\partial r_{\alpha\beta} \partial r_{\alpha\gamma}} \right). \tag{B.3}$$

I will now consider the component of the potential energy which diverges as particles μ and ν approach one another. It is expected that the diverging potential will be cancelled by a kinetic energy term involving the derivative of the wave function with respect to $r_{\mu\nu}$ in the same way as the Kato cusp condition which prevents the divergence of the local energy in three-dimensional systems [26]. The choices of terms which could cancel

the divergence are $\frac{\partial\Psi}{\partial r_{\mu\nu}}$, $\frac{\partial^2\Psi}{\partial r_{\mu\nu}^2}$, $\frac{\partial^2\Psi}{\partial r_{\mu\nu}\partial r_{\mu\rho}}$ or $\frac{\partial^2\Psi}{\partial r_{\mu\nu}\partial r_{\nu\rho}}$ for some other particle ρ. The kinetic energy term will include the addition $-\frac{1}{2\Psi R^2}\left(\frac{\partial^2\Psi}{\partial\theta_\mu^2}+\frac{\partial^2\Psi}{\partial\theta_\nu^2}\right)$ so the possibly relevant terms are:

$$-\frac{1}{2\Psi R^2}\left(\frac{\partial^2 r_{\mu\nu}}{\partial\theta_\mu^2}\frac{\partial\Psi}{\partial r_{\mu\nu}}+\frac{\partial^2 r_{\mu\nu}}{\partial\theta_\nu^2}\frac{\partial\Psi}{\partial r_{\mu\nu}}+\left(\frac{\partial r_{\mu\nu}}{\partial\theta_\mu}\right)^2\frac{\partial^2\Psi}{\partial r_{\mu\nu}^2}+\left(\frac{\partial r_{\mu\nu}}{\partial\theta_\nu}\right)^2\frac{\partial^2\Psi}{\partial r_{\mu\nu}^2}\right.$$
$$\left.+2\frac{\partial r_{\mu\nu}}{\partial\theta_\mu}\sum_{\substack{\gamma\neq\alpha\\ \gamma\neq\beta}}\frac{\partial r_{\mu\rho}}{\partial\theta_\mu}\frac{\partial^2\Psi}{\partial r_{\mu\nu}\partial r_{\mu\rho}}+2\frac{\partial r_{\mu\nu}}{\partial\theta_\nu}\sum_{\substack{\gamma\neq\alpha\\ \gamma\neq\beta}}\frac{\partial r_{\nu\rho}}{\partial\theta_\nu}\frac{\partial^2\Psi}{\partial r_{\mu\nu}\partial r_{\nu\rho}}\right) \tag{B.4}$$

Most of these terms will not contribute to the cancellation of the divergence. Firstly, $\frac{\partial^2 r_{\mu\nu}}{\partial\theta_\mu^2}=-\frac{1}{4}r_{\mu\nu}\to 0$ as $\theta_\mu\to\theta_\nu$ so the divergence cancellation cannot come from the first derivative terms as it does in the Kato cusp condition [26]. Next, as particles μ and ν approach the same position, $r_{\mu\rho}$ goes to $r_{\nu\rho}$ for a given third particle ρ, so $\left(\frac{\partial r_{\mu\rho}}{\partial\theta_\mu}\frac{\partial^2\Psi}{\partial r_{\mu\nu}\partial r_{\mu\rho}}\right)$ goes to $\left(\frac{\partial r_{\nu\rho}}{\partial\theta_\nu}\frac{\partial^2\Psi}{\partial r_{\mu\nu}\partial r_{\nu\rho}}\right)$. Then since $\frac{\partial r_{\mu\nu}}{\partial\theta_\mu}=-\frac{\partial r_{\mu\nu}}{\partial\theta_\nu}$, the mixed second derivative terms cancel. Finally, $\left(\frac{\partial r_{\mu\nu}}{\partial\theta_\mu}\right)^2\to R^2$ as $\theta_\mu\to\theta_\nu$, so the relevant diverging kinetic energy term is

$$T_{\mu\nu\,\text{diverging}}=-\frac{1}{2\Psi R^2}\left(R^2\frac{\partial^2\Psi}{\partial r_{\mu\nu}^2}+R^2\frac{\partial^2\Psi}{\partial r_{\mu\nu}^2}\right)=-\frac{1}{\Psi}\frac{\partial^2\Psi}{\partial r_{\mu\nu}^2} \tag{B.5}$$

Then the condition on the ground state wave function is: for each pair of particles μ and ν,

$$T_{\mu\nu\,\text{diverging}}+\frac{V_1}{r_{\alpha\beta}}=0, \tag{B.6}$$

$$\left.\frac{\partial^2\Psi}{\partial r_{\mu\nu}^2}\right|_{r_{\mu\nu}\to 0}=\left.\frac{V_1}{r_{\mu\nu}}\Psi\right|_{r_{\mu\nu}\to 0}. \tag{B.7}$$

Simpler expression for the Slater determinant of free particle wave functions

For the VMC method, it is important that the trial wave function can be evaulated quickly, as the optimisation process requires many function evaluations. Unfortunately, a Slater determinant of N single-particle wave functions will, in general, include $N!$ terms, each of which is the product of N single-particle wave functions. This dependence on N quickly makes the method unfeasible as the number of particles is increased. Fortunately, for free particle wave functions on the quantum ring, we can manipulate the expression for the Slater determinant into the Vandermonde determinant,

$$\begin{vmatrix} 1 & x_1 & x_1^2 & \cdots & x_1^{N-1} \\ 1 & x_2 & x_2^2 & \cdots & x_2^{N-1} \\ \vdots & \vdots & \vdots & \ddots & \vdots \\ 1 & x_N & x_N^2 & \cdots & x_N^{N-1} \end{vmatrix} = \prod_{\alpha<\beta}^{N} (x_\alpha - x_\beta), \tag{C.1}$$

which is equal to the product of just $\frac{N}{2}(N-1)$ terms and so its computation time scales much better with increasing numbers of particles.

The Slater determinant for an odd number of free particles on a quantum ring is

$$\Psi^N(\theta_1, \theta_2, ..., \theta_N) = \frac{1}{N!} \begin{vmatrix} \frac{1}{\sqrt{2\pi}} & \frac{\sin(\theta_1)}{\sqrt{\pi}} & \frac{\cos(\theta_1)}{\sqrt{\pi}} & \frac{\sin(2\theta_1)}{\sqrt{\pi}} & \frac{\cos(2\theta_1)}{\sqrt{\pi}} & \cdots & \frac{\sin\left(\frac{N-1}{2}\theta_1\right)}{\sqrt{\pi}} & \frac{\cos\left(\frac{N-1}{2}\theta_1\right)}{\sqrt{\pi}} \\ \frac{1}{\sqrt{2\pi}} & \frac{\sin(\theta_2)}{\sqrt{\pi}} & \frac{\cos(\theta_2)}{\sqrt{\pi}} & \frac{\sin(2\theta_2)}{\sqrt{\pi}} & \frac{\cos(2\theta_2)}{\sqrt{\pi}} & \cdots & \frac{\sin\left(\frac{N-1}{2}\theta_2\right)}{\sqrt{\pi}} & \frac{\cos\left(\frac{N-1}{2}\theta_2\right)}{\sqrt{\pi}} \\ \vdots & \vdots & \vdots & \vdots & \vdots & \ddots & \vdots & \vdots \\ \frac{1}{\sqrt{2\pi}} & \frac{\sin(\theta_N)}{\sqrt{\pi}} & \frac{\cos(\theta_N)}{\sqrt{\pi}} & \frac{\sin(2\theta_N)}{\sqrt{\pi}} & \frac{\cos(2\theta_N)}{\sqrt{\pi}} & \cdots & \frac{\sin\left(\frac{N-1}{2}\theta_N\right)}{\sqrt{\pi}} & \frac{\cos\left(\frac{N-1}{2}\theta_N\right)}{\sqrt{\pi}} \end{vmatrix}, \tag{C.2}$$

and for an even number of free particles on the ring:

$$\Psi^N(\theta_1,\theta_2,...,\theta_N)=\frac{1}{N!}\begin{vmatrix} \frac{\sin(\theta_1/2)}{\sqrt{\pi}} & \frac{\cos(\theta_1/2)}{\sqrt{\pi}} & \frac{\sin(3\theta_1/2)}{\sqrt{\pi}} & \frac{\cos(3\theta_1/2)}{\sqrt{\pi}} & \cdots & \frac{\sin\left(\frac{N-1}{2}\theta_1\right)}{\sqrt{\pi}} & \frac{\cos\left(\frac{N-1}{2}\theta_1\right)}{\sqrt{\pi}} \\ \frac{\sin(\theta_2/2)}{\sqrt{\pi}} & \frac{\cos(\theta_2/2)}{\sqrt{\pi}} & \frac{\sin(3\theta_2/2)}{\sqrt{\pi}} & \frac{\cos(3\theta_2/2)}{\sqrt{\pi}} & \cdots & \frac{\sin\left(\frac{N-1}{2}\theta_2\right)}{\sqrt{\pi}} & \frac{\cos\left(\frac{N-1}{2}\theta_2\right)}{\sqrt{\pi}} \\ \vdots & \vdots & \vdots & \vdots & \ddots & \vdots & \vdots \\ \frac{\sin(\theta_N/2)}{\sqrt{\pi}} & \frac{\cos(\theta_N/2)}{\sqrt{\pi}} & \frac{\sin(3\theta_N/2)}{\sqrt{\pi}} & \frac{\cos(3\theta_N/2)}{\sqrt{\pi}} & \cdots & \frac{\sin\left(\frac{N-1}{2}\theta_N\right)}{\sqrt{\pi}} & \frac{\cos\left(\frac{N-1}{2}\theta_N\right)}{\sqrt{\pi}} \end{vmatrix}. \tag{C.3}$$

For both determinants, we can take complex linear combinations of the columns and pull out constant factors to get for an odd number of particles

$$\Psi^N(\theta_1,\theta_2,...,\theta_N)\propto\begin{vmatrix} 1 & e^{-i\theta_1} & e^{i\theta_1} & \cdots & e^{-i\frac{N-1}{2}\theta_1} & e^{+i\frac{N-1}{2}\theta_1} \\ 1 & e^{-i\theta_2} & e^{i\theta_2} & \cdots & e^{-i\frac{N-1}{2}\theta_2} & e^{+i\frac{N-1}{2}\theta_2} \\ \vdots & \vdots & \vdots & \ddots & \vdots & \vdots \\ 1 & e^{-i\theta_N} & e^{i\theta_N} & \cdots & e^{-i\frac{N-1}{2}\theta_N} & e^{+i\frac{N-1}{2}\theta_N} \end{vmatrix}, \tag{C.4}$$

and for an even number of particles

$$\Psi^N(\theta_1,\theta_2,...,\theta_N)\propto\begin{vmatrix} e^{-i\theta_1/2} & e^{i\theta_1/2} & \cdots & e^{-i\frac{N-1}{2}\theta_1} & e^{+i\frac{N-1}{2}\theta_1} \\ e^{-i\theta_2/2} & e^{i\theta_2/2} & \cdots & e^{-i\frac{N-1}{2}\theta_2} & e^{+i\frac{N-1}{2}\theta_2} \\ \vdots & \vdots & \ddots & \vdots & \vdots \\ e^{-i\theta_N/2} & e^{i\theta_N/2} & \cdots & e^{-i\frac{N-1}{2}\theta_N} & e^{+i\frac{N-1}{2}\theta_N} \end{vmatrix}. \tag{C.5}$$

Then pulling out factors of $e^{-i\frac{N-1}{2}\theta_\alpha}$ from each row of the determinant (and rearranging the order of the columns), we get for an odd number of particles:

$$\Psi^N(\theta_1,\theta_2,...,\theta_N)\propto\left(\prod_{\alpha=1}^{N}e^{-i\frac{N-1}{2}\theta_\alpha}\right)\begin{vmatrix} 1 & e^{i\theta_1} & \cdots & e^{+i(N-1)\theta_1} \\ 1 & e^{i\theta_2} & \cdots & e^{+i(N-1)\theta_2} \\ \vdots & \vdots & \ddots & \vdots \\ 1 & e^{i\theta_N} & \cdots & e^{+i(N-1)\theta_N} \end{vmatrix} \tag{C.6}$$

and for an even number of particles

$$\Psi^N(\theta_1,\theta_2,...,\theta_N)\propto\left(\prod_{\alpha=1}^{N}e^{-i\frac{N-1}{2}\theta_\alpha}\right)\begin{vmatrix} 1 & e^{i\theta_1} & \cdots & e^{+i(N-1)\theta_1} \\ 1 & e^{i\theta_2} & \cdots & e^{+i(N-1)\theta_2} \\ \vdots & \vdots & \ddots & \vdots \\ 1 & e^{i\theta_N} & \cdots & e^{+i(N-1)\theta_N} \end{vmatrix} \tag{C.7}$$

Setting $x_\alpha=e^{i\theta_\alpha}$, we see that both of these determinants are equal to the Vandermonte determinant. Substituting $x_\alpha-x_\beta=e^{i\theta_\alpha}-e^{i\theta_\beta}$ in the simpler expression for the Vander-

monde determinant we get for both odd and even numbers of particles,

$$\Psi^N(\theta_1, \theta_2, ..., \theta_N) \propto \left(\prod_{\alpha=1}^{N} e^{-i\frac{N-1}{2}\theta_\alpha} \right) \left(\prod_{\alpha<\beta}^{N} e^{i\theta_\alpha} - e^{i\theta_\beta} \right). \tag{C.8}$$

Ideally, we would like to combine the two products into a single product. To do this I separate each factor in the left-most product into $N-1$ factors of $e^{-i\frac{\theta_\alpha}{2}}$. Having done this, I pair each $e^{-i\frac{\theta_\alpha}{2}}$ factor with a $e^{-i\frac{\theta_\beta}{2}}$ factor and multiply the two of them with their corresponding $\alpha\beta$-term in the right most sum. This gives

$$\Psi^N(\theta_1, \theta_2, ..., \theta_N) \propto \prod_{\alpha<\beta}^{N} e^{-i(\theta_\alpha+\theta_\beta)/2}(e^{i\theta_\alpha} - e^{i\theta_\beta}) \tag{C.9}$$

$$\propto \prod_{\alpha<\beta}^{N} e^{i(\theta_\alpha-\theta_\beta)/2} - e^{-i(\theta_\alpha-\theta_\beta)/2} \tag{C.10}$$

$$\propto \prod_{\alpha<\beta}^{N} \sin\left(\frac{\theta_\alpha - \theta_\beta}{2}\right) \tag{C.11}$$

$$\propto \prod_{\alpha<\beta}^{N} r_{\alpha\beta}, \tag{C.12}$$

which is far easier to evaluate than the original determinant.

Condition on the Jastrow trial wave functions

I now want to apply the previously derived condition on the second derivative of the wave function,

$$\left.\frac{\partial^2\Psi}{\partial r_{\alpha\beta}^2}\right|_{r_{\alpha\beta}\to 0} = \left.\frac{V_1}{r_{\alpha\beta}}\Psi\right|_{r_{\alpha\beta}\to 0}, \tag{D.1}$$

to the particular trial wave functions used in this thesis to find a condition on the parameters used to optimise the trial wave function. Both trial wave functions used in this thesis can be written in the form

$$\Psi_{\text{vmc}}(\boldsymbol{\theta},\boldsymbol{a}) \propto \prod_{\alpha<\beta}^{N} r_{\alpha\beta}^{*}\, e^{J(r_{\alpha\beta},\boldsymbol{a})}, \tag{D.2}$$

where $r_{\alpha\beta}^{*}$ is the signed inter-particle distance, $J(r_{\alpha\beta},\boldsymbol{a})$ is a polynomial of the positive inter-particle distance, $r_{\alpha\beta} = |r_{\alpha\beta}^{*}|$, and I do not worry about the normalisation constant which will cancel on both sides of equation (D.1). Now the first partial derivatives of the wave function is

$$\frac{\partial\Psi_{\text{vmc}}}{\partial r_{\alpha\beta}} = r_{\alpha\beta}^{*}e^{J(r_{\alpha\beta},\boldsymbol{a})}\frac{\partial J}{\partial r_{\alpha\beta}} \pm e^{J(r_{\alpha\beta},\boldsymbol{a})} = \left(\frac{\partial J}{\partial r_{\alpha\beta}} \pm \frac{1}{r_{\alpha\beta}^{*}}\right)\Psi_{\text{vmc}}, \tag{D.3}$$

where the plus or minus is determined by the sign of $r_{\alpha\beta}^{*}$. The second partial derivative is then

$$\frac{\partial^2\Psi_{\text{vmc}}}{\partial r_{\alpha\beta}^2} = \left(\frac{\partial J}{\partial r_{\alpha\beta}} \pm \frac{1}{r_{\alpha\beta}^{*}}\right)^2\Psi_{\text{vmc}} + \left(\frac{\partial^2 J}{\partial r_{\alpha\beta}^2} - \frac{1}{(r_{\alpha\beta}^{*})^2}\right)\Psi_{\text{vmc}} \tag{D.4}$$

$$= \left(\pm\frac{2}{r_{\alpha\beta}^{*}}\frac{\partial J}{\partial r_{\alpha\beta}} + \left(\frac{\partial J}{\partial r_{\alpha\beta}}\right)^2 + \frac{\partial^2 J}{\partial r_{\alpha\beta}^2}\right)\Psi_{\text{vmc}} \tag{D.5}$$

$$= \left(\frac{2}{r_{\alpha\beta}}\frac{\partial J}{\partial r_{\alpha\beta}} + \left(\frac{\partial J}{\partial r_{\alpha\beta}}\right)^2 + \frac{\partial^2 J}{\partial r_{\alpha\beta}^2}\right)\Psi_{\text{vmc}}. \tag{D.6}$$

Since $J(r_{\alpha\beta}, \boldsymbol{a})$ is a polynomial of $r_{\alpha\beta}$, $\left(\frac{\partial J}{\partial r_{\alpha\beta}}\right)^2 \Psi_{\text{vmc}}$ and $\frac{\partial^2 J}{\partial r_{\alpha\beta}^2}\Psi_{\text{vmc}}$ both go to 0 as $r_{\alpha\beta} \to 0$,

$$\left.\frac{\partial^2 \Psi_{\text{vmc}}}{\partial r_{\alpha\beta}^2}\right|_{r_{\alpha\beta}\to 0} = \left.\frac{2}{r_{\alpha\beta}}\frac{\partial J}{\partial r_{\alpha\beta}}\Psi_{\text{vmc}}\right|_{r_{\alpha\beta}\to 0}. \tag{D.7}$$

By comparing this to the original condition we get

$$\left.\frac{\partial J}{\partial r_{\alpha\beta}}\right|_{r_{\alpha\beta}\to 0} = \frac{V_1}{2}. \tag{D.8}$$

For the first Jastrow function used in this thesis with $J(r_{\alpha\beta}, \boldsymbol{a}) = (r_{\alpha\beta} - L_c)^3 \sum_{k=0}^{5} a_k r_{\alpha\beta}^k$, the first partial derivative is

$$\frac{\partial J}{\partial r_{\alpha\beta}} = (r_{\alpha\beta} - L_c)^3 \sum_{k=1}^{5} k a_k r_{\alpha\beta}^{k-1} + 3(r_{\alpha\beta} - L_c)^2 \sum_{k=0}^{5} a_k r_{\alpha\beta}^k \tag{D.9}$$

$$\left.\frac{\partial J}{\partial r_{\alpha\beta}}\right|_{r_{\alpha\beta}\to 0} = -L_c^3 a_1 + 3L_c^2 a_0, \tag{D.10}$$

so we require

$$a_0 = \frac{L_c}{3}\left(a_1 + \frac{V_1}{2L_c^3}\right), \tag{D.11}$$

to prevent the divergence of the local energy.

For the second Jastrow function, $J(r_{\alpha\beta}, \boldsymbol{a}) = \sum_{k=1}^{4} a_k r_{\alpha\beta}^k$, its first derivative is simply

$$\left.\frac{\partial J}{\partial r_{\alpha\beta}}\right|_{r_{\alpha\beta}\to 0} = a_1, \tag{D.12}$$

so we require

$$a_1 = \frac{V_1}{2} \tag{D.13}$$

to prevent the divergence of the local energy.

Bibliography

[1] D. R. Hartree. "The Distribution of Charge and Current in an Atom consisting of many Electrons obeying Dirac's equations". *Mathematical Proceedings of the Cambridge Philosophical Society* 25.2 (1929). Publisher: Cambridge University Press, pp. 225–236.

[2] V. Fock. "Näherungsmethode zur Lösung des quantenmechanischen Mehrkörperproblems". *Zeitschrift für Physik* 61.1 (1930), pp. 126–148.

[3] E. Gapon and D. Iwanenko. "Zur Bestimmung der Isotopenzahl". *Naturwissenschaften* 20.43 (1932), pp. 792–793.

[4] M. G. Mayer. "On Closed Shells in Nuclei. II". *Physical Review* 75.12 (1949). Publisher: American Physical Society, pp. 1969–1970.

[5] M. G. Mayer. "On Closed Shells in Nuclei". *Physical Review* 74.3 (1948). Publisher: American Physical Society, pp. 235–239.

[6] R. B. Wiringa, V. G. J. Stoks, and R. Schiavilla. "Accurate nucleon-nucleon potential with charge-independence breaking". *Physical Review C* 51.1 (1995). Publisher: American Physical Society, pp. 38–51.

[7] P. Ring and P. Schuck. *The Nuclear Many-Body Problem*. Springer Science & Business Media, 2004.

[8] S. G. Nilsson. "Binding states of individual nucleons in strongly deformed nuclei". *Dan. Mat. Fys. Medd.* 29 (1955). Number: CERN-55-30, p. 1.

[9] L. Coraggio, A. Covello, A. Gargano, N. Itaco, and T. T. S. Kuo. "Shell-model calculations and realistic effective interactions". *Progress in Particle and Nuclear Physics* 62.1 (2009), pp. 135–182.

[10] M. Lewin and S. Paul. "A Numerical Perspective on Hartree-Fock-Bogoliubov Theory". *ESAIM: Mathematical Modelling and Numerical Analysis* 48.1 (2014). arXiv:1206.6081 [math-ph], pp. 53–86.

[11] J. A. Sheikh, J. Dobaczewski, P. Ring, L. M. Robledo, and C. Yannouleas. "Symmetry restoration in mean-field approaches". *Journal of Physics G: Nuclear and Particle Physics* 48.12 (2021), p. 123001.

[12] M. C. Atkinson, W. H. Dickhoff, M. Piarulli, A. Rios, and R. B. Wiringa. "Reexamining the relation between the binding energy of finite nuclei and the equation of state of infinite nuclear matter". *Physical Review C* 102.4 (2020). Publisher: American Physical Society, p. 044333.

[13] M. Oertel, M. Hempel, T. Klähn, and S. Typel. “Equations of state for supernovae and compact stars”. *Reviews of Modern Physics* 89.1 (2017). Publisher: American Physical Society, p. 015007.

[14] J. R. Stone and P.-G. Reinhard. “The Skyrme Interaction in finite nuclei and nuclear matter”. *Progress in Particle and Nuclear Physics* 58.2 (2007). arXiv:nucl-th/0607002, pp. 587–657.

[15] A. Smerzi, D. G. Ravenhall, and V. R. Pandharipande. “Neutron drops and neutron pairing energy”. *Physical Review C* 56.5 (1997), pp. 2549–2556.

[16] B. S. Pudliner, A. Smerzi, J. Carlson, V. R. Pandharipande, Steven C. Pieper, and D. G. Ravenhall. “Neutron Drops and Skyrme Energy-Density Functionals”. *Physical Review Letters* 76.14 (1996). Publisher: American Physical Society, pp. 2416–2419.

[17] S. Viefers, P. Koskinen, P. S. Deo, and M. Manninen. “Quantum rings for beginners: Energy spectra and persistent currents”. *Physica E: Low-dimensional Systems and Nanostructures* 21.1 (2004). arXiv:cond-mat/0310064, pp. 1–35.

[18] C. Neill, T. McCourt, X. Mi, Z. Jiang, M. Y. Niu, W. Mruczkiewicz, I. Aleiner, F. Arute, et al. “Accurately computing the electronic properties of a quantum ring”. *Nature* 594.7864 (2021). Number: 7864 Publisher: Nature Publishing Group, pp. 508–512.

[19] N. Hernández, R. A. López-Doria, I. E. Rivera, and M. R. Fulla. “Refractive index change of a D2+complex in GaAs/AlxGa1-xAs quantum ring”. *Journal of Materials Science* 57.18 (2022), pp. 8417–8424.

[20] C. J. Judd, A. S. Nizovtsev, R. Plougmann, D. V. Kondratuk, H. L. Anderson, E. Besley, and A. Saywell. “Molecular Quantum Rings Formed from a π-Conjugated Macrocycle”. *Physical Review Letters* 125.20 (2020). Publisher: American Physical Society, p. 206803.

[21] R. W. Hasse. “Static criteria for the existence of Coulomb strings in storage rings”. *Physical Review Letters* 90.20 (2003), p. 204801.

[22] J. L. Zhu, Z. Dai, and X. Hu. “Two electrons in one-dimensional nanorings: Exact solutions and interaction energies”. *Physical Review B* 68.4 (2003). Publisher: American Physical Society, p. 045324.

[23] P. F. Loos and P. M. W. Gill. “Exact Wave Functions of Two-Electron Quantum Rings”. *Physical Review Letters* 108.8 (2012), p. 083002.

[24] S. S. Gylfadottir, A. Harju, T. Jouttenus, and C. Webb. “Interacting electrons on a quantum ring: exact and variational approach”. *New Journal of Physics* 8.9 (2006). arXiv:cond-mat/0511075, pp. 211–211.

[25] A. W. Bray and C. Simenel. “Fermions with long and finite-range interactions on a quantum ring”. *Physical Review C* 103.1 (2021), p. 014302.

[26] T. Kato. “On the eigenfunctions of many-particle systems in quantum mechanics”. *Communications on Pure and Applied Mathematics* 10.2 (1957), pp. 151–177.

[27] F. W. Olver, D. W. Lozier, R. Boisvert, and C. W. Clark. "The NIST Handbook of Mathematical Functions". *NIST* (2010). Last Modified: 2021-10-12T11:10-04:00 Publisher: Frank W. Olver, Daniel W. Lozier, Ronald Boisvert, Charles W. Clark.

[28] R. J. Needs, M. D. Towler, N. D. Drummond, and P. L. Ríos. "Continuum variational and diffusion quantum Monte Carlo calculations". *Journal of Physics: Condensed Matter* 22.2 (2010), p. 023201.

[29] R. J. Needs, M. Towler, N Drummond, and P. L. Ríos. *Casino Version 2.13 User Manual*. 2019.

[30] P. F. Loos and P. M. W. Gill. "Two Electrons on a Hypersphere: A Quasiexactly Solvable Model". *Physical Review Letters* 103.12 (2009), p. 123008.

[31] P. M. W. Gill and D. P. O'Neill. "Electron correlation in Hooke's law atom in the high-density limit". *The Journal of Chemical Physics* 122.9 (2005), p. 094110.

[32] J. D. Baker, D. E. Freund, R. N. Hill, and J. D. Morgan. "Radius of convergence and analytic behavior of the 1 Z expansion". *Physical Review A* 41.3 (1990), pp. 1247–1273.

[33] K. T. R. Davies, H. Flocard, S. Krieger, and M. S. Weiss. "Application of the imaginary time step method to the solution of the static Hartree-Fock problem". *Nuclear Physics A* 342.1 (1980), pp. 111–123.

[34] E. U. Condon. "The Theory of Complex Spectra". *Physical Review* 36.7 (1930), pp. 1121–1133.

[35] N. Metropolis, A. W. Rosenbluth, M. N. Rosenbluth, A. H. Teller, and E. Teller. "Equation of State Calculations by Fast Computing Machines". *The Journal of Chemical Physics* 21.6 (1953), pp. 1087–1092.

[36] H. Flyvbjerg and H. G. Petersen. "Error estimates on averages of correlated data". *The Journal of Chemical Physics* 91.1 (1989), pp. 461–466.

[37] R. Jastrow. "Many-Body Problem with Strong Forces". *Physical Review* 98.5 (1955), pp. 1479–1484.

[38] N. D. Drummond, M. D. Towler, and R. J. Needs. "Jastrow correlation factor for atoms, molecules, and solids". *Physical Review B* 70.23 (2004), p. 235119.

[39] Johnson, S. G. *The NLopt nonlinear-optimization package*. Version 2.7.1.

[40] D. R. Jones, C. D. Perttunen, and B. E. Stuckman. "Lipschitzian optimization without the Lipschitz constant". *Journal of Optimization Theory and Applications* 79.1 (1993), pp. 157–181.

[41] J. Mur-Petit, A. Polls, and F. Mazzanti. "The variational principle and simple properties of the ground-state wave function". *American Journal of Physics* 70.8 (2002). Publisher: American Association of Physics Teachers, pp. 808–810.